Scintillator Based Calorimetry for the SSC. A Subsystem Proposal

Boston University: T. Coane, S.T. Dye, E. Hazen, D. Higby, S.Klein, J.P. Miller, D. Osborne, B.L. Roberts, J. Stone, L. Sulak*, W. Worstell

Fairfield University: D.R. Winn

Florida State University: K. Johnson

FNAL: M. Atac, M. Binkley, A. Bross, T. Droege, G.W. Foster, J. Freeman, S. Hahn, J. Hauser, M. Lundin, C. Newmann-Holmes, J. Krebs, A. Para*, A. Pla, D. Theriot, S. Tkaczyk, R. Wands

KEK: M. Mishina (KEK and FNAL), F. Takasaki

Michigan State University: C. Bromberg, J. Huston, R. Miller

Northeastern University: T. Yasuda

Purdue University: V. Barnes, A. Garfinkel, A. Laasanen, J. Tonnison

Rockefeller University: P.Melese, R.W.Rusack, A.Vacchi, S. White

Rutgers University: T. Devlin

Texas A&M: T. Bowcock, P. Datte, F. Huson, P. McIntyre, R. Webb, J. White, S. Zaman

University of California-San Diego: D. Acosta, J. Branson, B. Ong, H. Paar, M. Sivertz, D. Thomas

University of Florida: S. Majewski, C. Zorn, P. Zorn

University of Illinois-Urbana: P.T. Debevec, R.A. Eisenstein, D.W. Hertzog

University of Michigan: R. Gustafson, M. Marcin, H. Neal

University of Rochester: A. Bodek, H. Budd, P. de Barbaro, M. Dixon, S. Olsen, W. Sakumoto, A. Sill, G. Watts

University of Tsukuba: Y.Funayama, F. Ioka, T.Inoue, A. Kaneko, S. Kim, K. Kondo, S. Miyashita, S. Mori, Y. Morita, R. Oishi, K. Takikawa, K. Yasuoka

University of Washington: V. Cook, R.Williams, K.Young

Yale University: P.Cushman, V.Singh

* contact

October 2 . 1989

Proposal Summary

We propose to design and engineer a calorimeter for an SSC detector based on scintillator as its active medium. The calorimeter will be well matched to the physics requirements. We will address optimization of large scale manufacturing techniques, including realistic construction schedule and cost estimate. Our goals include demonstrating survivability of the proposed detector in a high radiation environment of the SSC.

The main advantage of scintillating calorimetry is its intrinsic speed of response. Further, modularity, ease of construction and maintenance, hermeticity and a demonstrated performance in high rate environments and in large scale detectors (UA1, UA2, CDF, ZEUS...), are essential attributes of this technology. In addition, short and long term stability, simplicity and safety, compensation and excellent resolution are attractive characteristics of scintillators. Fiber based technology offers fine granularity, flexibility, and the best prospects for radiation resistance.

We will pursue a broad based experimental program, studying detector performance in areas such as energy resolution, hermeticity, electron-hadron separation, and radiation hardness. In parallel, we will study manufacturing and integration issues, as a part of a comprehensive costing program . Where required, we will pursue Monte Carlo studies to determine calorimeter performance requirements. Our three year R&D program will begin with several approaches, and will gradually focus on a specific detector technology.

Our collaboration has a great deal of experience with a variety of calorimeters using scintillator and other techniques. We propose to begin our experimental program by investigating the following approaches:

1. a single compartment fiber based calorimeter, with an effective depth segmentation given by projective geometry
2. a segmented fiber based calorimeter (i.e. containing an EM section followed by a hadronic one)
3. a calorimeter constructed of scintillating tiles which are read out by wavelength shifting fibers

The evaluation of these approaches will be made on the basis of experience with prototypes (some of which are currently operating or under construction), as well as engineering estimates of the cost and manufacturability of each. We will complete an engineered calorimeter design in time for the first round of SSC detector proposals.

Whereas calorimetry using scintillating fibers or tiles is a well established technology, applications to large scale, 4π detectors are still in their infancy.

Many of the system-wide issues appear and can be addressed only within the framework of a specific detector. We have chosen as an example a solenoidal detector with a coil placed inside the calorimeter. Most of the solutions appear to be readily adaptable to other geometries currently under discussion for an SSC detector.

The compensation phenomenon has received wide attention in relation to SSC calorimetry. The calorimeter designs we are considering involve various compensating combinations of lead, iron, and scintillator. We note the scarcity of experimental information on this subject, in particular for inhomogeneous absorbers and segmented calorimeters. In addition to test-beam measurements on our prototype calorimeter modules, we propose to make a dedicated experiment to address the issue of compensation in composite structures.

There are some potential problems with this type of calorimetry which need to be thoroughly examined. The principal ones are the radiation hardness, the maintenance of the calibration at the level of 1% and the total cost of the calorimeter including readout. Recent progress in radiation hardness of scintillators suggest that a calorimeter using this technology will survive in the SSC environment, while developments in calibration techniques imply that the strict requirements can be met. Our preliminary estimate of the total system cost indicates that the scintillator calorimetry is very competitive. All these important questions will be addressed in detail as part of our research program

TABLE OF CONTENTS

1. A SCINTILLATOR CALORIMETER DETECTOR FOR THE SSC

1.1. PHYSICS MOTIVATION AND REQUIREMENTS

Experimentation at the SSC requires the measurement of leptons and jets with a precision that allows determination of the underlying kinematics of multi-TeV collisions in terms of elementary constituents. This requires identification and energy measurement of photons, electrons, muons, quark and gluon jets, and neutrinos. At the SSC calorimetric measurement of particle energy is more accurate than is momentum measurement in a magnetic field. In addition to high precision, detectors must have a fast response and rapid cycle time so that they can function properly at the high event rate at the SSC. Working in concert with tracking and muon subsystems, the calorimeter will provide precise measurements of electrons, jets, and missing energy.

Many workshops have explored the physics questions to be investigated at the SSC[1]. All studies agree that a calorimeter will be a key element of an SSC detector. Its chief function will be:

a) To identify electrons and photons, and measure their energy and direction.

b) To measure missing transverse energy.

c) To detect and measure properties of high P_T quark and gluon jets.

d) To assist in the identification of muons and taus.

ϵ) To furnish fast signals for triggering on the above processes

A standard benchmark for calorimeter performance is the production of a Higgs + X, where the Higgs decays into a pair of W's or Z's, and one of the W's or Z's decays into two jets. The goal is to reconstruct the intermediate vector boson mass in the jet-jet system. Several studies were devoted to establishing detector parameters which are essential for this particular measurement[2]. These studies lead to the conclusion that short integration time is the most important parameter, since overlay of several minimum bias events degrades the two jet invariant mass resolution seriously (see Fig. 1). Plastic scintillator calorimetry, with an extremely fast response (see Fig. 2), provides a very powerful pile-up rejection.

Different physics signals impose some other requirements for calorimeter performance. The process $Z^* \rightarrow Z +$ jet.

$H \rightarrow ZZ \rightarrow ll\nu\nu$

$H \rightarrow ZZ \rightarrow jj\nu\nu$

$H \rightarrow WW \rightarrow l\nu jj$

are important signatures for Higgs physics. They demand finely segmented hermetic calorimetry to measure missing E_T and jets. Processes such as Z' -¿ e e and compositness will impose demands on energy resolution and linearity. A full specification of the calorimeter parameters in terms of physics to be studied at the SSC is an integral part of the work to be performed by this collaboration.

The initial goals for our calorimeter design are:

a) Fast response (tailored to the 16 ns repetition rate of the SSC) to ensure fast triggering,

b) Radiation resistance (for levels exceeding 10 MRad) to ensure operation for at least 10 years of running at the SSC.

c) Single particle energy resolutions of $\sigma/E < 50\%/\sqrt{E} - C_1$ for hadrons and $20\%/\sqrt{E} + C_2$ for electrons (positrons) and photons, with constant terms less than a few percent,

d) Good uniformity of response,

e) Full compensation with e/h between 0.9 and 1.1,

f) Jet energy resolution comparable to single particle resolution,

g) Good hadron-electron separation (better than 1000:1),

h) Fully hermetic construction (little or no cracks, dead areas or hot spots),

i) Fine granularity, with the electromagnetic and hadronic segmentation chosen to match physics requirements,

j) Compatibility with a central magnetic field

k) Self-supporting mechanical structure,

l) A large signal to noise ratio,

m) Ease of construction and maintenance

n) long and short time stability.

It is not always fully appreciated that a constant term in the fractional energy resolution will dominate at the SSC energies (E> 100 GeV). This term usually originates from variation in the response at different locations in the calorimeter. Our prototype calorimeter tests will evaluate this term by mapping the calorimeter response to electrons and hadrons at different energies and impact points.

1.2. EXAMPLE DETECTOR FOR THE SSC

A design of a complete calorimeter will be made after selection of calorimeter technology. It will include issues of construction, performance, mechanical support, calibration, trigger, and read-out. New problems may arise and some of the solutions adopted for small prototypes may become unacceptable when a global design of the entire detector is attempted. Interference with other detector components, the necessity of support structures, the need for penetrations for cables, etc. may degrade the performance of an otherwise acceptable detector.

Therefore, we plan to choose an example of a detector and generate a full physics and engineering design of a calorimeter for this detector. A non-magnetic detector poses far fewer constraints than a magnetic one, and for this reason we will develop a calorimeter for a detector with a magnetic field. Most of our solutions will be directly applicable to a non-magnetic detector, for which many problems are simplified. Our aim is to establish the feasibility and estimate the cost of scintillator-based calorimetry, rather than to propose a specific detector.

We choose a small solenoidal detector as the target for our calorimeter design. This detector is illustrated schematically in Fig. 3 . The selected geometry maximizes hermeticity of the detector. The inner tracking necessitates penetrations for the readout cables, cooling, gas, etc. We choose these penetrations at 90 degrees (where the particle density per unit length is minimal). We therefore envisage two superconducting coils (similar to the existing coil of CDF), with a barrel calorimeter split into two halves. Since the calorimeter read-out is outside of the magnetic volume, phototubes could be used for readout.

This design forces several constraints on the calorimeter design. The calorimeter structure must be strong enough to support itself. A viable calorimeter design must be able to accommodate the presence of large volumes of iron in the end cap calorimeters, to reduce the magnetic forces on the solenoids.

The initial results of our study should be completed in time for the first round of the proposals for an SSC detector. The design will include a mechanical support, a construction schedule, development of mass production techniques, prototype construction, and a cost estimate for a realistic calorimeter for the SSC.

1.3. THE CALORIMETER DESIGN: THREE OPTIONS

Physics requirements listed in section 1.1 are most easily satisfied with a scintillator based calorimeter. Although scintillator based calorimeters are well established, meeting physics requirements within constraints of the high rate environment and limitations of a magnetic detector poses a substantial challenge. Keeping in mind size, cost, maintenance and operation of the detector, we feel it is important to seek the simplest technical solution, rather than attempt to push performance of the calorimeter to its limits. The design must also address issues of large scale manufacturing. Past R&D projects and our experience suggest several designs of the calorimeter, each having its own particular advantages and problems.

We will explore scintillating fiber calorimetry, and a new variant of scintillator plates (Scintillating tiles with wavelength shifter fiber readout). Both of them have several advantages over the conventional scintillator plate technology with a wavelength shifter bars readout):

a) sensitivity to radiation damage is reduced by the short path of blue light in scintillator,

b) finer transverse segmentation can be realized.

c) excellent hermeticity is possible The liquid scintillator option is described in section 1.9.

Given the advantages and drawbacks of each scheme of scintillator calorimetry, we believe it is premature to settle on any particular design. We concentrate our work on the following designs, which we find the most promising:

1. A monolithic iron-lead laminated calorimeter composed of a single depth segment with scintillating fibers running from the front to the back. As the cross-sectional area of the calorimeter increases with depth, additional fibers are added to keep constant sampling fraction. An effective depth segmentation and consequent e/π separation capabilities are provided by reading out separately the fibers starting in front and those starting in depth. Monte Carlo simulation studies indicate an e/π separation power of the order of 1:1000 using this depth segmentation and taking advantage of the fine transverse granularity, although this clearly needs to be verified by studies in a test beam. This solution has the advantage of construction simplicity. Iron plates provide mechanical strength, and the number of independent modules is small.

2. A fiber calorimeter with two depth segments. The front (EM) segment of the calorimeter will be constructed of a lead-fiber mixture, probably using

a casting technique. The light from the EM section will be compressed into a readout area much smaller than that of the scintillating fibers using newly developed fibers with a wavelength shifting core. This light will be read out by splicing to small diameter (0.5 mm) clear readout fibers. The clear fibers from the EM calorimeter will either pass through the body of the hadronic calorimeter, or be led out via non-projective cracks. In this approach one is assured of achieving the usual e/π discrimination power of the segmented calorimeters, augmented by the fine transverse segmentation.

3. A scintillating-tile calorimeter read out by wavelength-shifting fiber. The EM section will be a Pb/scintillator sandwich, followed by a Pb/Fe/scintillator hadronic section. The tower structure is provided by appropriate segmentation of scintillator tiles, which are read out via the wavelength shifter fibers embedded in them. The volume occupied by these fibers in the calorimeter is negligible. This solution is an attractive alternative to a canonical scintillating fiber calorimetry owing to its relative simplicity of construction, similarity to existing large scale calorimetric detectors, and potentially lower cost.

1.4. Compensation Studies

A number of important questions for compensating scintillator calorimetry will be addressed by a large (80cm x 80cm x 2m) test beam calorimeter containing a Pb/Fe/Scintillating-tile stack which can be reconfigured to vary sampling fractions, material ratios, etc. Among these are:

a) Which combinations of Pb, Fe, & Scintillator are actually compensating?

b) What is the effect of a non-compensating EM front end on the hadron resolution?

d) How is compensation affected by inert hydrogenic materials?

d) How does calorimeter depth, and depth segmentation affect resolution?

e) What is the light yield & uniformity of a full sized Scintillating Tile calorimeter under beam conditions?

A reconfigurable calorimeter would also be ideal for studying radiation damage issues in a test beam environment.

1.5. PHOTOMULTIPLIERS AND READOUT

Each of the above calorimeter designs involves a bundle of readout fibers which must be collected and uniformly distributed to a phototube. In each design a trigger decision will be formed using some form of 'electromagnetic' and 'hadronic' pulse height. Photomultipliers, read-out and trigger design are therefore independent of the technical details of the proposed calorimeter.

A. Light Guides and Mixers

The fiber-to-fiber variation in the light output, transmission or optical coupling will lead to a constant term in the energy resolution. To avoid degradation of the performance of the calorimeter uniformity of the light collection system must be at the level of 5% or better. The SPACAL group has found a possible solution in the form of "light mixers", essentially plastic hexagonal light guides. (See Appendix F.3 for details).

Another significant contribution to the technology of light distribution was the development at Boston University of precision-machined fiber splicing plates, which provide a mass-termination splicing technology for bundles of optical fibers. This allows, for example, a removable and reproducible splice to be made from a large number of scintillating fibers in the body of the calorimeter to a bundle of clear readout fibers (See Appendix F.1).

B. PMT and Electronics Subassembly

An SSC calorimeter is expected to have perhaps 50.000 phototubes. The cost of the PMT's themselves is not daunting (5M$ at $100.00 apiece), but the cost of the associated trigger and readout electronics, power supplies, etc. may double or triple it. It is expected that significant savings can be realized by the engineering of a multi-phototube assembly. We envisage a single "card" containing 8-16 PMT's, with power supplies, magnetic shielding, readout electronics, trigger logic, etc. integrated in a single package (see appendix C). The module would be optically coupled to a mating array of the light mixers described above.

Authors on this proposal have been personally responsible for the design and construction of read out systems for several large arrays of PM tubes, as well as pipelined trigger electronics for detectors at hadron colliders. We see no technical problems in the approach we advocate above (indeed, there are many existence proofs of high-rate electronics in peaceful coexistence with PM tubes), and we feel that we should be able to produce workable prototypes and reasonable cost estimates during the period of this subsystem proposal.

C. Triggering and Data Acquisition System

The lowest level of components in the digital pipeline needed for an SSC

trigger will reside on the PMT/electronics module. The way that this module fits into the global scheme for the trigger will depend on other detector components. We propose two efforts related to the calorimeter first-level trigger.

First, one of the authors[3] has developed a conceptual design for a pipelined trigger which produces, on each beam crossing, a trigger decision similar to the CDF levels 1 and 2 triggers. Our design for the PMT front-end electronics will be compatible with such a system. Similarly, the first level components of the DAQ/readout system would reside on the integrated PMT/Electronics module.

At the same time, we see a need for studies of algorithms for isolating electrons, taus, and perhaps jets with a first-level trigger. Since a large part of the front-end calorimeter electronics will be devoted to first-level triggering, these algorithms must be chosen before the front-end electronics design can be completed. These studies will give efficiencies and background trigger rates as a function of trigger threshold. Because jets of a given momentum are essentially the same at the Tevatron as at the SSC, studies of background rates for electrons and taus using different trigger algorithms can be carried out using existing CDF data. Combining predicted SSC jet cross-sections with jet rejection factors determined from real data, we can derive realistic estimates of background trigger rates. Some of the studies will require Monte Carlo work as well. For instance, the monolithic scintillating fiber calorimeter will require an unusual scheme of electron triggering. We propose to carry out these trigger studies to a level where front-end electronics may be fully designed, and the rates which an SSC detector data acquisition system must be able to handle from calorimetry triggers are known.

1.6. CALIBRATION AND MONITORING ISSUES

A complete SSC detector will consist of the order of 50,000 channels to be calibrated. This clearly precludes a calibration of all towers in the test beams. For electromagnetic calorimeters, the SSC itself will provide a very powerful calibration tool in the form of a large number of Z^0's. The central magnetic field and tracking detector will permit another test of the absolute calibration by comparing momentum and energy measurements for electrons. (This technique has recently been very successfully employed by CDF in a precision measurement of the mass of the Z^0.) Because of the very large number of calorimeter channels, these methods may prove very cumbersome, however. In addition, there is no convenient signal from the SSC itself for the calibration of the hadron calorimeters. Hadronic calibration is further complicated by the fact that a typical hadronic shower will spread energy over several towers. In the case of the proposed single depth calorimeter with 'central' and 'side' fibers read out separately an additional

complication arises: gains of these two photomultipliers have to be adjusted to equalize the response. While it is expected that scintillators available for the construction of the SSC detector will be radiation hard, it is nevertheless important to be able to monitor possible radiation effects on the calorimetric response.

For the laminated fiber calorimeter we propose to address these questions by embedding a set of small diameter tubes into one of the steel plates at several depths of the calorimeter, with thin wires containing radioactive sources inside them. These sources will solve most of the problems mentioned above. By measuring a DC current as sources traverse several towers one can equalize the towers' responses, and moreover the gains of the 'central' and 'side' PMs can be adjusted. This greatly reduces the number of independent calibration constants which need to be determined/verified using the data itself. In the same way it will be possible to transport an absolute calibration of a tower from the test beam to the final detector, and to propagate the calibration to other towers. The techniques used will be based in part on our experience with the CDF Central and Endwall scintillator-based calorimeters[4].

By monitoring the response of the towers at different depths inside the calorimeter one will be able to monitor the effect of radiation damage with time.

In the case of magnetic flux return through the calorimeter one expects a change in the light yield of the scintillator. A suitable set of radioactive sources will be indispensable to calibrate out this effect.

Short term calibration of the pulse height and time measuring circuitry can be maintained with the help of a laser based calibration system, which will complement the absolute energy calibration system (radioactive sources). This will consist of a gain-stabilized nitrogen laser with photodiode feedback, a motor-driven attenuator intensity selector, Rayleigh diffuser/fiber selector box, quartz UV fiber delivery system, and diffuser couplers to the front and back ends of each calorimeter segment, integrated into the coupling system for the electro-optic readout. By selecting front or back fibers, the calorimeter optical transmission and the photodetector gains can be independently and relatively normalized to 1-2%.

In later stages of the subsystem R&D we may propose to:

a) fully integrate the calibration system into the hermetic design of the calorimeter system,

b) investigate more advanced and complete calibration equipment, in particular using compact accelerator technology to develop calibration sources with radiation, energy, temporal, and system-integrated properties uniquely suited for a very large calorimeter in the SSC detector environment.

1.7 ENGINEERING DESIGN AND COST OPTIMIZATION

The past few years have witnessed impressive development in scintillating calorimeter technology. Most of the R&D effort has been limited, however, to generic studies of the technology itself or to relatively small prototypes with simple Cartesian geometry. Our effort to design a complete calorimeter will address issues of construction, performance, calibration, read-out and triggering. The engineering aspects of this design will include mechanical support, construction schedule, development of mass production techniques, prototype construction, and a cost estimate of a realistic calorimeter of the SSC.

This work will be coordinated with a detailed Monte Carlo calculation of the effect of the support structure design on electron hadron and missing transverse energy resolution and acceptance. Emphasis will be placed on arriving at a design which minimizes adverse effects on the calorimeter performance. The relative simplicity of the scintillator based calorimeter will enable most of the design studies to be done using in-house expertise. Conceptual engineering design work will be carried out at Boston University and at Fermilab. This design will include a mechanical support system, assembly and disassembly procedures, and cable routing for the detectors (tracker, vertex chamber, pre-radiator) located within the cavity of the calorimeter.

Boston University's CAD /CAE system fully supports the commercial structural analysis, finite element codes NASTRAN and PATRAN developed for NASA. They will be heavily utilized to ensure the mechanical robustness of all calorimeter module designs. Preliminary stress and strain analysis has already begun for each of our three kinds of calorimeter modules and for both projective and Cartesian geometries. 4shows a composite of a CAD/CAE structural study of a barrel design for a lead/fiber calorimeter. The deflection and stress analysis for a vertical tower at $\eta = 0$ in this configuration is shown in Figure XII.

Fermilab's analytical tools include ANSYS and I-DEAS. Preliminary design of a complete laminated calorimeter, including support structure and magnetic field calculations has been completed. This initial work (see Fig. 6) is discussed in detail in Appendix A.6. The two in-house design teams will complete the conceptual engineering in the first year. The work can be undertaken largely independently of detailed optimization of each technology since the design of the overall calorimeter support structure is similar for all cases. As part of the engineering design, we want to develop a realistic construction schedule and a cost estimate of a complete calorimeter for the SSC. Manufacturing and assembly

procedures must be studied thoroughly so that mass production techniques can exploit the economics of scale. We will collaborate with industry to optimize our manufacturing and will rely on them to perfect the final detailed design work on the overall structural support for the calorimeter. Draper Laboratory has indicated a strong interest in participation, and has sent engineers to several of our collaboration meetings. Discussions have also started with Westinghouse.

1.8. Physics Simulations

We see a great need for detailed physics simulation studies to identify and specify the important calorimeter parameters. We see these as complementary to the studies at Snowmass and Berkeley workshops that identified likely signatures of new physics and evaluated analysis schemes.[5]

Since the calorimeter is the most expensive part of an SSC detector, one must not overdesign its specifications. In addition, it is often the case that improving the performance of one property of the calorimeter will result in degradation of other properties. An example of this is compensation: calorimeters with e/h=1 often have worse EM resolution than do calorimeters with e/h>1. The relative importance of each calorimeter parameter with respect to signal-to-background ratios for different physics processes must be known, so intelligent decisions about tradeoffs can be made. Properties like segmentation and time resolution must be chosen so that the signal is not swamped by the overlapping background events.

The signatures of new physics have been extensively explored at the Snowmass and Berkeley workshops. In these studies, signal to background issues were studied. However, in general, the studies were in the context of a fixed detector design. The possibilities of improving signal-to-background or of simplifying detector design by modifying the calorimeter design were not considered. A notable exception was a study done by one of the authors that considered in detail detector dependent contributions to the Higgs signature[6].

We plan on performing similar but more complete analyses of important calorimeter properties for a large set of possible new physics. We have at our disposal a complete set of analysis tools and simulation packages developed and used by the CDF collaboration. When appropriate we will use a calorimeter program developed for CDF by one of the authors (QFL. ref.) This program will allow us to study parameters such as EM and hadron segmentation, EM and Hadron compartment energy resolutions and constant terms. e/h, η coverage, calorimeter thickness, and effects of the central magnetic field and cracks in the coverage, and how choices of these parameters affect signal-to-background and triggering for processes such as Higgs production, supersymmetry, heavy top, tau

identification, and other interesting physics. We will collate and distribute the results of our studies in mid to late 1990.

Members of our group have extensive experience in simulation studies for 4π hadron collider experiments. We believe this experience will prove invaluable in this effort. We note that the interest in these studies is not limited to scintillator calorimetry alone, but spans all calorimetric techniques under consideration for SSC detectors.

1.9. Liquid Scintillator for Small Angle Calorimetry

It has been recognized that the radiation environment at small angles (below η=3) poses a challenge for all known calorimeter technologies. Use of a liquid scintillator offers a hope for an energy measurement in this difficult region of phase space. This active medium is very attractive because of the regeneration/replacement capability. Should the liquid scintillator lose light yield due to radiation damage or contamination, it can be circulated through the calorimeter and either rejuvenated or if necessary, replaced.

We propose to design a calorimeter with thin channels within the absorber (lead is the probable choice). The walls of these channels will be coated with a low refractive index material to ensure good light transmission. Our goal is to design, build and test a small electromagnetic module to demonstrate feasibility of such an approach. We expect to develop construction techniques making it possible to reconcile all necessary functions: good optical coupling, stability, liquid hermeticity, possibility of easy filling/venting and calibration.

1.10. PRE-RADIATOR

A finely segmented imaging preradiator can track the development of electromagnetic showers in the first few radiation lengths. Pulse-height measurements in the pre-radiator can help separate electrons from hadrons and, with good position resoltion, direct γ's can be separated from π^o's. To perform this task the preradiator needs to be finely segmented both transversely and longitudinally.

The Pre-radiator is therefore an important asset for the discovery of new physics where electrons or photons are produced. For example a finely segmented preradiator could eliminate most of the background in the search for the Higgs via its decay into two γ's.

Memebers of the collaboration from Rockefeller and Yale have been working on preradiators for the SSC for the past two years. They are currently building an imaging preradiator with 9000 fibers read out with image-intensifiers. This prototype will be tested this winter at FNAL.

Our program is to study study the performance of preradiators at the SSC and to develop the necessary technology for their implimentation. We will study their performance with Monte Carlo simulations and by testing our prototype preradiator in conjuction with the calorimeters that we will build. In this way we can study their mutual compatibility. The principal technical problem of installing a preradiator at the SSC is the individual readout of the fibers at rates compatible with the SSC bunch crossings. In Appendix E we describe in detail a possible solution to this problem that we would like to pursue. Our idea is to design and build an image-tube capable of working in a magnetic field with a high quantum efficiency photo-cathode and a pixel detector installed inside it to detect the photo-electrons with a good position resolution.

Since the design of the pre-radiator is strongly correlated with the design of the calorimeter, we want to pursue both these developments within this collaboration.

1.11. Radiation Hardness Studies

Several R&D studies over the past few years have revealed that large doses of radiation result in the degradation of the transmission of light in the bulk material due to the development of color centers. This effect depends strongly on the wavelength: short wavelengths are affected first. It has been shown that most of the scintillators exhibit an annealing phenomenon, greatly reducing the radiation damage after a few days. The rate of this effect can be dramatically increased by the presence of oxygen. Besides its effect on the attenuation, radiation affects the technical light output of the scintillator. This is probably due to the increased optical absorption of the base material in the absorption bands of the primary and/or secondary dyes, thus reducing the amount of light available for the final emission. Studies of rate dependent effects and of any cumulative damage (not subject to annealing) are of great importance.

We propose to carry out radiation damage studies along several lines:

a) testing existing plastic scintillators in the environment and geometry similar to the SSC conditions (Florida,Illinois)

b) mechanisms of the radiation damage, and their dependence on the material composition and properties, for example molecular weight

c) development of new base materials and/or new dopants (here studies of 3-hydroxyflavone and its derivatives look very promising).

d) environment dependence of the radiation damage.

The University of Tsukuba group plans to carry out a systematic study of the radiation damage and annealing processes and their dependence on the environment (both in the irradiation and in the annealing stage). University of Illinois, U. of Florida and Florida State will construct several electromagnetic test modules and expose them to an intense electron beam at U. of Illinois (see Fig. 7 for preliminary results). In addition we plan, to investigate the damage, as a function of depth in the calorimeter, in a geometry resembling the final setup. Other, more basic lines of research require dedicated facilities and sophisticated chemistry laboratories. MEMBers of Fermilab group have been investigating the physics of the scintillation process in polystyrene based scintillator. Two families of intra-molecular proton transfer compounds, 3-HF and HBT, have been studied in detail as possible dopants. Studies of radiation damage effects have addressed both the stability of the base polymer and of the dopants. The dependence of the radiation effects on the polymer molecular weight has been addressed too. All of the above studies will be vigorously pursued in this program. Similar work is also being carried out at Sandia Laboratory, Bicron and Kyowa Gas. We plan to collaborate with them on the formulation of the R&D program, and on testing of the new materials they develop. As an example we cite a new, multistep scintillator doped with Y7 and new, R13 dyes, which was developed by Kyowa Gas in collaboration with our collaborators at the University of Tsukuba. The long wavelength of its light by Kyowa (see fig. 8 is likely to ensure good radiation resistance. Similar scintillator, using 3-HF and Rubrene was developed at Fermilab , see fig. 9.

1.12. TEST BEAM REQUIREMENTS

Test beam studies form a vital and integral part of our proposed R & D program. We require particle beams to examine and optimize uniformity of response, linearity and resolution of the EM prototypes: to establish e/π separation capabilities of the monolithic design, for compensation studies and in-situ testing of read-out electronics. Our test beam requirements are presented in the following table:

TEST BEAM REQIREMENTS						
Test Prototype	Particle	Energy (GeV)	Intensity /sec	Days	Location	Date
EM Prototypes	e	< 10	10^3	5	FNAL	Summer 90
	π	< 10	10^3	5	FNAL	Summer 90
	e	> 100	10^7	5	FNAL	Summer 90
	π	> 100	10^7	5	FNAL	Summer 90
Hadron Prototypes	e	> 100	10^7	5	FNAL	Summer 90
	π	> 100	10^7	5	FNAL	Summer 90
Compensation	e	> 100	10^5	5	CERN	summer 91
	π	> 100	10^5	5	CERN	summer 91

2. BUDGET AND MILESTONES

2.1. BUDGET

We expect that the proposed R&D program will be carried out over the next three years. We have made a detailed evaluation of resources needed for a calendar year 1990. Directions of the R&D in the subsequent years depend on the results of the first phase, therefore it is not possible to make a detailed cost estimate.In 1991 we expect that emphasis will change in the direction of closer contact with industry and engineering companies to address of large scale manufacturing techniques, detailed cost estimates and production schedules.

EQUIPMENT REQUEST BY PROJECT ($K)			
PROJECT	TOTAL	INSTITUTIONS	PROJECT LEADER
Laminated Calorimeter Prototype	262.	Boston,FNAL*,MSU,Purdue,Rochester,UCSD	Para
Tile Calorimeter Prototype	68.	FNAL*,Michigan,Purdue,Rochester	Freeman
2-Stage/Electromagnetic Prototypes	49.	Boston*,FNAL,UCSD	Worstell
Specialized Tooling	118.	FNAL*	Mishina
Engineering Design	150.	Boston*,FNAL	Sulak
Fiber/PM Testing Equipment	40.	UCSD*	Paar
Calibration System	57.	Purdue*, Fairfield/Boston	Barnes
Test Beam	30.	Boston,FNAL*,MSU,Rochester,TAMU	Dye
Trigger/Front End and DAQ Electronics	110.	Boston,FNAL*,Rockefeller,Washington	Foster
Forward Scintillating Liquid Calorimetry	60.	Fairfield, TAMU*	Webb
Preradiator	50.	Rockefeller*,Yale	Rusack
Radiation Hardness/ Materials	75.	FNAL*,Florida,Illinois,Tsukuba	Bross
TOTAL EQUIPMENT REQUEST	1069.		

* Lead Institution

DIVISION OF REQUESTED FUNDS BY INSTITUTION

BUDGET BY INSTITUTION ($K)					
Institution	Operations	PDs (0.5 FTE)	Equipment	Task	Principal Investigator
Boston	189.	1	150.	Engineering	Sulak
		1	49.	EM Calorimeter	Worstell
Fairfield	24.		17.	Optical Calibration	Winn
FNAL	139.	1	262.	Laminated Hadron Calorimeter	Para
		1	53.	Tile Calorimeter	Freeman
		1	100.	Electronics	Foster
			118.	Specialized Tooling	Mishina
		1	30.	Test Beam	
Florida	20.			Radiation Hardness	Majewski
Florida State	20.			Radiation Hardness	Johnson
Illinois	31.		75.	Radiation Hardness	Hertzog
Michigan	10.		15.	Tile Calorimeter	Gustafson
MSU	40.	1		Hadron Calorimeter/Test Beam	Huston
Purdue	40.	1	40.	Source Calibration	Barnes
Rochester	72.	1		Hadron Calorimeter/Test Beam	Bodek
Rockefeller	52.	1	40.	Preradiator	Rusack
TAMU	79.	1	60.	Liquid Scintillator Calorimeter	Webb
UCSD	79.	1	40.	PMT/Fiber Test	Paar
Washington	65.	1	10.	Data Acquisition	Young
Yale	51.	1	10.	Preradiator	Cushman
TOTAL	911.	13	1069.		

2.2 MILESTONES AND SCHEDULE

Given a tight schedule for the R & D efforts for the SSC detectors it is of utmost importance to organize the work in the most efficient manner. This necessitates a prompt commencement of studies and prototype development so that we can rapidly converge on an optimized design. We propose the following timetable for the R & D efforts:

November 1989 - July 1990:

Laminated Calorimeter: Construct a 6 x 6 tower single depth laminated module. Beam tests of electron/pion separation capabilities.

Tile Calorimeter: Construct an electromagnetic prototype with tiles and wavelength-shifting fiber readout. Source, cosmic ray, and beam tests of resolution and uniformity.

Electromagnetic Front-End Prototypes: Construct and test cast, grooved lead, and liquid designs. Test beam studies of resolution and uniformity.

Conceptual Engineering Design: Preliminary structural design and analysis of support structures for large calorimeter and its components. Manufacturing engineering efforts for construction of prototypes to anticipate eventual mass production.

Calibration System: Design, construction and test of radioactive source and laser/optical calibration systems for prototype calorimeter beam tests.

Liquid Scintillator Forward Calorimeter: Design and construction of electromagnetic prototype for beam tests.

Preradiator: Design and construction of first-pass preradiator for use with laminated hadron calorimeter in test beam e/pi separation measurements.

Trigger/Front End and Data Acquisition Electronics: Preliminary design and specification of system requirements. Support of specialized electronics needs for beam tests.

Radiation hardness/materials: Preparation of radiation-hard plastics for irradiation at Illinois cyclotron and with a high-intensity Co^{60} source at Boston University. Long term exposure to mimic SSC conditions and evaluate self-healing of plastics.

July 1990 - January 1991:

Laminated Calorimeter: Evaluation of test beam results, design optimization. Upgrade of prototype to fully contain a hadronic shower (if laminated design is chosen as the most promising). Choice of hadronic detector design.

Tile Calorimeter: Evaluation of test beam results, design optimization. Test beam studies of resolution, linearity, and compensation in composite media through construction of a large "removeable tile" test device.

Electromagnetic Prototypes: Evaluation of test beam results, design optimization. Choice of most promising alternative, synthesis of techniques. Assessment of feasibility of 2-stage design. Radiation-hard liquid work continues for forward region.

Engineering Design: Engineering input into calorimeter design decision. Structural design and analysis, manufacturing engineering work on chosen hadronic detector design.

Calibration System: Evaluation of calibration system performance in beam tests, optimization of design for incorporation in hadron calorimeter.

Liquid Scintillator Forward Calorimeter: Design and development of full-size liquid hadronic forward calorimeter.

Preradiator: Design and development of preradiator for chosen calorimeter.

Trigger/Front End and DAQ Electronics: Design and development of triggering and data acquisition system for chosen calorimeter design.

Radiation hardness/materials: Assessment of radiation-hard materials for incorporation in chosen calorimeter design.

January 1991 - January 1992:

Hadron Calorimeter: Construct full-scale prototype and conduct detailed studies of compensation effects. Address issues resulting from earlier test beam studies. Address issues of large scale production techniques, with realistic cost estimate and production schedule.

Engineering Design: Full engineering design of hadron calorimeter, within the scope of a model detector. This will include complete design of mechanical support, construction schedule, development of mass production techniques, and cost estimate. Collaboration with industry (Draper Labs, Westinghouse, Martin-Marietta or equivalent) in complete design.

Calibration System: Design and development of mass-production quality control and mass-calibration techniques for full detector.

Liquid Scintillator Forward Calorimeter: Integration of liquid scintillator forward calorimeter (presuming this is chosen for forward region) into full calorimeter and detector design.

Preradiator: Integration of preradiator into full calorimeter design, with mass production techniques and cost estimate.

Trigger/Front End and DAQ Electronics: Final design and implementation of prototypes for system triggering and data acquisition electronics systems.

Radiation hardness/materials: Final evaluation and selection of radiation hard materials for central and forward calorimeter regions.

APPENDIX

A. TECHNICAL DETAILS OF PROPOSED CALORIMETERS

A.1. OVERVIEW

We are exploring in parallel three possible choices for scintillating calorimeter technologies: scintillating fiber with longitudinal segmentation generated by projective geometry; scintillating fiber with separate EM and hadron compartments: and scintillating tile with wavelength shifter fiber readout. Our plan is to build small but definitive prototypes based on the three technologies, and then expose them to test beams. The information gained in constructing and testing the prototypes will allow us to settle on a single technology for the fully engineered design. We will base our choice on ease of construction, cost, performance in the test beam, and results from structural analysis studies.

A.2. IMPLICATIONS OF THE MAGNETIC FLUX RETURN

When the calorimeter is placed outside of the magnet it is necessary that the solenoid is as thin as possible to minimize the effect on the electron identification and the energy measurement. However the solenoid must be able to sustain the compression forces caused by the magnetic flux lines crossing the current sheet. These forces are minimized when the distance between the solenoid and the flux return is minimal. This can be achieved by extending the solenoid beyond the endcap calorimeter and contending with the associated problems of read-out and combining data of the central and end-cap calorimeters. Alternatively, if the flux can be returned through the calorimeter itself then these problems can be avoided and it becomes possible to construct fully hermetic detector. Cable path for the inner tracker can be located at 90 degrees where the particle density per unit length is at minimum.

Combining the flux return and calorimetric functions has some disadvantages. For example, the magnetic field is known to change (increase) the light output of the scintillator via the Zeeman effect. This change, on the order of few percent, will require calibration. Another consequence of such a solution is a requirement to have a complete calorimeter in place for field mapping of the solenoid. While the decision regarding the geometry of the flux return must be left to the proponents of the detector, we feel it is important to provide for the possibility of such a solution. We note that in the case of a scintillator-based calorimeter a integrated flux return has the additional advantage of conveniently placing all read-out elements outside the magnetic field volume. Stray field outside the calorimeter can be easily shielded with soft iron/mu metal shields.

Another advantage of a calorimeter with a significant content of iron is that it can be used as a support for the coil of a solenoid with all loads transferred to the outside support structure. This will avoid problems with hermeticity usually resulting from requirements of the magnet support. The detector will be fairly compact and will have practically no cracks.

A.3. LAMINATED, IRON-LEAD, SINGLE DEPTH SEGMENT FIBER CALORIMETER

Scintillating fiber based calorimetry is by now an established technique. Fiber calorimeters are in use in Fermilab experiments E774 and E687, and the JETSET experiment at LEAR; the calorimeter for this latter experiment was constructed at University of Illinois. Also, the R&D efforts of SPACAL collaboration at CERN and Takasaki et al. at KEK have produced a number of modules which have been tested with beam. The most attractive features offered by this technology are, in our opinion, the intrinsic speed of the scintillator and the excellent hermeticity which can be obtained in a full calorimeter. However, application of this technique to a large scale 4π detector does pose several challenges. These include: the development of sound construction techniques, minimization of the effects of non-uniformities leading to a constant term in the fractional energy resolution and, demonstration of the electron/pion separation capabilities of a calorimeter with a limited depth segmentation.

The R&D efforts mentioned above are addressing some of these issues. However, many of the proposed solutions are easily applicable to only small-scale prototypes, or optimize one parameter at the expense of others worsening the overall performance for SSC detectors. We propose to investigate the performance of a calorimeter built in a simple and manageable manner which can be incorporated in an SSC detector with some confidence. Construction techniques will use present-day technologies and no heroic efforts will be made to address issues which might have only marginal gains. While it is quite likely that the outcome of some of the R&D projects will make it possible to construct a far better detector in the future, it is important to establish what today's capabilities are.

Construction techniques. Segmentation. Projective geometry.

The calorimeter is constructed from 2 mm iron plates interspersed with 2.5 mm lead plates. U-shaped grooves, 1.05 mm deep, on both sides of the lead plate are filled with 1mm diameter scintillating fibers (see Fig. 10). Fiber-to-fiber distance is 2.5 mm. The effective composition of the calorimeter is therefore : Fe - 40%, fibers -17.8%, Pb - 42.2%. The iron and lead plates are oriented such that all plates are (to a good approximation) radial in both the barrel and the endcap. Therefore, in a cylindrical coordinate system the produced particles enter the calorimeter nearly parallel to the plane of the laminations (the Θ direction).

To construct the calorimeter modules grooved lead strips are bonded to iron plates. The specific bonding technique which will be used is being investigated. The simplest technique would bond using a glue, such as Bicron 650. However, the radiation resistance of the glue and its influence on the compensation mechanism are a concern. It is very important to rule out changes to the glue after irradiation that could either cause damage to the fibers or weaken the mechanical strength of the laminations. Alternatives which avoid glue altogether, such as brazing or low temperature soldering are also being investigated.

Projective towers require tower size to grow with depth. In the theta direction this is realized by appropriately shaping the lead strips; the strip width increasing with depth in the calorimeter. New grooves and fibers are started on each side of the strip to maintain a uniform sampling fraction as shown in Fig. 11 . Projective geometry in phi direction (perpendicular to the laminations) is realized by adding

new iron/lead plates on the sides of the tower. These plates are progressively shorter and will be tapered at the front edge to form the wedge shape of the tower as shown in Fig. 12 . In the endcap region the new plates will change shape and will have a tapered edge in both directions to form the projective towers.

An effective depth segmentation is realized by grouping onto one photomultiplier tube all fibers in a given tower which run the full length of the calorimeter while those fibers which start at depth are read out by second tube. This effective depth segmentation will be important in our later discussion of the e//*pi* separation characteristics of this design. An intermediate stage of light mixing between the end of the fibers and the phototube face will also be necessary to avoid problems with the non-uniform response of the photocathode.

Physical segmentation of the calorimeter and logical segmentation (i.e. tower structure) are decoupled. The iron plates extend over many lead strips and, consequently, cover many towers in eta (see Fig. 11). Therefore, the number of independent mechanical modules can be smaller than the number of towers by at least an order of magnitude, thus reducing the potential for problems due to the accumulation of tolerances.

Electron identification and triggering.

The identification and energy measurement of electrons are crucial functions of the calorimeter. The electron identification problem can be defined only with some specific physics processes in mind. In a first approximation the physics separate into a problem of electron identification for isolated electrons, and electrons in jets or near jets. The dominant background for an isolated electron is the unusual fragmentation of a QCD jet into, primarily, a single charged hadron. To set the scale of rejection needed we note that at a given Pt the cross section for jet production typically exceeds that for electron production by about a factor of 10^5 and studies of jet fragmentation [ ] show that less than 1% of jets fragment into a charged particle carrying most of the jet energy. Therefore, it should be sufficient to provide a rejection factor against charged hadrons of 10^3 to reduce the background to the electron signal level. An isolation cut provides a further discrimination against charged hadrons by rejecting events with any residual jet energy in nearby towers. For electrons in or near hadronic jets much less stringent isolation cuts are possible. We expect that the fine lateral segmentation of the proposed calorimeter will be essential here both in the reconstructed data and at the trigger level.

Electron/pion separation is traditionally achieved via depth segmentation: electrons deposit all of their energy in the front section of the calorimeter, whereas hadronic showers typically extend well into the rear section. Although the proposed calorimeter has no explicit depth segmentation, an effective depth segmentation is provided by projective geometry. Given an aspect ratio of 2, typically, 3/4 of fibers start at depth in the calorimeter and are read out by a separate photomultiplier. These are called the 'side' fibers as they surround the 'central' core of fibers in a tower. The first level of electron/pion discrimination is achieved by a combination of the fine lateral segmentation throughout the calorimeter and the effective depth segmentation resulting from the projective geometry. We rely on the fact that hadron showers will typically spread over a large number of towers and deposit a large fraction of their energy in the 'side' fibers. The results of a monte carlo simulation of 100 GeV electromagnetic and hadronic showers using

GEISHA are given in Fig. 13 . This study indicates that the two criteria can provide a rejection factor of 10^{-3} at 100 GeV. The addition of a preshower detector (now a standard in all calorimeter configurations) should result in another factor of 10 rejection, uncorrelated with the previous cuts. Our electron trigger would require that in a cluster of four towers a large energy is deposited in the 'central' fibers and little energy is deposited in the 'side' fibers. The expected electron/pion rejection at the lowest trigger level is 10^{-2}, as shown in Fig 13 . Matching a track to a shower using a fast track processor at the second level trigger should provide another factor of 10. The preshower information can be used in the higher level trigger, if needed.

Resolution, compensation. Uniformity of response.

The calorimeter will be used to measure the energy of electrons and hadronic jets. The expected resolution is quite different for these two cases. Electromagnetic showers are confined to a very small volume, few mm across and some 30 cm long. Sampling fluctuations will contribute a term of the order of $\frac{20\%}{\sqrt{E}}$ to the resolution. Measurement of the light yield for a bundle of scintillating fibers exposed to Bi 207 source gives an estimate of 1000 - 1400 photoelectrons per GeV of energy deposited in the calorimeter (using the EGS predicted sampling fraction of 2.3%). Thus photoelectron statistics are not expected to contribute to the resolution, even after the unavoidable losses due to the light attenuation and/or a shift to longer wavelengths.

Due to the small lateral dimensions of an electromagnetic shower the majority of the light is generated in only a few fibers. Therefore, fiber-to-fiber variations in the response (due to variations in the fiber dimensions, light attenuation, optical couplings, etc..) are important contributions to the resolution. Even with efforts to spread the shower over a reasonable number of fibers (by tilting) in order to keep the constant term in the resolution below 1.5 % it is necessary to control the fiber-to-fiber variations to below 5%.

Another consequence of the small size for the core of an electromagnetic shower (when comparable to the fiber lattice spacing) is a substantial variation of the response depending on the impact point. This leads in turn to long tails in the pulse height distribution, and to a substantial constant term in the resolution, see Fig. 14 . These problems are greatly reduced when calorimeter is tilted with respect to the incident particle's direction, causing the electromagnetic shower to cross media boundaries more frequently and equalizing the response. In our particular geometry to reduce the constant term to 1-1.5% an effective tilt on the order of 10 degrees is needed. This tilt is most effective if it is in the phi direction; a tilt in the theta direction will not cause showers to average over the iron-lead structure. The required tilt angle of 10 degrees is very large compared to the typical tower size of 1.7 degrees, therefore tilting of the entire tower is not an adequate solution. Therefore, we propose to bend the iron plates as shown in Fig. 15 . This solution presents large angle to the incoming photon/electron over the first 10 Xo, while preserving the geometrical properties of the projective towers.

Another sort of uniformity problem will arise at the tower boundaries. This will be especially true in the end-cap region where tower dimensions grow with radius. We propose to build several short electromagnetic modules to verify that

over the face of the proposed calorimeter an adequate uniformity in response (hence a small constant term in the resolution) is achieved, and to investigate the transition regions at the tower boundaries. It is usually assumed that the electromagnetic calorimeters are 'linear', i.e., the amount of charged produced produced by the PM is strictly proportional to the incoming energy. Considering the large dynamic range which an SSC calorimeter must cover we feel that this conjecture should also be tested experimentally.

Energy resolution for hadrons is usually discussed in connection with so called 'compensation'[8]. It has been realized that large fraction of the energy of hadron induced showers is deposited in a form of low energy neutrons. All of these neutrons end up in the scintillator, irrespectively of the sampling fraction. It is possible, therefore, to choose the sampling fraction in such a way, that the response of the calorimeter to electrons (which is proportional to the sampling fraction) and to hadrons (which contains a piece independent of the sampling fraction) to be equal (compensation).

Using results of ref.[8] one may expect that iron-lead- scintillator calorimeter with the relative volumes of 5:5:2 should have e/h ratio very close to 1. The chief interest in compensation is to optimize the energy resolution for high pt jets by removing a contribution due to the fluctuation in the electromagnetic component. Compensation is usually achieved by compromising the energy resolution of electrons (by reducing the sampling fraction). At the SSC energies, where the constant term limits the resolution, the reduction in signal does not seriously affect the resolution. In the case of longitudinal fibers an additional complication arises, due to different attenuation of the signal of the electromagnetic and hadronic components of the jet. It reduces the electromagnetic signal, thus permitting a better sampling fraction for the calorimeter. The expected attenuation length of the fiber depends on the details of the construction (fiber type, diameter, filters, dopants, read-out elements, etc..). Fig. 16 shows how the e/h ratio changes as a function of the attenuation length. We hope to achieve attenuation lengths on the order of 4 - 5 meters by shifting the scintillation light to longer wavelengths where longer attenuation lengths are possible. Detailed studies of the attenuation mechanism are presently being conducted by the Particle Detector Group at Fermilab. We hope to avoid mirroring the far end of the fibers as it would introduce another contribution to electron resolution.

With our sampling fraction we expect the energy resolution of the order of $\frac{50\%}{\sqrt{E}}$ for single hadrons. Energy resolution for jets should be comparable. The constant term in the energy resolution will probable come chiefly from the fluctuations in the longitudinal shower development coupled with the attenuation of light along the fiber. Fig. 17 shows the expected contribution to the resolution from this effect as a function of the attenuation length in the fiber. For attenuation lengths in the range of 4-5 meters a constant term on the order of 4% must be expected.

List of the R&D projects

Most of our expectations for this single-depth laminated calorimeter need experimental confirmation. Three stages of tests are planned to fully explore the abilities of this calorimeter design:

a) four, short, electromagnetic modules will be constructed to test the feasi-

bility of bending the iron and lead plates at the front of a module. Tests of the uniformity of response across the face and across tower boundaries will determine the level of the constant term for electromagnetic showers. The estimated costs total $10000.

b) a full length (2m) module consisting of a 6x6 matrix of 36 projective towers will be constructed. The towers shapes will be square, 6 cm on a side at the front and expanding to 12 cm on a side at the rear. This prototype will test the feasibility of the construction on a larger scale verifying the expected mechanical strength based on calculations. The primary goal of the beam tests will be to verify the electron/pion separation capabilities of a single depth segment calorimeter. The estimated costs total $240000.

c) additional modules, enlarging the prototype of b) to the transverse size necessary to fully contain hadronic showers, will be constructed. With this large calorimeter we plan to address the issues of the energy resolution for single hadron induced showers as compared to jet showers by using 'poor man jets' generated by placing a thin absorber in front of the calorimeter. The tests of 'compensation' will measure the response to electrons and hadrons for an inhomogeneous absorber medium and its dependence (linearity) on the energy. The time structure of the compensating signal and therefore the effects of an integration gate will also be investigated. The estimated costs total $250000

Negative results of these tests at any stage may terminate this path of R&D.

A.4. Fiber Calorimeter with Two Depths

If the longitudinal segmentation can be achieved without jeopardizing hermeticity. it potentially has some advantages over single segment design. The e.m. segment is only 3careful design to fulfil the more stringent requirements such as the energy resolution and uniformity for electron measurement. and also because it is exposed to the incident particles directly it has to be highly hermetic. The hadronic segment. on the contrary. composes more than 95the major factor in the total cost. Since the energy resolution requirement is much looser and the lateral shower profile is much larger than that of electromagnetic shower, design can be much less stringent. Also because it is hidden behind the e.m. segment, minor crack or irregularity of the fiber pattern does not affect the performance. Thus by dividing the projective tower into an e.m. and a hadronic segment, one can optimize the design of the calorimeter for e.m. signal and hadron/jet signals independently.

POSSIBLE STRUCTURE

A possible structure of the calorimeter is shown in Fig. 18 schematically. E.m. segment is a block of lead with 1.2 mm diam. scintillation fibers embedded longitudinally with the lead to fiber volume ratio of 4 to 1. The fibers are individually read out by a clear fiber which is brought to a phototube at the rear end of the hadronic segment through a gap on the side of the hadronic tower. In order to minimize the gap, the cross section of the fiber bundle has to be compressed significantly from the cross section of the scintillation fiber . An idea developed by one of our collaborators (G.W.F) is illustarted in Fig. 19. A wave-length-shifter doped core is embedded through the axis of a scintillation fiber and only the cross section of the wave-length-shifter core will be spliced to a clear fiber for readout, thus gaining a sizable reduction in the cross section. The core must have a low refractive index clad around it and the core must be also scintillating. A Monte Carlo calculation showed the efficiency of absorbing the original scintillation light into the wave-shifter doped core is about 1/4 to 1/2 only weakly dependin g on the ratio of the cross section of the core to the outer scintillating part down to 1/40. Therefore one can squeeze the readout fiber cross section substantially without being affected by Liouville's theorem directly. The outer surface has to be reflective and has to be polygonal instead of round shape in order to reflect back the light efficiently into the core. An optimal choice considering the shape of the hole in the lead and also matching with the readout fiber is hexagonal or octagonal profile. Examples of the ray traces are shown in Fig. 20The Mote Carlo calculation result was confirmed by a test in which four 1 mm wave shifter doped fibers were inserted into a block of scintillator, 1 cm x 1cm x 5 cm, irradiated by a Bi-207, 1.06 MeV beta source. Thus with a cross section reduction factor of 1/30, we observed a half of the light we observed directly from a bundle of scintillation fibers. Several hundred meters of such fiber has been drawn as a sample. Fig. 21is a photograph of the magnified cross section of the sample fiber. The outer shape of the fiber is hexagonal and the wave shifter-doped core is round . The outer scintillator and the inner core are polystyrene and are both cladded by PMMA. The centering of the core looks excellent. We are in the process of measuring the properties of this fiber, light yield and the transmission. The process to draw such fibers is not difficult and therefore the price will not be high. In the final design, possible choices of the

parameters are 1.2 mm as the outer diameter of the scintillator and 0.4 mm as the core diameter. The clear readout fiber must be slightly oversized and will be about 0.5 mm to avoid alignment problems . As a result the reduction in the cross section is about 1/6. Therefore at the front face (rear end) of the hadronic segment the read- out fiber bundle subtends 3.5If one asumes 25 rad. length deep e.m. segment whose radiation length is 7 mm. it corresponds to 0.9 int. length (interaction length of lead-fiber is 20.3 cm) and the gap the clear readout fiber craeates behind it will be well smeared for the hadron/jet induced shower. It is also conceivable to guide the fiber bundle through non-projective holes in the hadronic segment. The lateral dimension of the projective tower grows about 10dimension after the first 25 rad. length. It is possible to flare the fiber layout accordingly in order not to have a discontinuity of the fiber density at the tower boundary. Then it is possible to build the e.m. segments into a large lateral block because the tower is defined by the bundling of the readout fiber. Such a fiber layout can be realized by lead casting technique which is not constrained to a parallel geometry. Once the hadronic segment is designed to be independent and hidden by the e.m. segments. the design of the hadronic segment can be relaxed to match the hardon/jet energy resolution. We propose to use 2 mm diam. fibers in the hadronic segment . Maintaining the same lead to fiber ratio (4:1) the total length of the fiber is reduced by a factor of 4 . A preliminary survey indicates the cost of fibers is approximately proportional to the diameter. Therefore we expect a factor of 2 reduction in the cost compared to the 1 mm fiber case. The cost for the readout fibers is about 1/4 compared to the case in which 1mm fibers are used for hadronic segment. Since the number of the phototubes is the same as the single compartment design, the overall cost is slightly less than the single compartment design.

LEAD CASTING TECHNIQUE FOR E.M. SEGMENT Fermilab/KEK group has developed a technique of casting a lead block with holes for the scintillation fibers. The method is to hold hard stainless steel tubings with proper geometry by perforated metal plates while lead is casted. The tubings are etched out afterwards. In this technique only lead matrix is left and there is no need for extremely thin wall tubings nor deburring work to remove sharp edges of the tube ends. After a systematic tests, we have established the conditions for etching such as the type of the agent, concentration, and the temperature so that the process does not take more than a few hours. This method has been used to fabricate sevaral lead blocks already.

FIBER SPLICING An issue vital to the two segment design is how to splice the clear fibers for readout to the core of the scintillation fibers. A technique for collective splicing of fibers developed by the Boston University group seems promising for this purpose. A conceiveble example of this technique is sketched in Fig. 22. About 1 cm thick slice will be cut out from the very end of the e.m. segment lead block as a jig to hold the clear fibers to match the pattern exactly to the fiber pattern in the e.m. segment. The alignment of the jig to the block of the e.m. segment relies on dowel pins at the four corners of the block. These dowel pins are hollowed to allow the fibers to penetrate. In order to make precise fiber by fiber alignment. insert ferules will be made. either out of aluminum or plastic molding, which have a 0.5 mm hole at one end and forming a funnel with a larger, 1.8 mm, hole towards the other end to ease the insertion of the 0.5 mm fibers. Taking into account the tolerances of the holes we expect

perfect alignment. A similar splicing scheme will be applicable to the readout for the hadronic segment. Such splicing is advantageous to the direct coupling of the scintillation fibers to the phototube because delicate work of bundling the fibers and gluing them to the diffuser and then to the phototube can be done on a bench and can be tested before it is mounted onto the calorimeter body. The key issue for this splicing technique is how to control the possible fiber to fiber variation of the light transmitance to better than sevaral per cent. This is one of the most important subjects to be adressed in this R&D. The very first step is to cut the fiber ends precisely. The surface has to be perfectly perpendicular to the axis of the fiber and of mirror quality . Even for the modest prototype module the number of fibers is quite large and it is crucial to minimize the time for cutting enormous number of fibers with such a quality. Based on the experience at Fermilab, we are designing a diamond cutter which can cut fibers in high speed. High quality finish is expected so as to eliminate further polishing process. A fallback scheme for the e.m. segment is fiber by fiber splicing using appropriate ferules as illustrated in Fig. 23. The work can be done on a bench semiautomatically and the fibers can be inserted to the lead block after fiebr by fiber screening. Since we have made similar. in dimensions and tolerances, ferules for other purposes out of metal with automatic machining, we know that the mass production of such pieces out of metal is practical technically and cost-wise. We have also contacted with a plastic molding company and found that the dimensions and the tolerances we require was within their capability. We are in the process of trying both ways for a small quantity for the initial test.

STRUCTURE OF HADRONIC SEGMENT Since the hadronic segment is very long (9.1 int.l.= 1.85 m),the fibers will be put down in a parallel pattern and the projective tower shape is realized by shaping the side of the tower. The absorber material of the hadronic segment is either of lead or lead-iron composit, depending on the choice of detector system design whether the magnetic flux is guided through the barrel calorimeter. If it is lead. the lead to fiber volume ratio is 4:1 and if lead-iron composit is chosen, the ratio is 5:5:2 to fulfill the requirement of e/h compensation. In either case the nuclear interaction length is about 20 cm. In case of lead-iron composite structure, one possible way alternative to what is described in the previous section for the single compartment design is shown schematically in Fig. 24 . About 0.16 mm thick perforated steel sheets are laminated along the depth of the tower. Precise alignment is achieved by sevaral dowel pins. The lamination is welded on the side with or without reinforcement panels. An excellent example of such structure is the collar of the TEVATRON magnet in which precisely punched sheets are laminated into a 21 ft long column and welded seams on the sides hold the entire length. If necessary additional bonding by either of soldering or epoxying will be considered. The lead composition is added by inserting lead tubing and fibers are to be threaded into the center bore of the lead tubing. Thus the fiber pattern and lead iron composition has a perfect symmetry. We have confirmed that lead tubings of the required dimensions and tolerances are within the range of the products in the market. We are fabricating a module of a realistic tower dimensions, 6 cm x 6 cm and 12 cm x 12 cm as the front and rear face, respectively, and 1.8 meter deep, out of commercially available perforated steel sheets. The module will be examined to study the mechanical and magnetic properties, which we expect to be excellent. In case of end plug, there is a magnetic force on the calorimeter of the order of

900 tons in total if the flux is guided to the side. A natural structure to hold the module is to extend the reinforcement panel welded onto the side and hold it with a support structure on the back of the end plug. It should be noted that the magnetic force on the lamination is mainly compressive parallel to the beam axis at any depth and hence there is no delaminating force.

PRERADIATOR

Two segment design explicitly takes advantage of the difference between the radiation length(7mm) and the interaction length(20cm) by examining the tail of the shower to determine whether it is electromagnetic or hadronic. However it has been known that it is not an easy task to achieve an e/pi separation of the order of 1/1000 even with finer longitudinal segmentation. Therefore most likely we need another shallow layer of longitudinal segmentation at the front end of the e.m. segment to augment the e/pi separation capability by measuring the the early development of shower. Another role of the shallow layer is to measure the shower centroid before it is blurred. Such a layer is also useful for single photon measurment. Several conditions can be discussed. a) On the average the energy deposit in the first few radiation length is less than a few smaller at SSC energy domain. Hower there is a large fluctuation and event by event measurement seems to be necessary. Based on the data by CDF, rather a crude energy measurement, 5b) It is desirable that the readout of the pre-radiator is done loaclly so as not to disturb the hermeticity of the main body of the e.m. segment. c) In order to measure the shower centroid to an accuracy of a few mm, scintillation fiber coupled to some type of solid state readout device is an excellent candidate. Possibly such fiber layers have to be placed behind a few radiation length in order to have a reasonable S/N ratio. An optimum design will be pursued through a simulation and by the beam test.

ADVANTAGES OF TWO SEGMENT DESIGN To summarize this chapter, we discuss the possible advantages of two segment design. In principle it adds adjustable parameters while there is no cost increase over the single compartment design beacause of large saving from using 2 mm diam. fibers in the hadronic segment which is 95volume of the calorimeter. 1) Simpler electron triggering and software e/pi separation. The energy deposit in the e.m. segment can be conveniently used for the clean electron trigger and also e/pi separation in the software. Although hadronic shower spreads laterally into a large diameter, there is a relatively small core in which most of the energy is concentrated. For example pure lead (iron) contains 70(60case of 300 GeV protons. Such core right behind the e.m. segment which was hit by an electron like enrgy deposit can be directly examined to distinguish hadrons against electron signals. 2) The fabrication of the e.m. segment is freed from the fabrication technique for the large hadronic segment so that the lead casting technique can be used to fabricate the e.m. segment into an ideal geometry. 3) Complete hermeticity/seamlessness The fibers in the e.m. segment is layed in a flared geometry and as a result the e.m. segment can be built continuously over large lateral area without any physical boundary. The tower boundary is solely defined by the bundling of the readout fibers. As a result the fraction of the crack at the boundary of the fabrication unit for the e.m. segment . if any, is significantly small.The hadronic segment is constructed in a parallel geometry and has tower by tower boundary but is well hidden behind the 0.9 int.l. thick e.m. segment. 4) The channelling effect,

positive or negative can be dealt by the e.m. segment and since the hadronic shower is large in the lateral profile and also because it is hidden behind the e.m. segment most likely the hadronic segment can be rigourously projective. As a possible options besides a simple tilting of the e.m. tower, we are investigating a method to make fibers into helix. Helix has an advantage that the lateral profile of the narow e.m. shower is preserved almost exactly. A loose helix can easily provide the necessary angle(8 degree) at any part of the fiber with respect to the incident particles. 5) Minimal e.m. shower leakage. The e.m. segment is physically isolated from the hadronic section and it is possible to insert a thin lead sheet between them to prevent low energy component of the e.m. shower after 25 X0 to leak into the hadronic segment through the fibers which is essentially an opening of 20of the absorber cross section. Also general mismatching of the patterns of the 1.2 mm fibers in the e.m. segment and 2mm fibers in the hadronic segment makes the leakage problems smaller. 6) Independent e.m. and hadronic signal manipulation. For example it is possible to have a different timing for the e.m. segment in order to minimize the pile up. It should be reminded that 1.8 m long fiber in the hadronic segment has a 9 nsec dispersion of timing even for one end readout. If the front end of the fibers is mirrored in order to obtain a effectively long attenuation length, the situation is worse. In the two segment design electon signals, which is always important and vulnerable from pile up, can be measured cleanly. Also if a perfect e/h compensation is required for jet measurement,the timing for the hadronic segment has to wait 100 nsec to fully accomodate slow neutron components and soft photons from nuclear excitations. Also it allows us to have a different weight for the two segments if the composition turned out to be slightly off from the ideal unity e/h or due to different timing as mentioned above. 7) 2 mm fibers have significantly better attenuation length and hence should give a better longitudinal uniformity for long hadronic module. Additional effect of the attenuation is the fiber to fiber variation of attenuation length which is on the order of 5 avalable fiber and does not seem to be improved drastically in the near future because it is mainly due to the absorption in the fiber material and also absorption at every time of numerous internal total reflection at the clad boundary. Therefore the amount of attenuation must be kept minimal. 8) Clear minimum ionization constraint for muon identification. Two segments individually constrains the minimum ionization signel while single compartment may misidentify low energy pi-zero overlapped with low energy charged tracks as minimum ionizing. 9) Possible lateral profile measurement to help small isolation criterion for electrons or muons by using segmented anode phototube or wire mesh dynode phototube. If one can measure the lateral distribution of the hadronic shower it is possible to require much smaller isolation criteria for electrons or muons thus opening a new capability of finding leptons in jets.

A.5. TILE CALORIMETERS

The technique of scintillating tile with wavelength-shifter optical-fiber readout eliminates many problems found in conventional scintillator-plate/light-guide-readout calorimeters or scintillating-fiber calorimeters. In addition, it possesses advantages that the other techniques do not.

In a conventional scintillator plate calorimeter, the plates are perpendicular to the incident direction of the showers. In this configuration, there is no fine-scale variation in the fraction of scintillator/radiator the shower traverses as the shower impact point is scanned across the calorimeter face. Recall that this is not the case with a fiber calorimeter, where either the shower hits a fiber, or it doesn't. The lack of a sampling-fraction variation causes the conventional scintillator stack calorimeter to give uniform response, with non-uniformity occuring only if the light collection efficiency varies with shower impact point. Unfortunately, scintillator-stack calorimeters do in general suffer positional variation in light collection efficiency. For example,in devices where the scintillator plate is coupled along its edge to a wavelength shifter bar/light guide, there are typically variations of 10% or more. In addition, light guides generate large cracks in the calorimeter coverage. For example, CDF, with light guide readout of the scintillator, has about 10% cracks in the central region. Finally, the conventional coupling scheme forces the scintillation light to travel a relatively long path in the scintillator before it is captured in a light guide. The longer light path causes an increased sensitivity to radiation damage (form degrading the optical attenuation length of the scintillator).

We believe we have identified a technique that avoids the problems of fiber calorimeters or conventional scintillator plate calorimeters: The calorimeter is built of conventional scintillator tiles, and wavelength shifting optical fiber is used to read the tile out. A wavelength shifter fiber is glued into a groove in a scintillator plastic tile. The flexible fiber is then carried to the outside to the phototube.

This idea was developed by Albrow, et al.[9] as a replacement for the UA1 Gondola EM calorimeters. Two prototypes were built and studied in a test beam. Although the test beam studies were promising, the idea was not pursued. The principal reason for this was that at that point in fiber development the (1.5 mm diameter) fibers were not flexible and had to be bent with a large radius of curvature. In addition, the difficulty of manufacturing these (hand-made) fibers did not suggest the use of a large quantity for a large device.

In the UA1 prototype, 0.25 X 20 X 20 cm plates were read out by a single 1.5 mm WLS fiber running along the diagonal. Alternate plates in depth had the fiber running along the opposite diagonal. About 1% of the plate area was covered by the fiber. Test beam studies found the light yield to be 3 photoelectrons/minimum-ionizing particle per plate. Uniformity studies found about a 10% positional variation in response due to a drop in light for scan points far from the fiber. However, a scan was conducted that crossed the fibers along a line where they were separated by 6 cm. In this region, where fibers were close together, the spatial variation was found to be 0.7 % . In our design, we envision fibers even closer spaced, 1 cm apart. Test bench studies of our prototypes, using a UV laser for excitation of the scintillator, show readout uniformity of the order

1% or better. Our measurements are also consistent with measurements made on D0 prototypes [16].

Experiment E814 at Brookhaven has built a hadron calorimeter based on the tile/fiber idea using 2.5 mm thick scintillator plate and 1 cm thick lead plates. The scintillator plates are pie-shaped, 22.5 degrees wide, and with a radius of 60 centimeters. The scintillator plates are read out by a single fiber on the phi edge of the plate, with the side alternating in depth. They achieved a resolution of 0.45/sqrt(E) for pions. The light yield for their device is 4.5 photoelectrons per minimum-ionizing particle per scintillator plate (after the light travels 60 cm along the fiber to the phototube). This corresponds to 250 PE per GeV in their compensating calorimeter.

Finally, D0 is constructing their inner-cryostat detector with this technology.

Advantages of this scheme are:

(*i*) High light yield. The E814 calorimeter has a light yield per GeV approximately 9 times larger than that of the CDF central EM calorimeter which uses a conventional WLS bar/lightguide readout. With our choice of the fraction of scintillator covered by WLS fiber (10%), we anticipate about 500 photo-electrons per GeV for a compensating lead calorimeter.

(*ii*) High uniformity. Expected positional uniformity is better than 1%.

(*iii*) No cracks. Projective cracks can be totally avoided by carrying the WLS fibers to the outside along a non-projective path. In addition, since the fibers have a very small volume, there are only very small non-projective cracks. We estimate that at the back of the hadron calorimeter, only 0.2% of the area is occupied by WLS fibers.

(*iv*) Radiation Hardness. Since the light is collected relatively locally by the fiber, the optical path of the light is short. Radiation damage induced changes in attenuation length are expected to have little effect on the light yield. Monte carlo studies predict only 10% change in light after a degradation of the scintillator bulk attenuation length from 2 meters to 0.5 meters. This corresponds to a radiation dose of more than 10**7 rads.

(*v*) Arbitrary choice of depth segmentation. Since the fibers from all depths of the calorimeter tower are present at the outside, complete information about the depth development of the shower is available. A choice of depth segmentation of 3 EM depths and 2 hadron depths, for example, is feasible.

(*vi*) The ability to have position sensing chambers imbedded in the calorimeters. For example, a strip chamber positioned at EM shower-max can be easily accomodated.

(*vii*) Great mechanical strength. A possible SSC Calorimeter design, sketched below, would have mechanical strength approaching that of solid iron. It would be self-supporting and could also support the solenoid without the need for structural ribs.

(*viii*) Arbitrary choice of mechanical modularity. The mechanical modularity is determined by issues such as crane lifting capacity, and not by tower segmentation requirements, as it is for conventional plates or fiber. This means that the design can be made for fewer mechanically separate mod-

ules. easing installation problems and reducing any problems at module boundaries.

(*ix*) Low cost/Ease of construction. Preliminary investigations suggest that this technology. using scintillator plates rather than fibers. and flat-rolled iron and lead plates. can be substantially less expensive than fiber calorimetry.

Prototyping Efforts to Date

We have built several types of prototypes to explore issues of uniformity and light yield. Scans with a UV laser have confirmed the uniformity seen by UA1 and D0. A UV laser scan is shown in figure 25. The measured uniformity is approximately 1%.

Cosmic ray studies have given estimates of expected light yield. Fig. 26shows a photograph of a stack of 28 tiles used to observe cosmic rays. The light yield for this device is 20 photoelectrons per minimum ionizing particle per centimeter of scintillator plastic traversed. This corresponds to a light yield of about 275 photoelectrons per GeV for a totally compensating lead/scintillator calorimeter. Our conceptual design for this technique has a somewhat larger ratio of wavelength shifter fiber area to total scintillator area. with a projected light yield of 500 photoelectrons per GeV.

We have developed a sophisticated optics monte carlo program to model expected response of tiles. We have verified the program using our own measurements. and those of D0 and UA1. This program allows us to predict light yields and uniformities for different geometries of tiles, as well as model effects like radiation damage of the plastic.

We are researching techniques of mass-production of the tile. Working with Laser Machining. Inc.. Summerset. Wisconsin. and with Laser Services. Westford. Mass.. we are developing techniques to laser-cut the polystyrene tile, and then use the laser to "mill" the groove in the tile. Preliminary trials were successful. Use of a computer controlled laser cutter makes the tile manufacture very inexpensive. approximately $2 per tile.

Structural analyses using ANSYS are in progress for the goal of a conceptual design using this technique.

A Tile SSC calorimeter

As an example of the large scale application of this technology, we are making a conceptual design of a small solenoid SSC detector calorimeter. Our performance goals are those outlined in chapter 1.

In our design. we choose to have a single EM depth compartment. and a single hadron compartment. The barrel calorimeter would be composed of wedges that can be stacked in free-standing arches.(a la CDF). There would be two rings of arches. allowing for splitting the detector at 90 degrees. The number of wedges would be determined by crane capacity. A possible choice is 24 wedges per ring or 48 total. Each wedge would have 8 phi tower segments for the EM compartment, and 4 for the hadron. We will choose lead as the radiator in the EM compartment. For hadron absorber. we will pick equal parts lead and iron.

The detail of a tile is shown in fig 27. The scintillator plastic plate has a groove cut into it in which is placed a wavelength shifting fiber. Tiles are grouped into units to be inserted into the calorimeter wedges, as shown in this figure.

A cross-section of the EM compartment is shown in fig. 28. The mechanical structure is 0.030 inch steel plate, with 0.2 inch lead bars bonded to it. The lead bars are staggered in depth. The resulting structure is mechanically rigid, and provides slots for the insertion of the scintillating plastic tiles. The structure prevents any force from being exerted on the plastic. The readout fibers bend and progress along a serpentine milled slot to the outside.

We envision the hadron compartment built of a lamination of iron and lead plates. The lead plates are again staggered (as in the EM compartment) to provide slots for the scintillator plastic tiles. The lead and iron plates are bolted together, with the bolts going from iron to iron. A possible internal structure is shown in figure 29.

This design is expected to meet to outlined list of calorimeter requirements. In the design, there are no projective cracks. In addition, since the fibers have a very small volume, there is only 0.2% non-projective cracks. Compensation is obtained by the choice of thickness of plastic for the 2 compartments. 2mm thick scintillator in the EM compartment, and 5 mm in the hadron compartment will generate compensation values inside of our design window. Since this design has separated EM and hadron compartments, conventional techniques for E/pi separation can be used. We can be confident that the E/Pi separation goal can be met.

Proposed R&D

The application of tile technology to a 4π calorimeter is a new idea. At the moment, there is not adequate test beam experience with this technique to be able to confidently predict light yield and other properties. We propose to construct an EM calorimeter prototype to evaluate tile calorimeter performance.

Our prototype will be composed of 5mm lead plates, interleaved with 2mm scintillator tiles, with a total depth of 24 radiation lengths. It will be divided into 4 (non-projective) towers to allow for scans across tower boundaries. The estimated size of this device is 20 X 20 X 20 centimeter. Its estimated cost is approximately $10,000.

In addition, we will conduct studies of tile technology. We plan to make special radiation damage studies of tile prototypes to see if there are limitations in this area. We will explore strategies of inexpensive tile manufacture: laser machining, NC milling, and casting. We will investigate tile-to-tile uniformity, and techniques to control it (Laser-trimming the wavelength shifter fiber to a uniform gain with a computer-controlled CO_2 laser and feedback circuit, in a vein similar to laser-trimming resistors) We will also do preliminary structural analyses of tile calorimeters. Results from these studies and from the construction and its test beam analysis of the prototype will allow us to determine if tile calorimetry has a viable future at the SSC.

A.6. Mechanical Support of Detector Components

A model of a possible detector geometry, with module and solenoid support systems, is shown in Fig. 30 . The following calculations and discussion will show the feasibility of the major mechanical features of the model. Conceptual design was made and structural calculations were performed for the laminated calorimeter case, other cases will be very similar.

Structural Analysis Approach

The conceptual phase of a design requires strength calculations which are simple enough to allow consideration of several alternatives in a reasonable amount of time, and accurate enough to identify inadequacies. In this work, hand calculations and small finite element models determine the primary structural behaviour thought to be most important in a practical detector component support system. The specific issues addressed are:

1. Endplug module support ear design
2. Barrel module support ear design.
3. Design of endplug support structure. This support system must resist electromagnetic and weight loads and allow the endplug to be withdrawn from the barrel and solenoid assembly.
4. Design of barrel support structure. This support system must resist electromagnetic and weight loads and allow separation of the barrel halves for access.
5. Support of the solenoid from the barrel module assembly. This support system must resist radial and axial electromagnetic loads and weight loads and allow the separation of the barrel halves.

Calculation of Loads

Module and Solenoid Dead Weight

This can be calculated from a volume averaging of the lead and steel content of a module. This proposal considers lead plates which are 2.5 mm thick (0.098 in.) and steel plates which are 2 mm thick (0.079 in.). The densities of lead and steel are 0.411 lbs/in3 and 0.284 lbs/in3, respectively. The volume averaged density of a module (neglecting the lead removed for slots) is 0.354 lbs/in3.

A cross section of the detector assembly is shown in Fig. 31 . The volumes and weights of each module, obtained from a computer solid model, are listed in Table I.

The dead weight of the solenoid can be approximated by scaling the weight of the CDF solenoid according to the slightly larger radius assumed here. The result is an estimated solenoid weight of 30000 lbs.

The total weight of one-half of the detector (one endplug, six barrel assemblies, and one solenoid) is $4.4*10^6$ lbs, or 2200 tons.

Table I. Detector Component Weights		
Component	Number	Weight
Endplug module A	24 modules	3185 lbs/module
Endplug module B	48 modules	3257 lbs/module
Endplug module C	72 modules	3277 lbs/module
Endplug module D	144 modules	2193 lbs/module
Barrel module A	24 modules	44200 lbs/module
Barrel module B	24 modules	49400 lbs/module
Barrel module C	24 modules	55510 lbs/module
Solenoid	1	30000 lbs

Note: Figures are for one-half of the detector.

Electromagnetic Forces

A two-dimensional axisymmetric finite element model was generated to calculate the axial magnetic forces on the solenoid and the endplug module assembly for a central field of 1.7T. The laminated structure of the modules was approximated by smearing the iron permeability over the module region. The finite element model and flux plot are shown in Fig. 32 . In this analysis, two separate solenoids were assumed, with their dimensions scaled from those of the CDF solenoid at Fermilab[11].

The axial forces are related to coil separation, endplug proximity to the solenoid, and installation of the solenoids with their magnetic centers axially displaced from the magnetic center of the iron. The magnetic analysis shows that, for a symmetric installation of the coils about the midplane of the detector, the end iron proximity can be adjusted to bring the axial forces to nearly zero. Some installation error can be expected, however. An estimate of this displacement for one solenoid is 0.025 mm, or about 1 in. Because two solenoids are involved, there are several ways in which these displacements may combine. Previous work on an 8m by 16m solenoid for the SSC indicates that the simultaneous displacement of both solenoids toward the center produces the largest force[12].

The force calculated by the finite element model is 300000 lbs for this case. For design purposes, an axial decentering force of 500000 lbs will be assumed to allow for uncertainties.

Radial decentering force calculation requires three dimensional modeling, which is beyond the scope of this preliminary work. However, a previous analysis (2) has shown decentering forces about 45000 lbs might be expected on each solenoid. For design purposes, this force will be assumed to act in the same direction as the solenoid weight, giving a total radial force support requirement of 75000 lbs.

The endplug experiences large forces which pull it toward the detector mid-plane. If a uniform field of 1.7T is assumed over the endplug area. then the force can be calculated as

$$F = \frac{B^2}{2 \times \mu_0} \times \text{area}$$

or 11 MN ($2.47*10^6$ lbs). The finite element model. using a more realistic field distribution over the endplug. gives 8.7 MN. or $1.95*10^6$ lbs. For design purposes. a force of $2*10^6$ lbs will be used for the endplug axial magnetic force.

Mechanical Properties

The modules consist of bonded laminations of 2 mm steel plates and 2.5 mm lead plates. Lead has a Young's modulus of $2*10^6$ psi, and a density of 0.411 lbs/in^3. Steel has a Young's modulus of $29*10^6$ psi. and a density of 0.284 lbs/in^3. For the purposes of finite element analysis, the properties of the materials are 'smeared' homogeneously throughout the material by volume averaging. and are given a value of $14*10^6$ psi for Young's modulus. and 0.354 lbs/in^3 for density. The steel is unspecified. but assumed to be equivalent magnetically to AISI 1020 steel. Module stresses calculated below are within the capacity of available 0.2

Endplug Module Support Ear Design

The steel plates in a barrel or endplug module may be extended to form ears from which the module may be supported. An ear geometry which provides acceptable access to the module is shown in Fig. 33 . The stress area available for a one inch length of this ear is 0.44 in^2, and the allowable load is

$Pa = 0.44Sa$

where Sa is the maximum allowable stress in tension of the steel. This stress will be taken as 2/3 Sy. where Sy is the minimum specified yield stress of the material.

The module support scheme requires that these ears resist bending loads when modules are cantilevered. In the case of an endplug module. shown in Fig.34 . ears appear along azimuthal lines around the assembly. Therefore, both the bending stiffness of the module and the orientation of the ears change with position within the assembly. which results in ear stress distributions of either uniform tensile stress over the length of the ear. or a linearly varying bending stress. A three-dimensional analysis of a similar endplug module assembly has shown a strong tendency for modules with their weak bending axis oriented horizontally to distribute a large portion of their weight to the modules below them, which become more stiff as the weak axis is rotated toward the vertical. There are indications that the calculation of ear strength based on the requirement that each module support only it's own cantilevered weight (no redistribution to adjacent modules) in it's weakest orientation is the 'worst case' for the endplug modules. Table II gives the module ear lengths. moments. and resulting ear stresses for this case. The largest stress is 18500 psi.

The electromagnetic axial force on the endplug of $1.95*10^6$ lbs will increase the stress in the ears of the endplug modules by approximately 1500 psi. The

largest total ear stress is then 20000 psi, which requires a steel with a minimum specified yield stress of 30000 psi.

Table II. Stresses due to Cantilevering		
Endplug Module	Moment	Maximum Stress
A	76720 in-lbs	16800 psi
B	114700 in-lbs	17400 psi
C	114000 in-lbs	18500 psi
D	114500 in-lbs	18400 psi

Barrel Module Support Ear Design

In contrast to the endplug assembly, the barrel assembly presents the same ear orientation at each module and the same bending stiffness relative to moments produced by dead weight in a radial plane. This geometry is amenable to a simple, 2-d finite element analysis which can include the effect of module interaction.

Fig. 35 shows the finite element model of half of a barrel assembly and the deflected shape. (The support structure analysis is detailed below) The modules are modeled as discreet units, interacting only azimuthally with adjacent modules; i.e., they are free to slide radially relative to adjacent modules. The stiffness of these modules is that of the combined steel-lead assembly. The assembly is assumed to be 2 meters deep, and has a total weight of 808000 lbs. This weight is approximately 10the heaviest barrel assembly of Fig. 30 .

Table III summarizes the resultant moments and normal forces on the modules. Barrel module 10 has the largest moment/normal force combination, and requires 48 linear inches of ear. Fig. 36 shows a possible scheme for acquiring the necessary ear length by using six 8-inch long ears on each edge of the module. An important issue which must be addressed in the final analysis is the shear strength of the lead/steel bond and it's effect on ear placement.

Table III. Moments and Forces on Assembled Barrel Modules		
Barrel Module	Moment (in-lbs)	Normal Force (lbs)
1	$-1.37*10^6$	64000
2	$-3.62*10^6$	48000
3	$-5.15*10^6$	21000
4	$-5.50*10^6$	-15000
5	$-4.45*10^6$	-54000
6	$-1.91*10^6$	-90000
7	$1.81*10^6$	-115000
8	$5.70*10^6$	-127000
9	$8.70*10^6$	-125000
10	$9.69*10^6$	-113000
11	$7.95*10^6$	-96000
12	$3.14*10^6$	-84000

Note: Positive normal force produces tension in ears

Support of Endplug Module Assembly

The endplug support structure cantilevers the endplug modules into the bore formed by the barrel module assemblies. It must allow the 390 ton endplug to be drawn away from the bore for access to the solenoid and upstream endplug region. A possible support design, shown in Fig. 37 , uses concentric rings of 2 inch steel plate, connected by webs at 30 degree increments between the rings. The inner and outer radius ears on the endplug modules are attached to the rings, and external support plates attach to the outermost ring and ride on beams projecting from the front of the barrel assemblies. During operation, the endplug contacts the downstream barrel assembly at several points about it's outer circumference, transfering the large electromagnetic axial endplug force through the barrel assemblies.

A three-dimensional finite element model of the endplug support structure was created to calculate support stresses. This is shown in Fig. 38 . The endplug modules were approximated by modeling a network of spar elements (not shown) projecting from the concentric rings to the center of gravity of the endplug, at which point a vertical force equal to the endplug weight was applied.

The stress intensity in the endplug support structure is shown in Fig. 38 . The maximum stress is 19700 psi, which is within the capacity of structural steels. A more detailed analysis will be necessary to consider the effects of sta-

bility, welding and other issues. However, there is considerable space available for additional support material and a support structure of the type shown here should be feasible.

Support of Barrel Modules

The proposed barrel module support structure consists of arches constructed of 2 inch steel plate, which provide for attachment to the ears of the barrel modules, while leaving as much space as practical for access. Six arches are used on each half of the detector, and can be drawn back to provide access to the solenoid and the inner radius of the barrel modules themselves. Each arch consists of two arch plates, connected by plates parallel to the detector axis. The exact size and number of these plates will be determined by a detailed analysis of the axial and dead weight forces.

The simple two-dimensional finite element model of the barrel assembly can be used to examine the stresses in the arches. It is not known at this time how the arch itself will be supported on the ground, so the assumption of self-support was made. Fig. 39 shows the stress intensity in the 2 inch steel arch plate. The module weight appears near the base of the arch, due to the azimuthal weight transfer, and produces very little bending in the plate. Stresses are very low, and given the conservatism of the analysis, which uses only one 2 inch plate instead of the two required by a practical support, a structure of this type should provide adequate module support. As with the endplug support, this analysis suggests feasibility, but the final analysis must address other important structural issues.

Support of Solenoid from the Barrel Module Assembly

The solenoids are supported from the barrel assemblies at the detector midplane and the upstream ends. Axial forces are reacted at the midplane through 15 degree plate segments of 2 inch steel as shown in Fig. 40 . This arrangement allows half of the azimuthal area at the midplane to be available for cable routing. The force on each plate is 41700 lbs. If it is assumed that the plate segment acts as a cantilever beam and that the force acts at a distance of three inches from the fixed end of the beam, then the bending stress is 9100 psi. This is within the capacity of common structural steels. The issue of bearing against the barrel modules must be investigated, but the axial orientation and large number of module steel plates available should provide adequate bearing strength.

The upstream support is designed for dead weight and radial decentering forces only. Attachment is made directly to the bent steel plates at the inner radius of the barrel modules by extending the plates and pinning or bolting them to the solenoid. The support requirement is one half of the total dead weight of the solenoid and the radial decentering force, or 37500 lbs. Sufficient plate area exists for support: Detailed analysis must consider the interaction of the bent plates and the possibility of attachment schemes which provide shear resistance and allow the full bending strength of a group of plates to be generated.

The solenoid dead weight is less than half of the total radial design force, and it should be possible to support the solenoid from one half of the barrel arches, allowing the other half to be pulled back for access to detector components.

Mechanical Integrity of Individual Calorimeter Modules

Indepedent of the final structural details of the overall calorimeter support structure, the mechanical robustness of each of our 3 types of calorimeter mod-

ules will be firmly established well before hand. To this end, we are currently calculating, using the NASTRAN finite element computer code, stress and displacement fields within each of the calorimeter module types. We will also perform adequate mechanical tests to verify key issues such as the sheer strength of lead/steel bounds and epoxy/plastic interfaces. Our goal is to have a thorough and verified mechanical design of our calorimeter modules finished before detailed design work on the overall calorimeter support structure is started.

A.7. Compensation Studies

A number of important issues for compensating scintillator calorimetry will be addressed by a large (60cm x 60cm x 2m) test beam calorimeter containing a Pb/Fe/Scintillating-tile stack which can be reconfigured to vary sampling fractions, material ratios, etc. Among these are:

a) Which combinations of Pb, Fe, & Scintillator are actually compensating?

b) What is the effect of a non-compensating EM front end on the hadron resolution?

c) In a 3-component laminate, does the compensation depend on the sequence of materials: i.e. is Pb/Fe/Scint equivalent to Scint/Fe/Pb?

d) How is compensation affected by "dead" plastic?

e) How does calorimeter depth, and depth segmentation affect resolution?

f) What is the light yield & uniformity of a full sized Scintillating Tile calorimeter under battle conditions?

A reconfigurable (i.e. piecewise disposable) calorimeter would also be ideal for studying radiation damage issues in a test beam environment.

B. TECHNICAL DETAILS OF PROPOSED FRONT-END ELECTRONICS AND TRIGGER SYSTEM

B.1. PMT and Electronics Subassembly

The number of phototubes (50.000) required for an SSC detector falls in the range accessible to high-volume commercial fabricating techniques. The general experience with PM tubes in high-energy physics is that the cost of the tubes themselves has been equalled or exceeded by the cost of the associated trigger and readout electronics, HV supplies, bases, connectors, etc. We expect that expected that significant savings can be realized by engineering of a multi-phototube assembly. We envisage a single "card" containing 8-16 PMT's, with power supplies, magnetic shielding, readout electronics, trigger logic, cooling, calibration system, etc. integrated into a single package. The module would be optically coupled (in a pluggable manner) to a mating This approach has a number of advantages:

- The front-end electronics is greatly simplified by removing the cable separating it from the PM tube.

- A PM with a small number of stages (6-7) can be used, resulting in increased gain stability and further simplifications of the electronics & HV power supply. A low-gain PM tube is especially useful in the high-rate environment of the SSC, and where high dynamic range and linearity is important.

- The HV power supply is conveniently shared among the 8-16 channels on a PM, with the individual tube gains being trimmed via a single adjustable voltage on one of the last dynodes.

- No HV connectors exist anywhere in the system, and no dangerous charges are built up on HV distribution cables. All HV components up to and including the PMT bases are collectively potted.

- Inexpensive molded parts can be used for mechanical support, magnetic shielding, etc.

- On-site detector maintenance is greatly simplified by the monolithic nature of the PMT/electronics module: you "change the card and solve the problem", without regard to whether the problem is in the PM tube, power supply, amplifier, ADC, trigger logic,... or some combination of the above. The PMT/electronics module arrives at the detector as a completely tested subassembly, so that the number of system-level interference possibilities is greatly reduced at the time that the detector is deployed.

We propose to build and test a first-round prototype module of this type during the term of this subsystem proposal. This is mainly an engineering task (as opposed to R&D), since one can point to a number of experiments in which PM tubes have been successfully operated in conjunction with high-rate electronics. Although a fully engineered design will require several design cycles before production for an SSC detector could begin, we anticipate that our experience with this design will enable us to generate realistic cost estimates for the readout of a PMT-based SSC calorimeter.

B.2. FRONT-END ELECTRONICS

AMPLIFIER/CHARGE INTEGRATOR We propose to investigate two possibilities here:

1) Charge integrating amplifiers of the same type used on the CDF. They have demonstrated excellent linearity over wide dynamic range. They require only very modest gain from the photomultiplier. Their noise level can be made so low as to be much less than other errors. We have extensive experience with these designs and can predict performance. Obtaining the bandwidth necessary to fully settle in the the 16ns crossing time requires further R&D.

2) A gated charge integrator which uses an emitter-coupled current switch to distribute the PM current from each 16ns crossing onto a sampling capacitor. A number of capacitors (probably 2-4) are operated in a round-robin manner. After the charge from a crossing is deposited, the capacitor voltage is then digitized, and the capacitor is reset before its use in a subsequent crossing. This scheme has the advantage of being completely DC-coupled so that there will be no rate-dependent effects. It has the disadvantage that one may need multiple calibration constants per channel, e.g. for the odd/even crossings. Switching times on the order of 100 psec can be realized with an emitter-coupled current switch, so that extremely accurate charge sampling gates may be obtained.

ADC SELECTION/DESIGN AND PROCUREMENT. We forsee three possible ADC schemes for this detector:

1. Multiple Flash Encoders with Digital Memory. This is a brute-force approach which one could design today, and the cost of which would somewhat exceed that of the PM tubes. In order to obtain the required dynamic range (a least count of 20 MeV to measure minimum-ionizing depositions, and a full scale of 10 TeV) one requires 19 bit digitization. This could be obtained, for example, by four 10-bit flash ADC's which are offset by 3 bits of gain. Such an approach may well become economically attractive as the cost of Flash ADC's continue to decline in the marketplace.

2. Logarithmic Pipelined Encoder with Digital Memory. In this approach each bit in the final digital word represents a multiplicative factor, the product of which gives the final result for the digitized voltage. Each bit decision is made sequentially in an analog pipeline, using switched capacitors as the delay element. This scheme has the advantage of having only a single comparator for each bit decision, whereas a Flash ADC with N bits has 2**N comparators and commensurately higher power. This digitization method has been used successfully in radar systems at clock frequencies lower than the 60 Mhz required for the SSC, but will require further R&D to determine what accuracy and dynamic range which can be obtained at this frequency.

3. Analog Memory with Conventional ADC (Superconducting Delay Line, Charge shift register of various types...). This approach offers potential cost savings at the expense of increased system complexity. In particular, since flash digitization at some level will be necessary for trigger purposes, at present we prefer a scheme in which the trigger relies on the same digitized information that is available in software.

CALIBRATION AND TESTING. We would propose three calibration modes. Our experience with CDF indicates that these calibrations can be done to required accuracy with little difficulty. Firstly we would provide charge injection on an individual amplifier. This allows checking the amplifier gain, allows tests of the trigger system, and tests everything downstream of the amplifier. Next we would provide LED light flashers on each phototube. This checks the phototube gain, but would not be considered a primary calibration. The third calibration would be accomplished by pulling a source through the towers. The DC current produced would be monitored by measuring the voltage across the feedback resistor on the integrating amplifier. This can be done to high precision and measures the combination of phototube gain and possible aging of the scintillator.

CLOCK DISTRIBUTION. Each modular group of phototubes will require a clock. We would propose to provide electronic de-skewing of the clock signals through a DAC controlled delay.

B.3. TRIGGERING AND DATA ACQUISITION.

The lowest level of components in the digital pipeline needed for an SSC trigger will reside on the PMT/electronics module. The way that this module fits into the global scheme for trigger and data aquisition will depend on the overall design of the detector. However, the main trigger & DAQ components on our proposed PMT/Electronics module (digitization of every crossing, storage of 100 crossings worth of data, a digitally pipelined triggering scheme, deadtimeless readout of digitized events, etc.) are likely to fit in well with any reasonable trigger design.

One of the authors [Ref GWF Breckenridge] has developed a conceptual design for a pipelined trigger which produces, on each beam crossing, a trigger decision equivalent to the CDF level 0.1 and 2 triggers. It relies on a custom digital gate array which provides for:

1) digital storage for Flash ADC data from each crossing.

2) accumulation of transverse energy sums and lepton lists via a "bucket-brigade" which passes trigger information up to the 90-degree crack in a digital pipeline. When the trigger information from a crossing arrives at the 90-degree crack, it is put into phi-coincidence with tracking information to form a fully pipelined trigger decision.

3) pipelined communication along dedicated cables between "nearest-neighbor" towers to determine lepton isolation and to identify electrons which straddle tower boundaries.

4) DAQ readout for triggered buckets via dedicated digital cables.

5) Full diagnostic capabilities. In particular, the ADC memories can be loaded and "played back" to allow full speed testing of the (all-digital) trigger system.

Our design for the PMT front-end trigger electronics will be compatible with such a system. Similarly, the first level components of the DAQ/readout system would reside on the integrated PMT/Electronics module. The gate array design for the trigger logic will be investigated on the IC design facilities at BU and at FNAL. The first-round prototype will in all probability not make use of a custom gate array, but will simply provide digital storage and readout, and a simple digital trigger, through the use of standard components.

C. Liquid Scintillator Calorimeter

Several key design issues must be optimized in designing a liquid scintillator calorimeter. First, the basic structure liquid-filled channels must be imbedded in an absorber matrix. Second, the tubes must be lined with a suitably chosen material to allow for TIR of the light emitted by the scintillator. Next the structure must be designed to provide for filling and venting so that no air bubbles interrupt the light transmission and so that the oil can be recirculated or replaced. Also provision must be made to terminate each tube into some form of light guide to transmit the light to the photodetector readout. This structure must be able to accommodate a wedge geometry without sacrificing its compensation properties or light readout. Further, consideration must also be given to the issues of calibration and performance monitoring over the long durations of typical SSC experiments. Lastly, this calorimeter must be **hermetic**. There can be no cracks or dead regions and certainly no dripping oil.

A. Lead/Tube Assembly

One way to produce the desired pattern of tubes in a lead matrix is to stamp or roll these grooves in lead sheets and stack them together. Several commercial firms as well as a number of the collaboration's university groups have recently demonstrated their ability to make such sheets using hardened lead. When these sheets are stacked, the mating grooves form cylindrical tubes. The 4:1 absorber/

scintillator ratio can be provided by appropriate choice of dimensions. Channeling effects may be reduced by "wiggling" the groove pattern on the stamping die, with an amplitude of $\approx$ 1mm and a wavelength as shown in Fig. 41 .

B. TIR lining

The required TIR lining can be provided in a number of ways depending on the material being used(Teflon or polymethylsiloxane). We are currently experimenting with using commercially available Teflon tubing and adhesive backed sheets, or surfaces which we paint with these polymethylsiloxane materials. In either case, it is fairly straight forward to coat or line these grooved plates for constructing these modules.

C. Filling and Venting

In order to provide for filling and venting each calorimeter module, all tubes within a layer must be interconnected at their two extreme ends to accommodate cross-flow. For the grooved plate construction, this can be achieved by milling a narrow transverse channel across each surface of each plate near each end as shown in Fig. 42 . These channels form fill/vent manifolds within each layer of tubes. The outermost tubes on each side of the layer can be connected to external manifolds to provide fill and vent lines to the entire layer. Because the outermost tubes sample light only from the rearmost portion of the calorimeter module (see later discussion of wedge configuration), the dedication of those two tubes of each layer for fill/vent has no significant effect on calorimeter response.

D. Light Readout

The interface between the liquid filled channels and the necessary light collection system can be accomplished by glueing non-scintillating fibers into each of the liquid channels at the exit end of the calorimeter. For the coupling to the assembly of grooved plates, the TIR coating is terminated a few millimeters from the exit of the calorimeter block to allow for the insertion and glueing of the bundle of light collecting fibers. A technique must be developed to align and glue these large bundles of light collecting fibers to facilitate mass production of a large number of such modules. Further, these light collecting fibers can be coated with a low-index film (e.g. polyvinylacetate) so that light from the liquid scintillator will enter the fiber efficiently and will be TIR-channeled everywhere, even within the short region of the glue joint.

E. Wedge Geometry

For both barrel and end-wall calorimeters, it is desirable to configure each calorimeter module as a projective wedge. For the grooved plate construction the wedge shape can be achieved in one dimension by simply tapering the plate width as shown in Fig. 43 . This geometry has the advantage that there are two distinct types of fibers in this module, those that extend the entire length of the wedge located in the center of the wedge, and those that begin at various depths in the calorimeter and only exit the back of the calorimeter stack. By choosing the size of the wedge to have the central core a fraction of the size of a typical hadron shower, one can use the lateral spread of energy in this calorimeter structure to help separate electrons from pions without a separate electromagnetic compartment. This configuration is shown in Fig. 42 .

F. Calibration

Calibration can be accommodated by milling transverse slots at several locations along selected absorber plates and installing a small bore (0.5 mm diameter)

tube which runs a closed circuit along one flanking tube, across the channel, and out an opposite flanking tube, as shown in Fig. 42 . A loop of wire containing an encapsulated isotope source can be run through the tube to provide source calibration at selected depths whenever desired. This technique is patterned after the system used for the CDF central wedge calorimeters[4] .

G. Hermeticity

Each calorimeter module must be hermetic. This means two things: it must not leak energy (cracks between modules, dead regions), and it must not leak oil The structure illustrated in Fig. 42 can meet both criteria. The active medium of the module extends right out to its boundary. A thin (0.5 mm) steel skin can be used to enclose the outer boundary of each module to provide a smooth hard surface for stacking and to provide a light-tight enclosure. All appurtenances - light fiber bundles, calibration fibers, phototube assemblies, and fill/vent lines can be enclosed within the projective (θ, ϕ) profile of the module. Modules can then be stacked upon a superstructure with NO CRACKS. Regarding oil hermeticity, the layers can be epoxied pairwise at their boundaries, sides and ends. The complete module should therefore be an oil tight assembly. The seal integrity can be checked before filling by evacuating the entire manifolded tube assembly and helium leak-checking. The oil fill can also be done under vacuum to assure elimination of air voids.

Current Activities

Our current efforts on developing liquid scintillator for spaghetti calorimetry are focussed on setting instrumentation to measure the "totally internally reflecting"(TIR) light transmission of Teflon(n = 1.35) and polymethylsiloxane(n = 1.40) coated surfaces for application in the construction of a prototype calorimeter.

In an effort to confirm the expected light transmission properties of these liquid scintillator filled channels, we have setup a test counter to make such measurements. The aim of these tests is to measure the light yield and attenuation length for a collection of liquid filled channels.

The setup that we have assembled is shown in Fig. 44 . It consists of 60, 1 meter long and 1mm i.d. quartz tubes, laid out in a rectangular close-packed array to simulate a conventional *paddle* counter geometry. These tubes are then lined with Teflon by inserting a standard thin walled PTFE Teflon tube(24 AWG) into each channel. The glass tubes in this configuration are used to support the Teflon tubes and contain the liquid scintillator(BC 517). The two ends of this assembly are then viewed by separate 2" diameter fast linear focussed photomultipliers.

We have just begun to perform tests on this device using both cosmic rays and radioactive sources. With this setup we expect to measure the absolute light output per *mip* and the light attenuation length of this light collection system.

We are also currently preparing to test several aspects of the groove channel design mentioned earlier. We have obtained samples of the grooved plates that were rolled at Purdue University. Once we have developed the necessary coating techniques required to produce the TIR channels, we will assemble these coated plates into a counter for tests of light output and attenuation length.

Program Objectives

We propose to conduct a program of design, hardware development and testing to produce an optimum liquid scintillator fiber calorimeter for use at the SSC and evaluate its performance in a test beam at Fermilab. Our program objectives include the following components:

Material Choices. We plan to obtain samples of stamped hard lead sheet and evaluate dimensional stability, surface quality and tensile properties. Our study will also include a careful evaluation of available liquid scintillators for performance in collider calorimetry. In particular, we will investigate their light yield, attenuation length, response time and sensitivity to radiation damage. These studies will also include an evaluation of the various materials available (eg. Teflon and polymethylsiloxane) and their coating techniques, in order to produce the requisite TIR structure for these calorimeters.

Simulation. The state of simulation codes for modelling the performance of electromagnetic and hadronic cascades and the resulting ionization response has improved dramatically in recent years. It is now possible to establish reasonable agreement between experiment and simulation for a variety of calorimeter designs. We plan to use the current codes to simulate the response in the geometries of a liquid scintillator calorimeter. We hope to then use these results to fine tune the geometry for the test module. The beam test results will then be used to check the validity of the simulations.

Module Fabrication. In parallel with our studies of materials and their properties, we will also be focusing on the design and construction aspects of producing a workable SSC calorimeter using this technique. These studies will involve developing procedures for coating the channels in the absorber matrix and for coupling the light from these channels to the readout photodetector. Given the strict requirement of oil tightness, we will carefully study the design of the oil seal of the final assembly.

Beam tests and Calibration. In the test beam, we plan to carry out a systematic study of the performance of a prototype module. Our plan is to install this unit in a Fermilab test beam for testing during the fixed target running in 1990. The test beam measurements will include studies of energy resolution, linearity, compensation and e/π separation over the largest feasible energy range. We would also like to conduct above the measurements for several selected liquid scintillators in order to optimize compensation in this device. Lastly, we will evaluate the practical precision of source calibration procedure and study its ability to track changes in the response of the module due to radiation aging and other time dependent changes.

D. TECHNICAL DETAILS OF PRERADIATOR

D.1. IMAGING PRE-RADIATOR

SUMMARY

We propose a three year program to develop a full scale design for an imaging pre-radiator based on a matrix of lead and scintillating fibers and aimed at the physics requirements of an SSC detector. A major task will be to develop a system that will be capable of reading out images from systems of several hundred thousand scintillating fibers that fully exploits the high speed and excellent granularity of such a system. By placing a pixel detector, such as those currently being developed by D. Nygren and his group at LBL, inside an image tube, a fast high-density read-out system can be implemented at a reasonable cost.

INTRODUCTION

The importance of lepton and single-γ signatures for SSC physics is quite generally recognized. For a Higgs mass that is $M_H \geq 2M_Z$, the Higgs is expected to decay into one or two lepton pairs, which, in order to be recognizable above the abundant QCD background, places a very strong requirement on the ability of the detector to correctly identify electrons. For the mass range $M_H < 2M_Z$, the $H^0 \rightarrow \gamma\gamma$ decay mode has been suggested as the most feasible experimental signature, which puts a premium on good single-γ/π^0 discrimination. In addition, there are the semi-leptonic decays of the heavy quarks, both seen and yet to be seen.[13] Leptons are also expected to provide important signatures for a variety of new physics, such as, for example, searches for supersymmetric particles,[14] searches for Z*'s, heavy recurrences of the Z,[15] and many others. A detector capable of identifying electrons within complicated events could have a great advantage over one that has to make an isolation cut. For example, this could be important for decay modes such as $Z^* \rightarrow Z + \text{jet}$.[16] Since the ability to identify electrons and single-γ's will be an important physics signature at the SSC, we have been investigating the possibilities of using a pre-radiator in conjunction with calorimeters to enhance these features of proposed SSC experiments.

As part of this program, we have been developing an imaging pre-radiator composed of ribbons of scintillating fiber (SF) interleaved with lead (Fig 1). The high speed, excellent granularity and ability to function in a magnetic field, make fibers ideal for such a device. However, there are no currently available techniques for reading out such systems that do not compromise some or all of these properties. Imaging detectors currently in use are read out with CCD pixel devices, which are severely limited by the long time it takes for their serial readout. Recently, there has been considerable progress on randomly accessible pixel devices; this is an area of technology that has been receiving considerable attention. Here we propose a program of research that applies these new technologies to imaging SF devices. While our present focus is on pre-radiators, progress in their readout systems should be equally applicable to SF tracking devices and calorimeters.

Pre-radiators

The use of pre-radiators, devices that give detailed information about the early development of electromagnetic showers, is a common experimental technique in high energy physics. Recently, rather complex pre-radiators have been

implemented in both the UA2 and CDF experiments at $p\bar{p}$ colliders. In particular, UA2 has demonstrated that an imaging pre-radiator can greatly enhance the quality of data.

Pre-radiators supply detailed position information with a precision that is characteristic of tracking devices and, thus, of considerably higher accuracy than can be generally obtained using energy sharing between calorimeter modules. This is a technique that exploits the short development length of electromagnetic calorimeters: they are of little use for hadronic showers since the start of these showers is spread over a much larger depth region within the calorimeter.

Imaging pre-radiators have considerable potential for SSC experiments. They can provide information about the detailed structure in a complex event that would would be unobtainable with presently conceived trackers and calorimeters alone. Moreover, they would also provide redundant information that could be important for interpreting complex events. They provide a link between tracking detectors and calorimeters which, at the SSC, will be essential for:

1. Improved electron/hadron rejection in isolated events and electron identification within complicated events where isolation cuts can't be applied:
2. Separation of direct single-γ's from π^0's on an event-by-event basis:
3. Tagging of high energy electrons by the detection of the synchrotron radiation (SR) emitted it emits as it bends in a magnetic field:
4. The precise determination of the location of the starting point of an electromagnetic shower;
5. Reduction of fake electrons due to accidental π^0/charged-track overlaps.
6. Unambiguous assignment of the shower with bunch crossing;

The capability of performing these tasks is limited by the quality of the track measurement and the physics of the shower development. We will discuss each of the above-mentioned items in turn.

Electron identification in calorimeters is based on the differences between electromagnetic and hadronic shower development. The lateral and longitudinal development of a shower, as well as the time development of the sampling pulses, are different for electrons and hadrons. With methods based on these signals, rejections of the order of $0.1 \sim 1.0\%$ can be achieved. However, the different calorimeter signatures are highly correlated since the major source of mis-identification comes from a hadron shower that converts most of its energy into π^0's early in the calorimeter, which subsequently create electromagnetic showers. A pre-radiator that samples the early shower development can provide additional information that is uncorrelated to the other measurements. This has been demonstrated by measurements using a pre-radiator at a shower depth of 1.5 $RL^{[17]}$ and for other lead-scintillating fiber configurations by Monte-Carlo calculations. Furthermore, when an electron is accompanied by a hadron, calorimetric methods fail, restricting electron identification to isolated tracks only. An imaging pre-radiator does not suffer from these limitations and can separate electrons from other particles at distances as small as a few millimeters, enabling some electron identification inside of jets.

To separate direct single-γ's from π^0's on an event by event basis, the pre-radiator has to be able to distinguish the two photon showers from a single one.

The minimum opening angle of a π^0 is given by

$$\theta_{\min} = \frac{2m_\pi}{p_\pi}.$$

Thus. for a 100 GeV/c π^0. , the two decay photons are separated by a distance of $\geq$ 2.6 mm per meter of flight path. This separation has to be measured sufficiently deep in the calorimeter so that the two photons have a high probability of converting, but not so deep that the two showers begin to merge. This is a task for which an imaging pre-radiator is particularly well suited.

The technique of using synchrotron radiation to tag electrons in a preshower detector has some very interesting possibilities.[18] While the study of this technique has been motivated by the possibility of using a small (R $\sim$ 1 m), high field (B $\sim$ 6 T) detector configuration;[19] our Monte-Carlo studies have shown that it would be feasible for p $\sim>$ 50 GeV/c electrons in a B $\sim$ 2 T, R $\sim$ 2 m. configuration. (Our test beam measurements, planned for the near future, should provide further information on this lower limit.) It is important to note that SR signatures for electrons are uncorrelated with those based on shower development.

The rejection of fake electrons due to π^0-charged track overlaps would be particularly important for non-magnetic detectors being considered for the SSC and for magnetic detectors in the forward direction. While it would be less of a problem for magnetic detectors where E/p cuts can be made, it would still provide independent information that would further reduce these backgrounds. The finer the granularity of the preshower detector, the better it performs in this regard.

Some magnetic detectors under study for the SSC have the electromagnetic calorimeter outside a thin (ΔR $\sim$ 2 RL) coil. In this case. layers of the pre-radiator could be placed both inside and outside the magnetic coil. The ones inside of the coil could be used to distinguish electrons from π^0's with overlapping tracks and for detecting synchrotron radiation. The ones placed outside the coil would be useful for single-γ identification.

We are studying ways by which pre-radiators could be introduced without compromising the requirements for complete hermeticity.

In principle, the energy resolution of an EM calorimeter should not be affected by the presence of a pre-radiator since that device is also capable of measuring the energy deposited in it. In any case, a $\sim>$ 50GeV electron only deposits .1-.3% of its energy in the first 3 radiation lengths.

In addition to providing unique capabilities, a pre-radiator can be useful for determining charged track multiplicities in jets as well as crude momentum measurements, thus providing some redundancy to the tracking information. With fibers of radius 0.5 mm, track separations as small as 1 mm in the bend plane and 5 mm normal could be recognized. The high speed of SF can be used to eliminate the calorimeter backgrounds from events in neighbouring buckets.

Imaging Readout Devices

The most difficult task to be faced in the construction of an imaging pre-radiator for the SSC is the readout. Imaging pre-radiators have to date been read

out with Charge-Coupled Devices (CCD's) coupled to image intensifier tubes. This system provides the necessary position resolution, but, as each pixel is read out serially, it is too slow for the high rate environment at the SSC. The only proven system, that we are aware of, which is fast enough for use at the SSC is the position-sensitive photomultiplier.[20] The position information is provided by multi-anode cells or crossed anode wires. The readout time is naturally fast, but the position resolution is limited in the case of multi-anode (3mm x 3mm cells are the smallest achieved and Hamamatsu claims this is near the limit). Crossed anode wires cannot be operated in a high B-field and suffer from multi-hit ambiguities. Solid state photomultipliers (SSPM) have also been proposed for the readout of fiber bundles.[21] These devices, while they can achieve the necessary position resolution, since there is one SSPM for each fiber, and have a 60% quantum efficiency, to be compared with 15% for ordinary image-tubes, they do have some drawbacks. The cost of the SSPM and the read out can be optimistically expected to be around $10 per channel, which would result in a total cost of $24 million to read out the pre-radiator that we are designing. Besides the cost there is also the additional problem that they have to operate at temperatures below 7°K and thus they require cryogenics for their operation. We are in close contact with the group that is performing R&D into the SSPM and we will maintain that contact during the course of the proposed research.

An advance over the CCD readout schemes currently used for image readout is the pixel detector being developed by D. Nygren at LBL for use in tracking at the SSC. It consists of a silicon PIN diode array bump-bonded to a readout chip developed by Hughes Aircraft which has been tested radiation hard to 1 Mrad. The particular feature of this pixel detector which makes it suitable for an SSC imaging pre-radiator or tracker is the read out which works in the following way. Each row and column of the pixel array is connected to a shift register where a bit is set if the row or column contains a hit. The shift registers are clocked every 15 nsec and are deep enough to allow the first level trigger decision to be made. When an event is selected, only the pixels with a row and column bit set for that bunch are read out at a rate of 200 nsec per pixel.

We want to build an image-tube with a pixel detector placed inside it, where it would be used to detect the electrostatically accelerated photo-electrons (approx. 10 KeV) with a high position resolution and thus satisfy the requirements of a readout for fibers at the SSC.

D.2. PROPOSED RESEARCH

We propose to continue research and development on imaging pre-radiators, of the style pioneered by the UA2 group at CERN, for use in a magnetic field.

In our design the pre-radiator would consist of $\sim$ 2 m long fibers forming a cylindrical shell just inside the solenoid coil. Four such cylinders would be required for an 8m long solenoid. Layers of fibers would be aligned at angles of -15, 0 and -15 to the magnet axis. The 500μm fibers would be read out individually with an image-tube inside the magnetic field. There would be 4 super-layers each consisting of 6 layers of fibers located in the first 1.5 RL of lead. The exact number of layers and the lead thickness will be determined in the near future in our forthcoming FNAL beam tests. Assuming the magnet to

be 8m long and to have an inner radius of 2m there would be 600k fibers for each super-layer or 2.4 million fibers in all. The total sensitive photo-cathode area that would be required for the pre-radiator would be 6000 cm^2. This would require 1500 image-tubes 2cm square.

Outstanding Issues

There are two major issues in the design of the pre-radiator which can only be settled with further R&D. The first of these is the level of complexity that is required by the physics. If the pre-radiator is sensitive to the synchrotron radiation emitted by the electron as it traverses the magnetic field, this point could be even more important. It is therefore urgent to begin the physics simulations to help decide these and other related questions.

The second is the feasibility of the image-tube readout. There are two different issues which must be addressed. The first is the fiber occupancy and the second is the technical feasibility. The former requires a good physics Monte-Carlo and the latter a prototype. A proto-type of this tube has to be built to demonstrate that it can work.

In the detector we are considering, which has 2m long fibers placed 2m. from the beam axis, the fiber occupancy, computed from the expected interaction rates at $L=10^{33}$, is approximately 20KHz. Each fiber is read out with 10 $100\mu m^2$ square pixels, giving an expected pixel occupancy of 2kHz. At these rates a 4 cm^2 pixel readout consisting of 40 thousand pixels would have on average 1 pixel hit per bunch crossing. Even taking into account the correlations in hits due to clustering neighboring fibers into the same image tube (factor of 10 more), the readout would be able to operate comfortably. However, since this is a very important question for these detectors it should calculated as accurately as possible with Monte-Carlo computations.

The pixel detector uses a $2\mu m$ polysilicon getter which the photoelectron would have to penetrate before it can deposit detectable charge in the pixel detector. It has to be determined how thin this getter can be made without effecting the properties of the device.

When image-tubes are made the manufacturing process includes a bake out stage where the temperature of the tube is raised to 400^0 C. This temperature is close to the melting temperature of conventional alloys used in indium bumping. The correct alloy has to be selected for use in the image-tube which must have a low vapour pressure and a high melting point. Alkali-poisoning of the silicon is also a danger, but this has been avoided in the past by enclosing the silicon in a glass ampule which is later cut internally using a current-carrying resistive wire.

The choice of the pre-radiator affects the required granularity of the calorimeter. If an imaging pre-radiator is feasible at the SSC, considerable cost could be saved in the calorimeter design. Therefore, for the engineering design to take into account the possibility of a pre-radiator, a first level prototype of the image tube has to be built in the coming year to prove its feasibility.

A number of other questions about the pre-radiator will be settled by forthcoming tests at Fermilab (Rockefeller/Yale). In particular the optimum lead/fiber configuration, the effect of albedo on the pre-radiator, and the interaction between pre-radiator and calorimeter especially as regards energy resolution.

R&D efforts to date

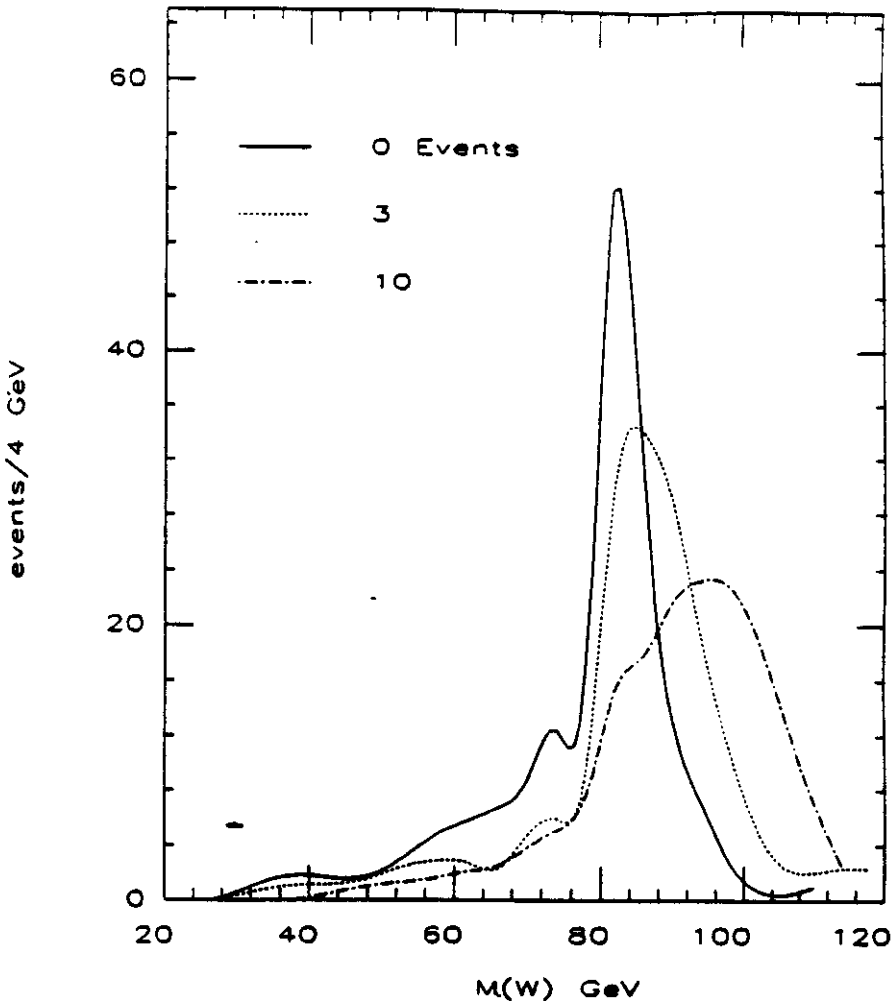
0 Events
3
10
events/4 GeV
M(W) GeV
0
20
40
60
80
100
120

Fig. 1

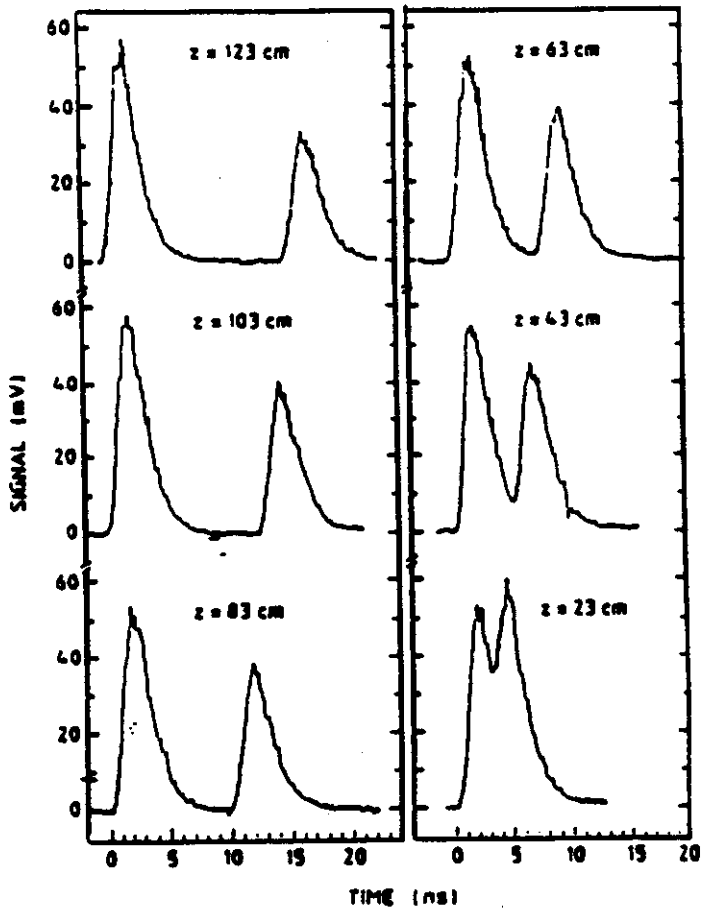
z = 123 cm
z = 63 cm
z = 103 cm
z = 43 cm
z = 83 cm
z = 23 cm
SIGNAL (mV)
TIME (ns)

Fig. 2

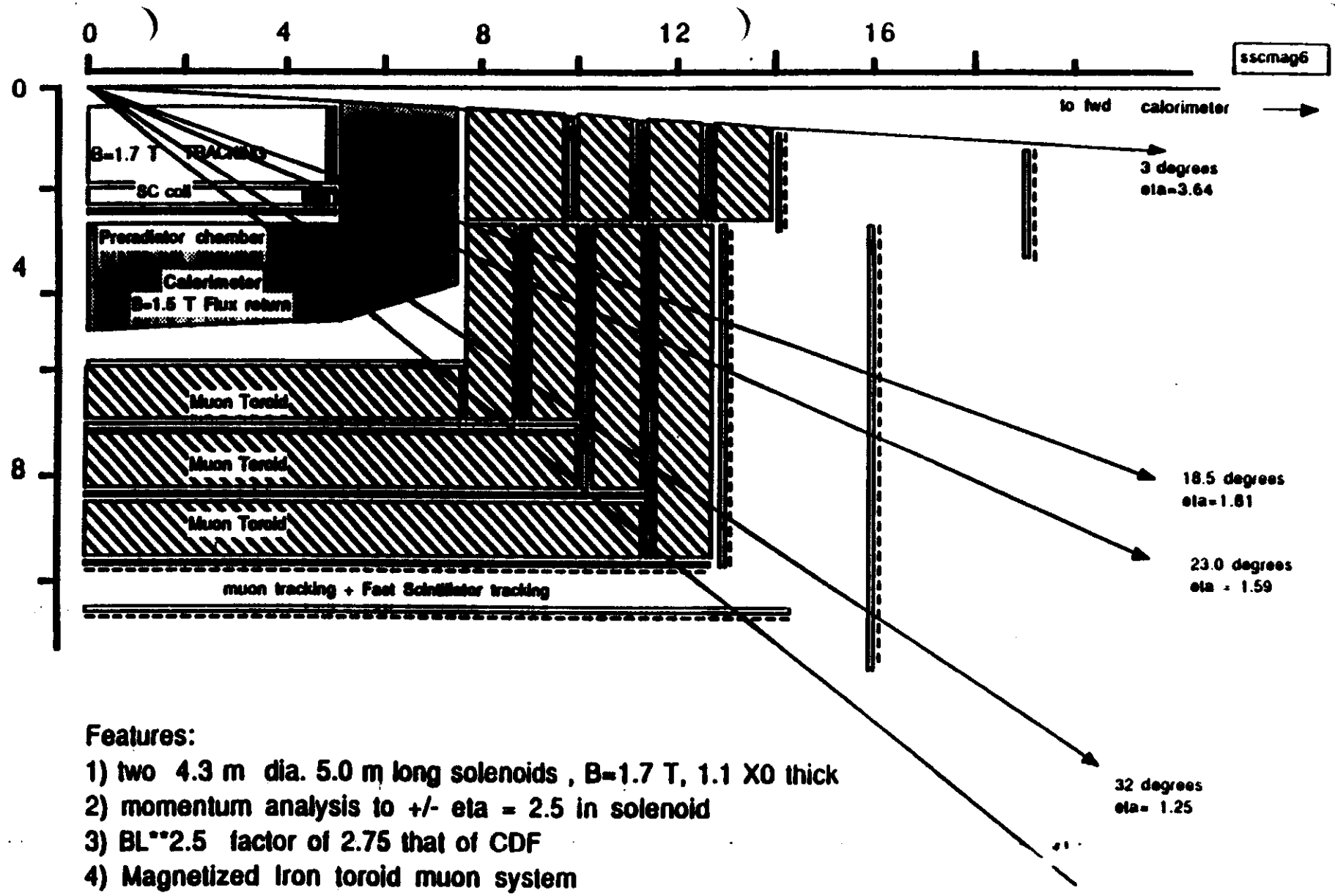

Features:

1) two 4.3 m dia. 5.0 m long solenoids , B=1.7 T, 1.1 X0 thick
2) momentum analysis to +/- eta = 2.5 in solenoid
3) BL**2.5 factor of 2.75 that of CDF
4) Magnetized Iron toroid muon system
5) muons over +/- eta =3.5, e's over +/- eta=2.5

Fig. 3

Fig. 4

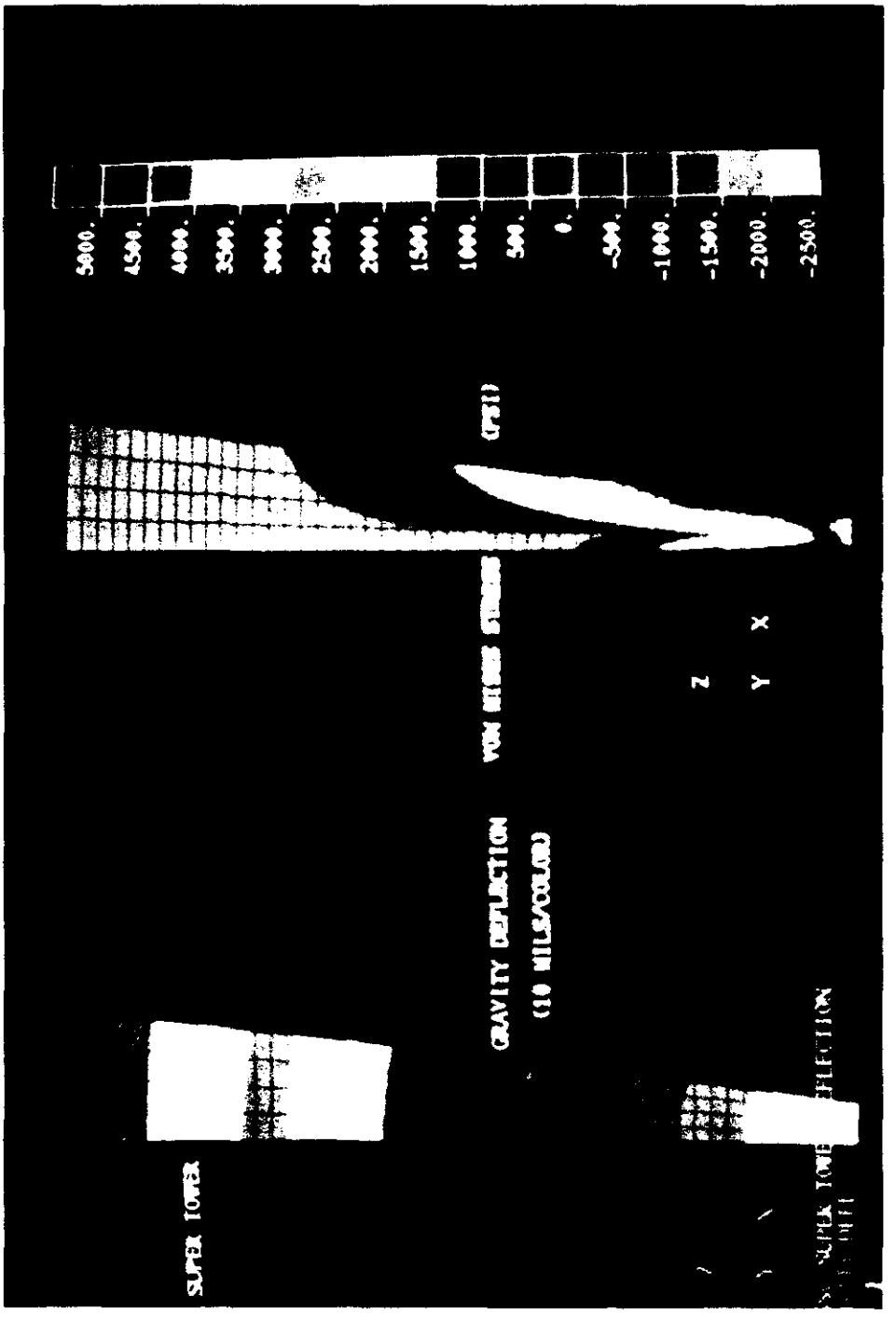
500.
450.
400.
350.
300.
250.
200.
150.
100.
50.
0.
-50.
-1000.
-1500.
-2000.
-2500.
SUPER TOWER
CAVITY DEFLECTION
(10 MILS/COLOR)
Z
Y
X

Fig. 5

Fig. 6

3HF fiber
(green)
Kyowa Gas

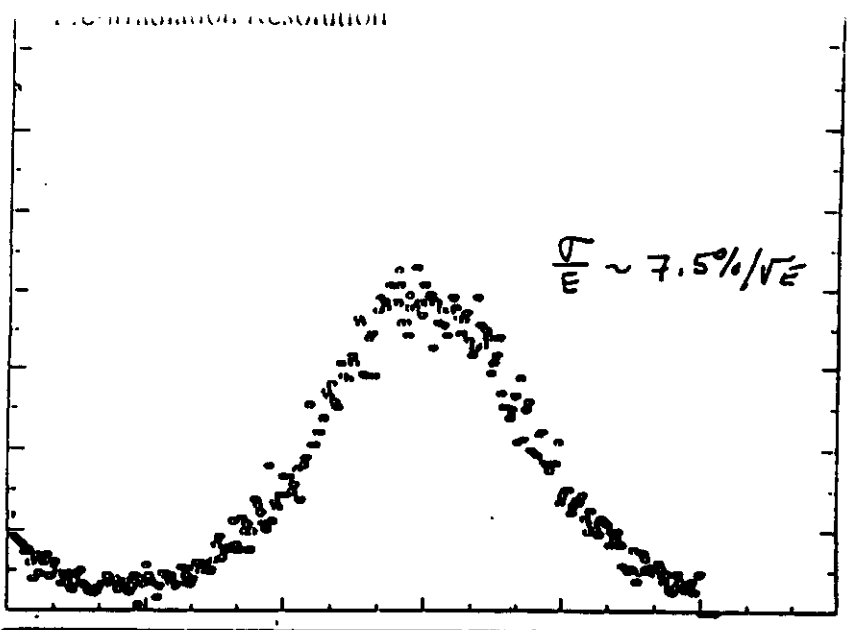

100 MeV e

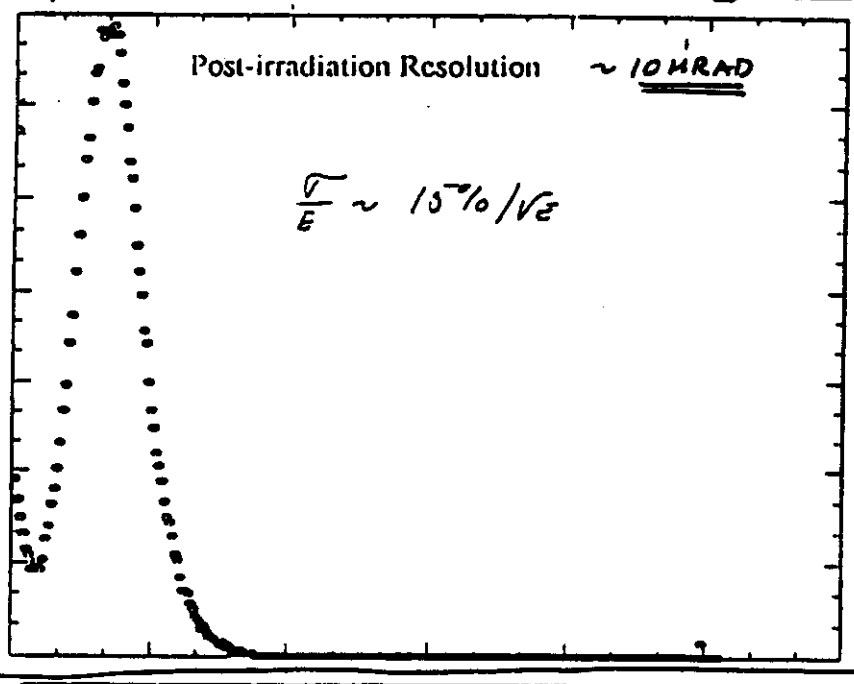

100 MeV e⁻
(15 minutes in

Different
"Absolute" ADC
Scale

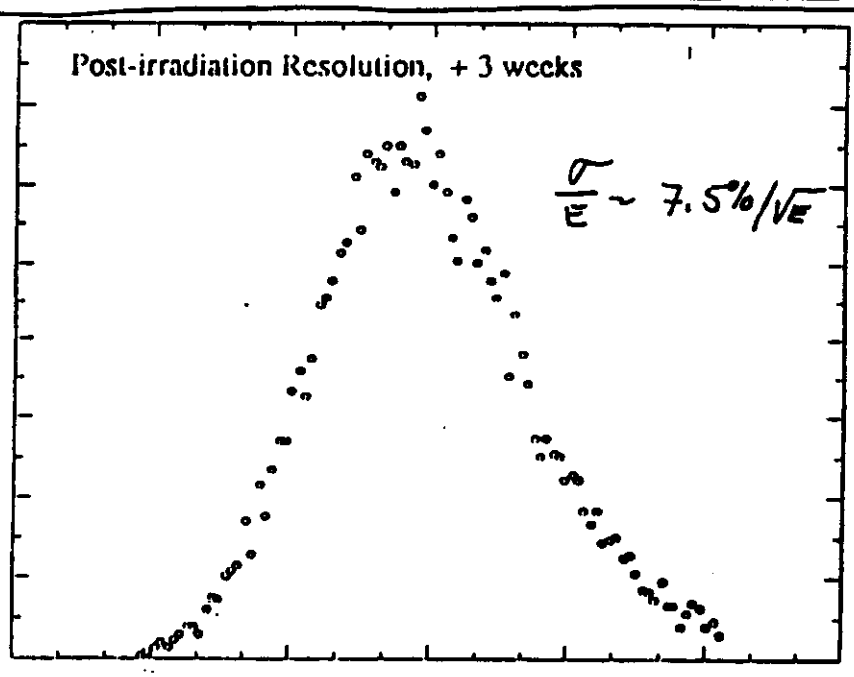

88 MeV e

Fig. 7

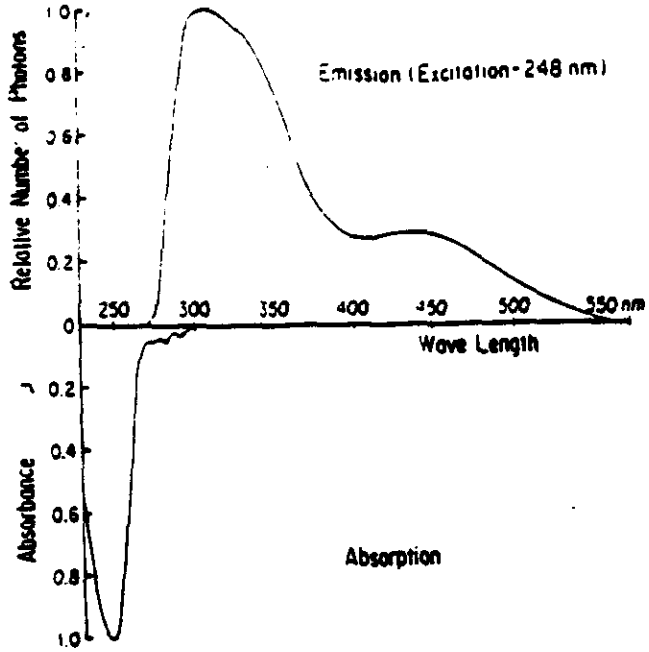
Emission (Excitation - 248 nm)
Relative Number of Photons
Wave Length
Absorbance
Absorption

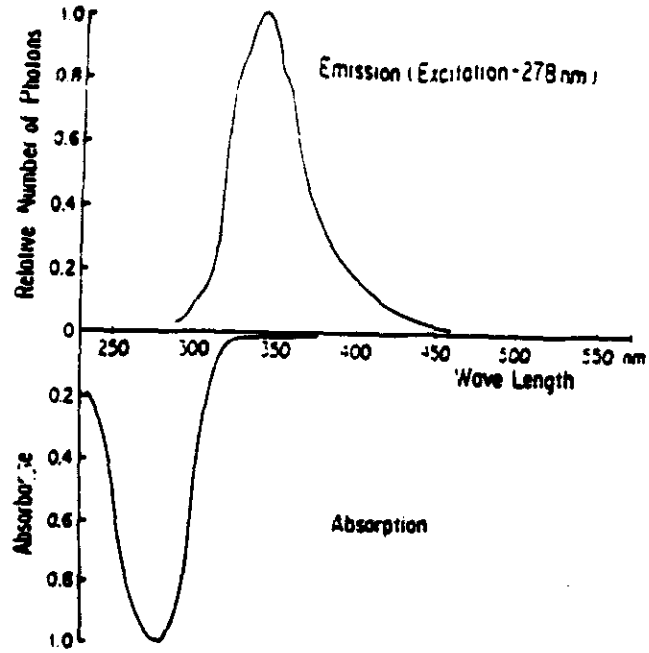
Emission (Excitation - 278 nm)
Relative Number of Photons
Wave Length
Absorption

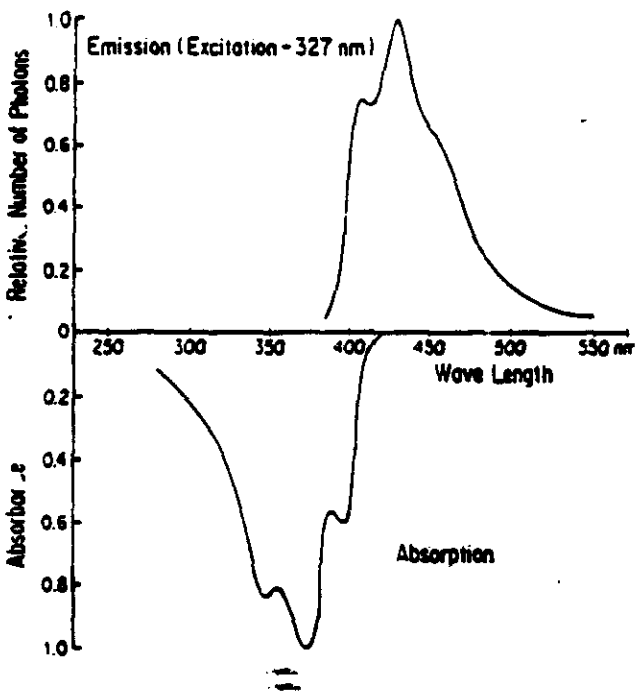
Emission (Excitation - 327 nm)
Wave Length
Absorption

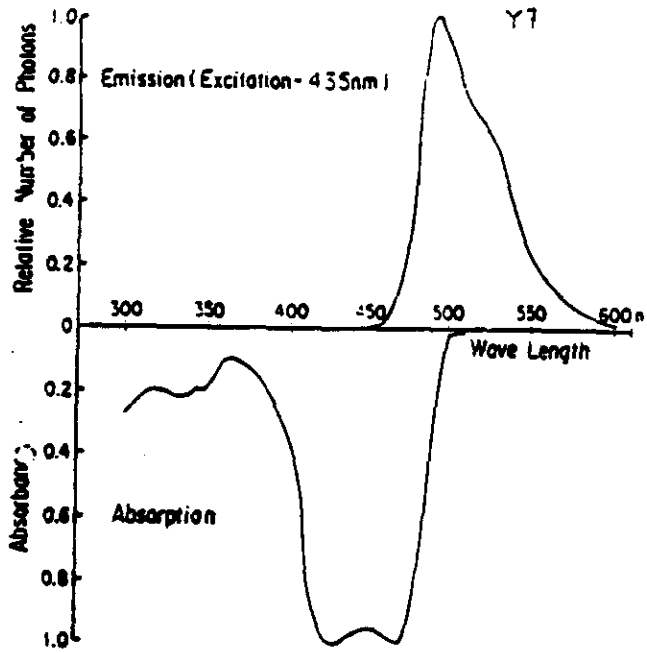
Emission (Excitation - 435nm)
Wave Length
Absorption

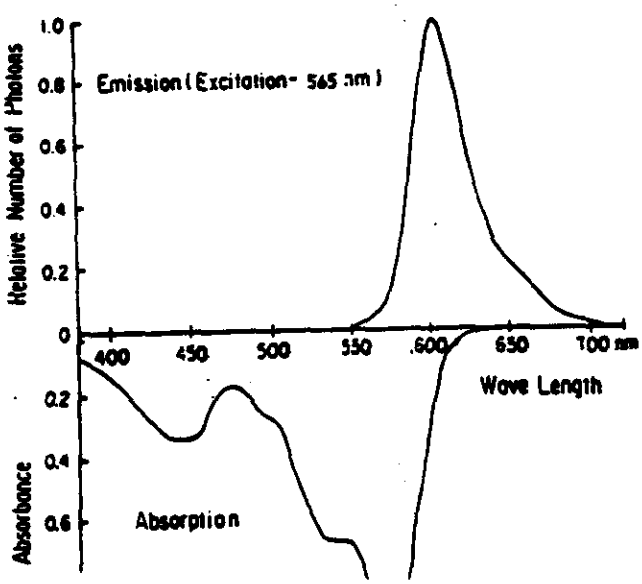
Emission (Excitation - 565 nm)
Relative Number of Photons
Wave Length
Absorbance
Absorption

Fig. 8

ABSORBANCE
3
2.5
2
1.5
1
.5
0
400
450
500
550
600
650
700
750
800
WAVELENGTH (nm)

Fig. 9

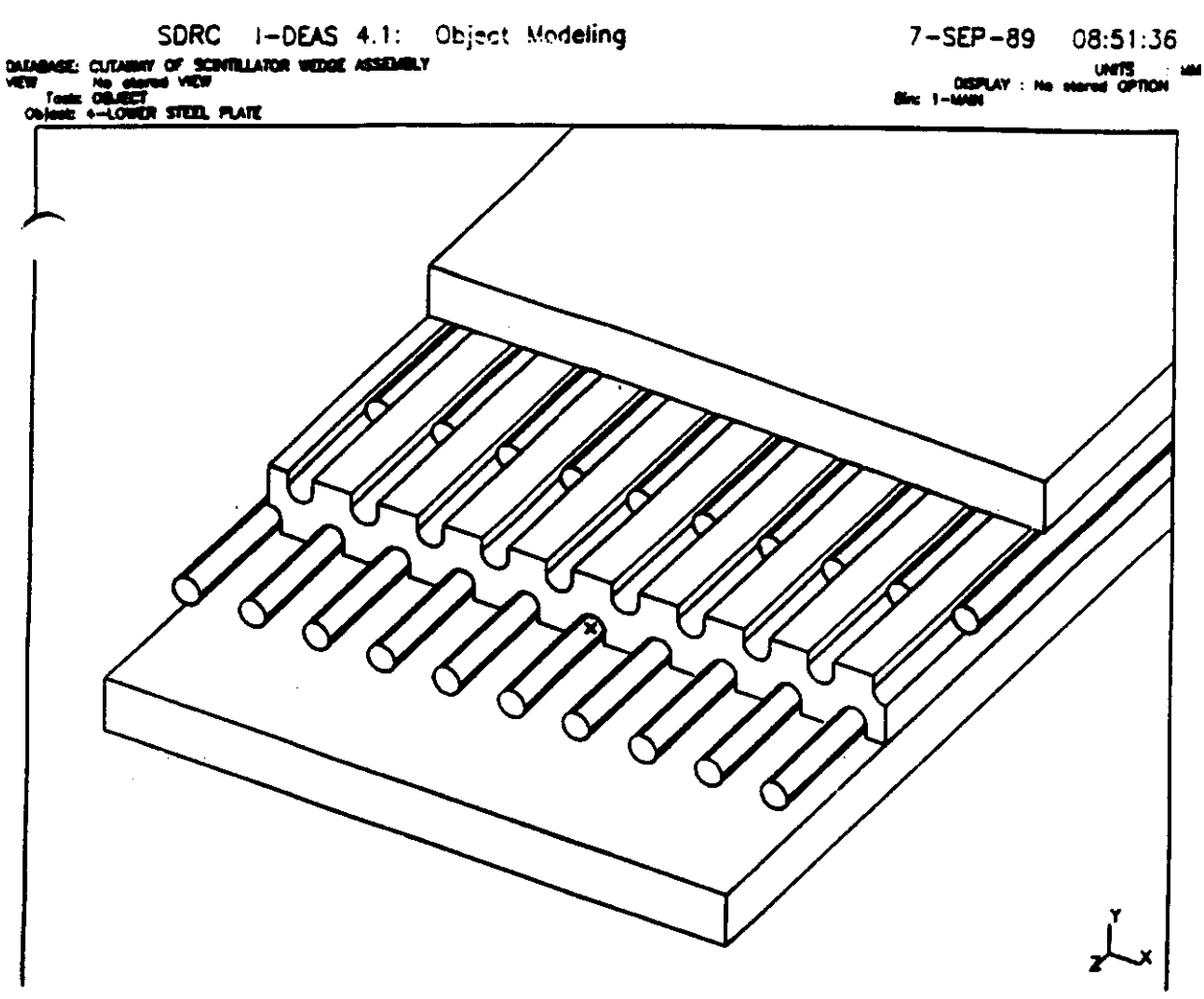
SDRC I-DEAS 4.1: Object Modeling
7-SEP-89 08:51:36
DATABASE: CUTAWAY OF SCINTILLATOR WEDGE ASSEMBLY
VIEW : No stored VIEW
Task: OBJECT
Object: 4-LOWER STEEL PLATE
UNITS : MM
DISPLAY : No stored OPTION
Disc 1-MAIN
Y
Z
X

Fig. 10

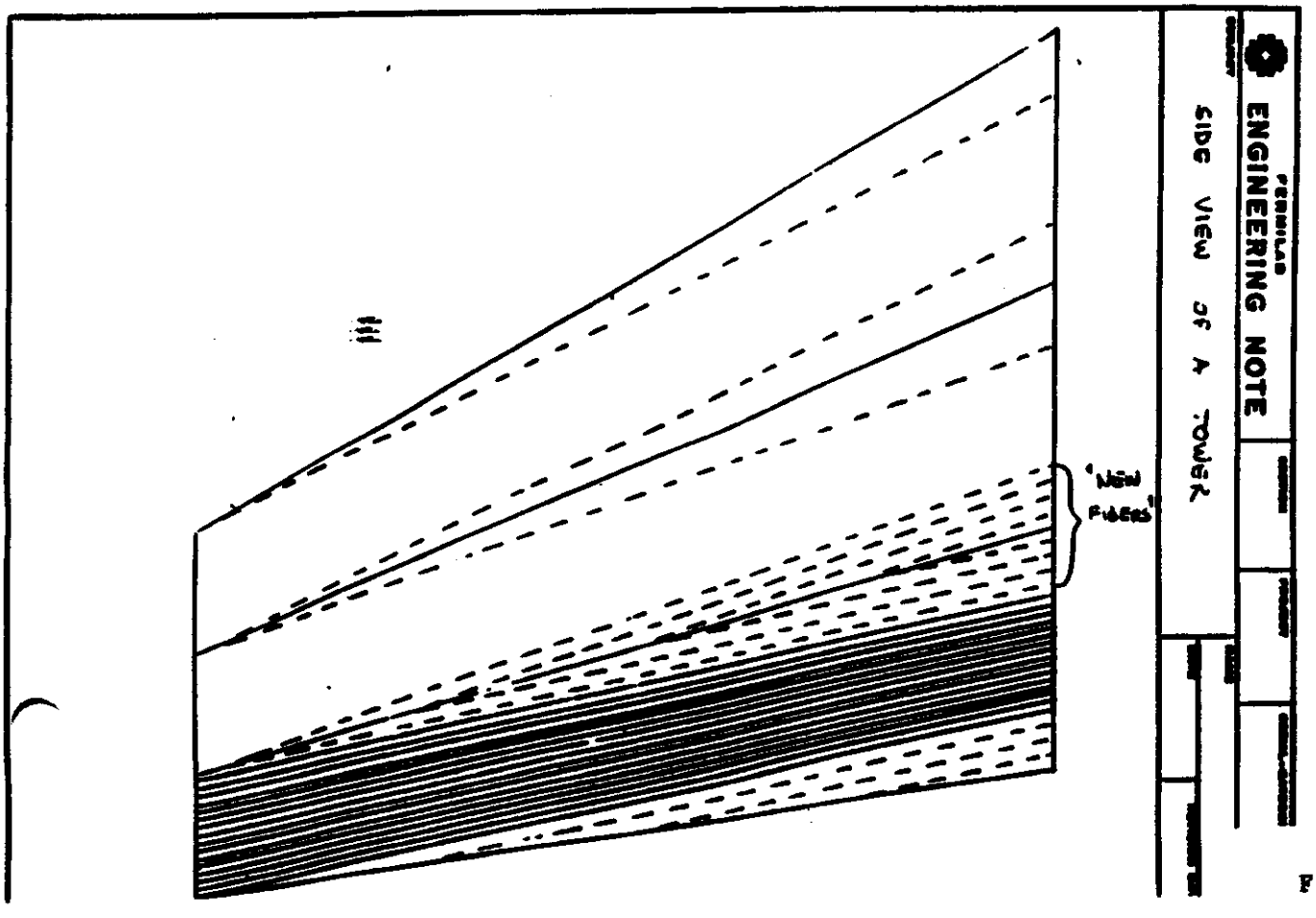
ENGINEERING NOTE
SIDE VIEW OF A TOWER
"NEW FIBERS"

Fig. 11

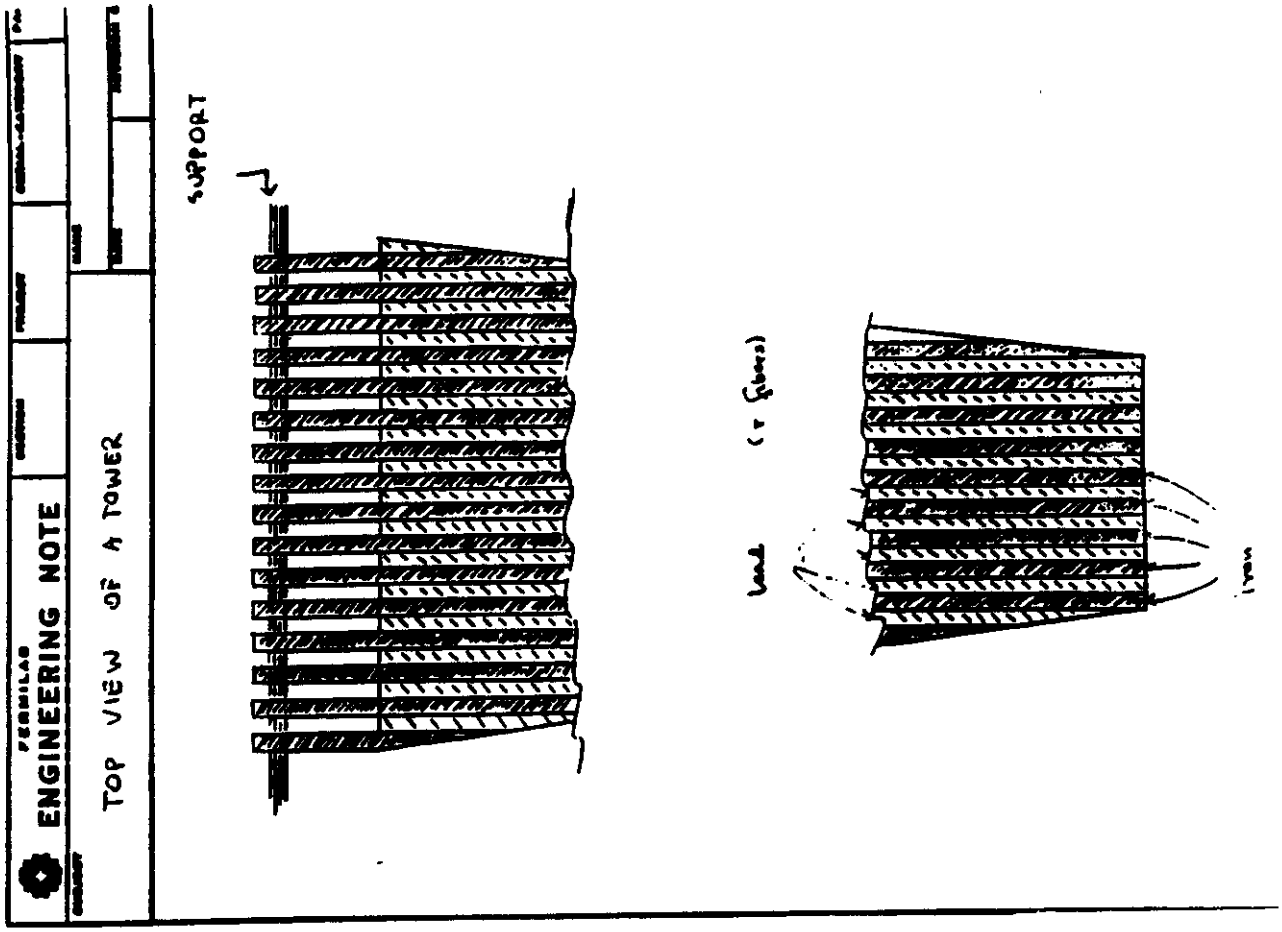
FERMILAB
ENGINEERING NOTE
TOP VIEW OF A TOWER
SUPPORT

Fig. 12

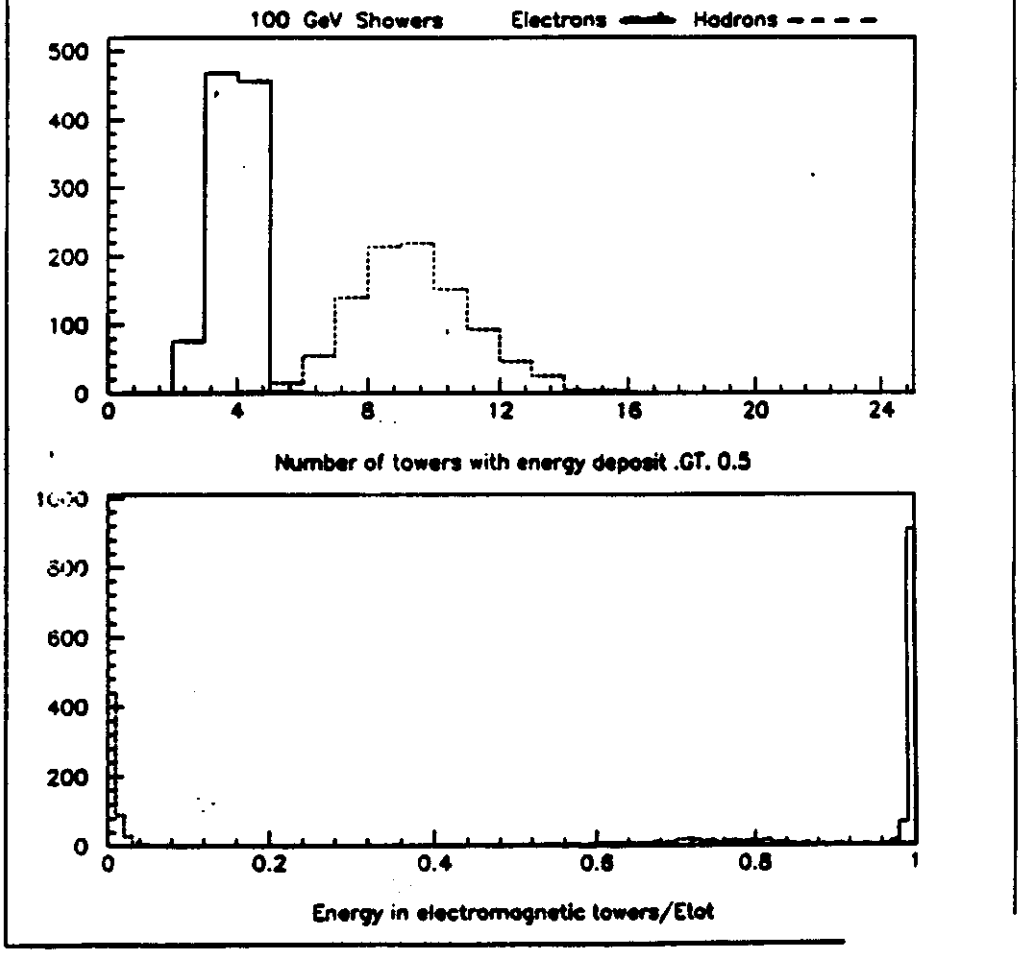
100 GeV Showers
Electrons
Hadrons
500
400
300
200
100
0
0
4
8
12
16
20
24
Number of towers with energy deposit .GT. 0.5
800
600
400
200
0
0
0.2
0.4
0.6
0.8
1
Energy in electromagnetic towers/Etot

Fig. 13

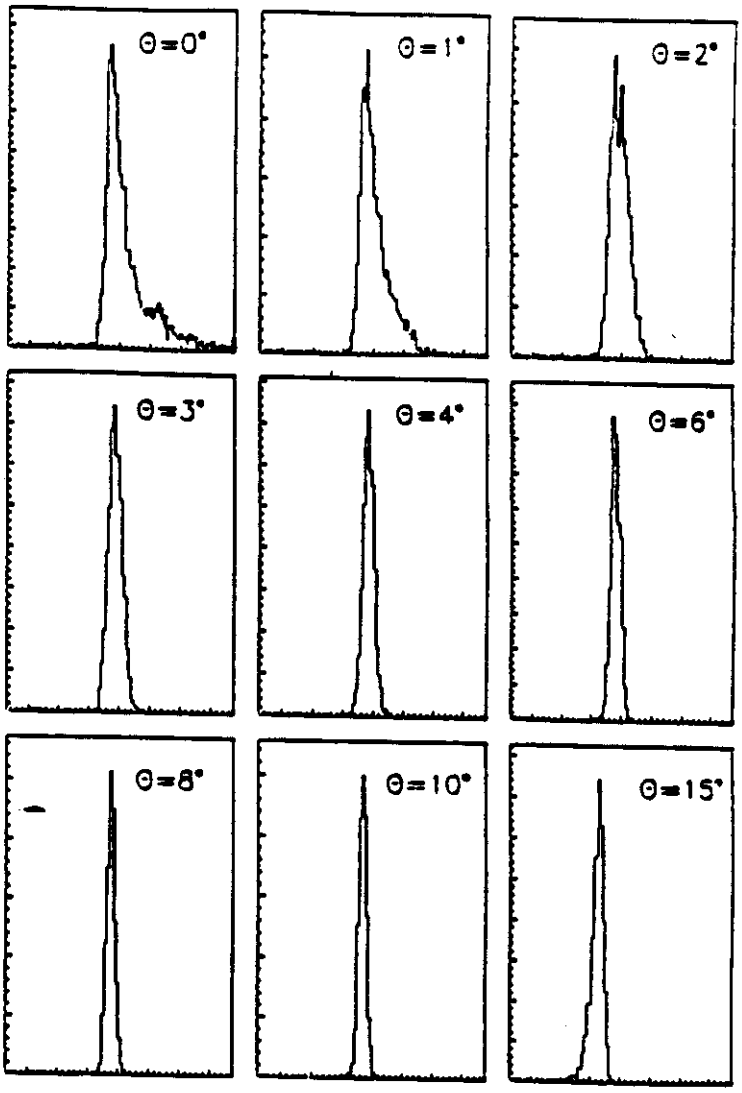

Fig. 14

Fig. 15

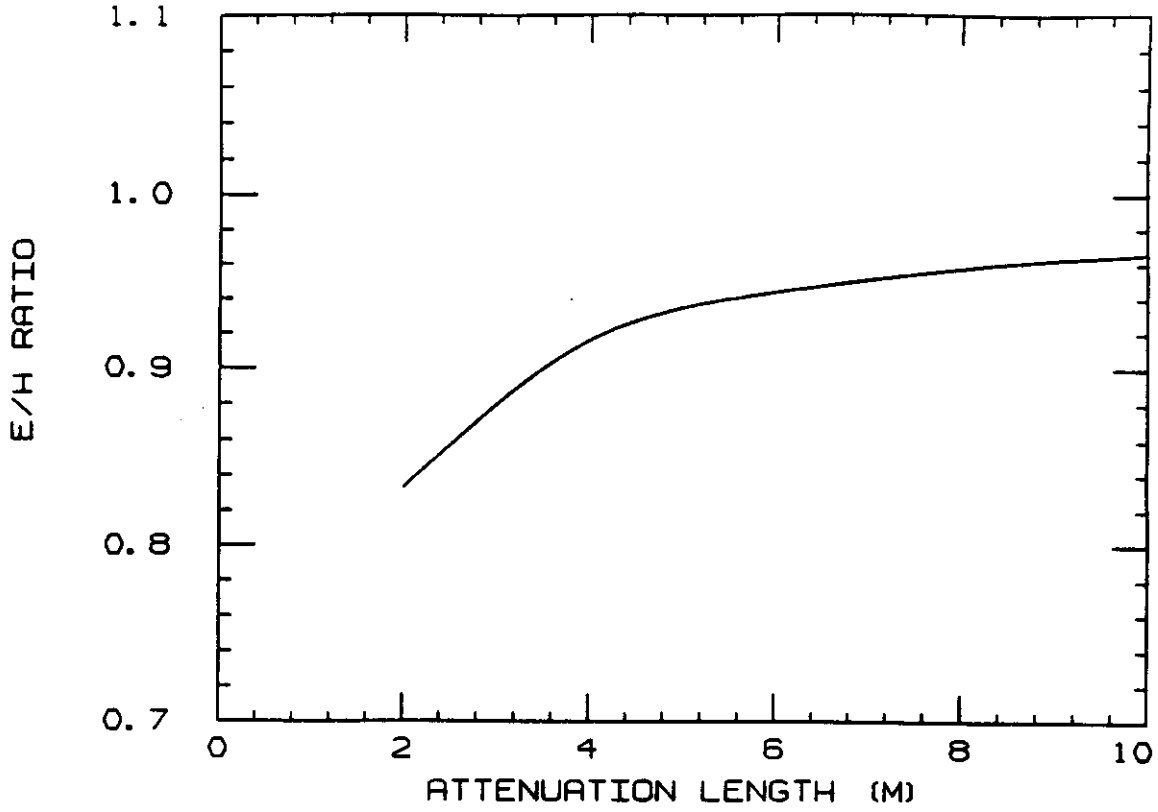
E/H RATIO
1.1
1.0
0.9
0.8
0.7
0
2
4
6
8
10
ATTENUATION LENGTH (M)

Fig. 16

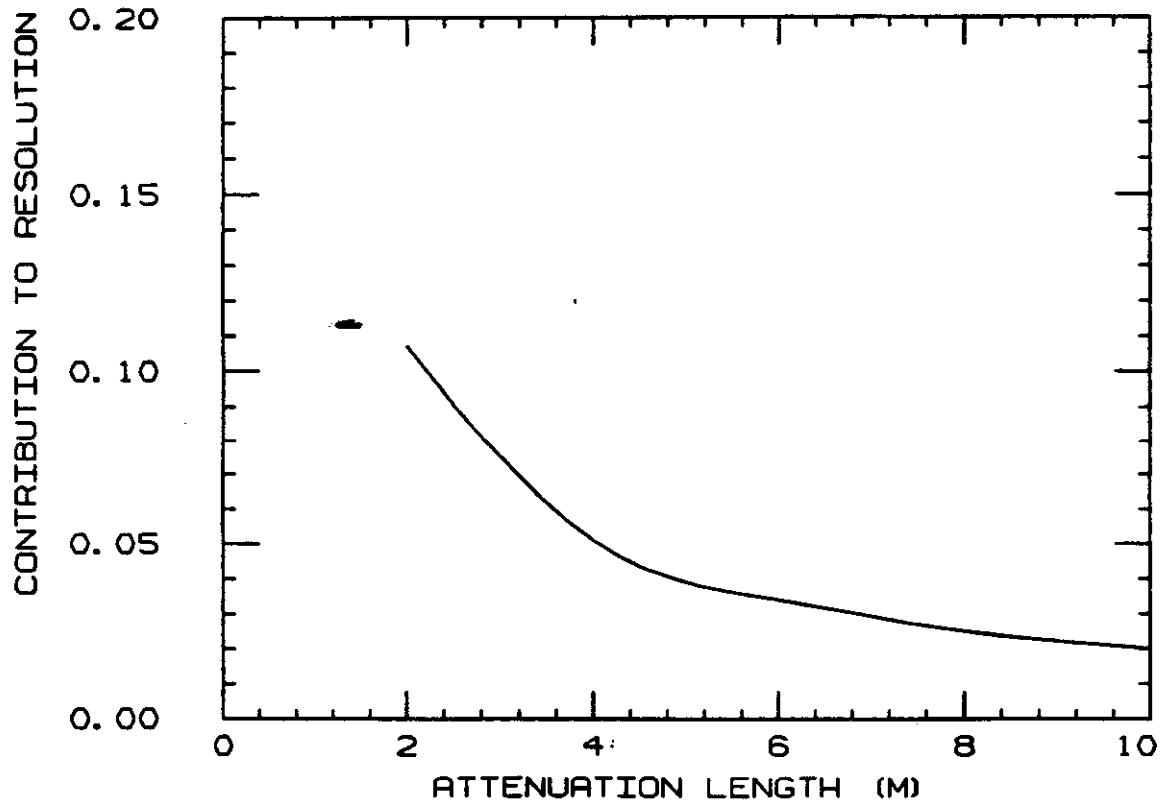
CONTRIBUTION TO RESOLUTION
0.20
0.15
0.10
0.05
0.00
0
2
4
6
8
10
ATTENUATION LENGTH (M)

Fig. 17

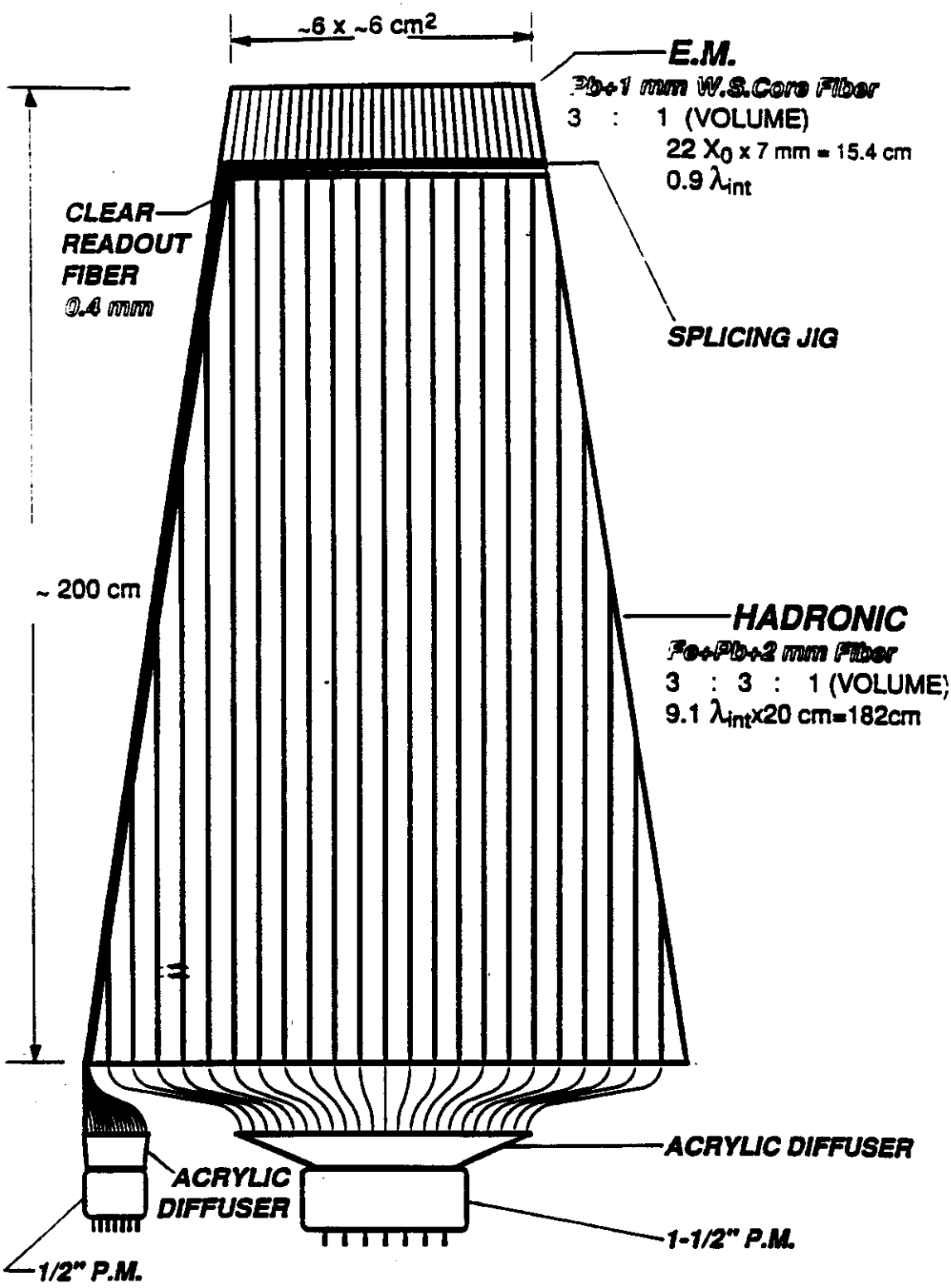
~6 x ~6 cm²
E.M.
Pb+1 mm W.S.Core Fiber
3 : 1 (VOLUME)
22 X0 x 7 mm = 15.4 cm
0.9 λint
CLEAR READOUT FIBER 0.4 mm
SPLICING JIG
~ 200 cm
HADRONIC
Fe+Pb+2 mm Fiber
3 : 3 : 1 (VOLUME)
9.1 λint x20 cm=182cm
ACRYLIC DIFFUSER
ACRYLIC DIFFUSER
1-1/2" P.M.
1/2" P.M.

Fig. 18

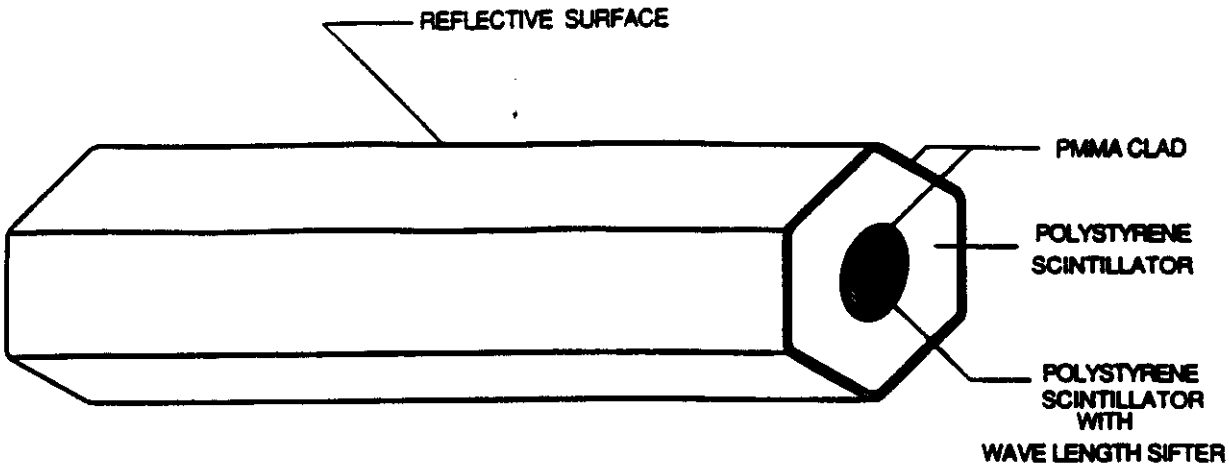

SCINTILLATION FIBER w. WAVE-LENGTH-SHIFTER-CORE

Fig. 19

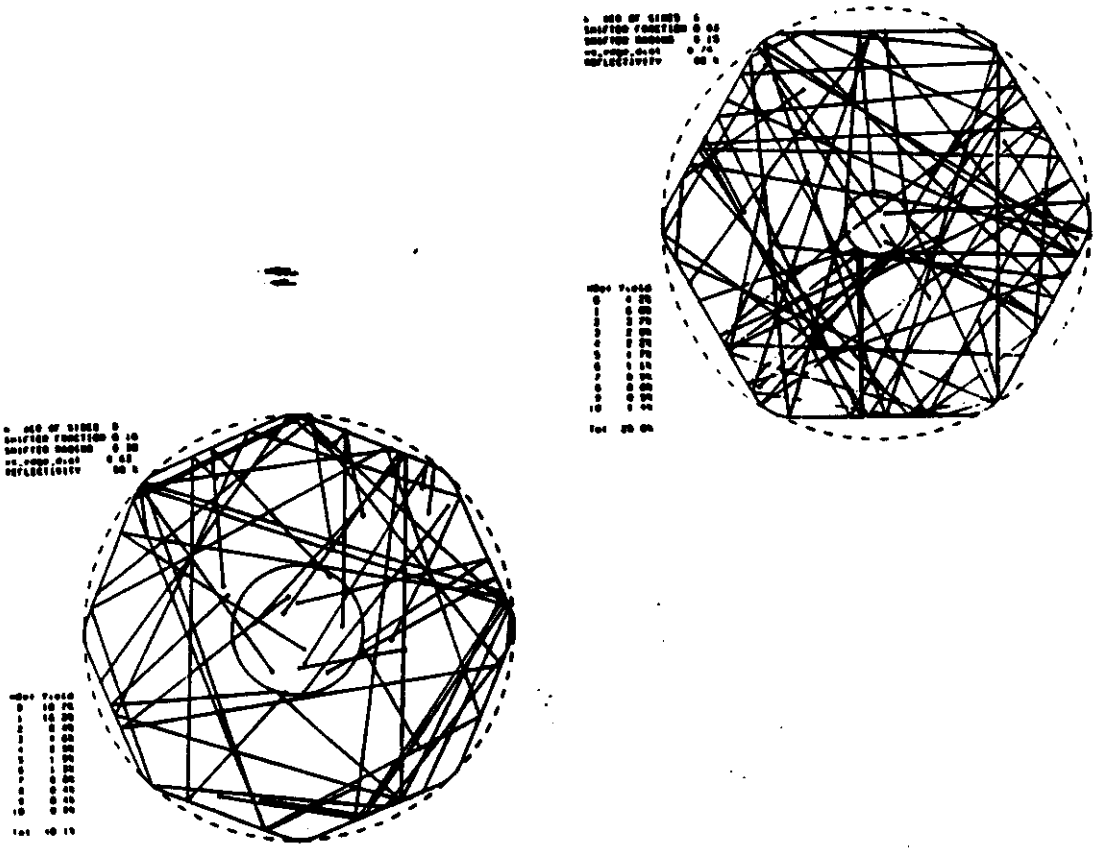

Fig. 20

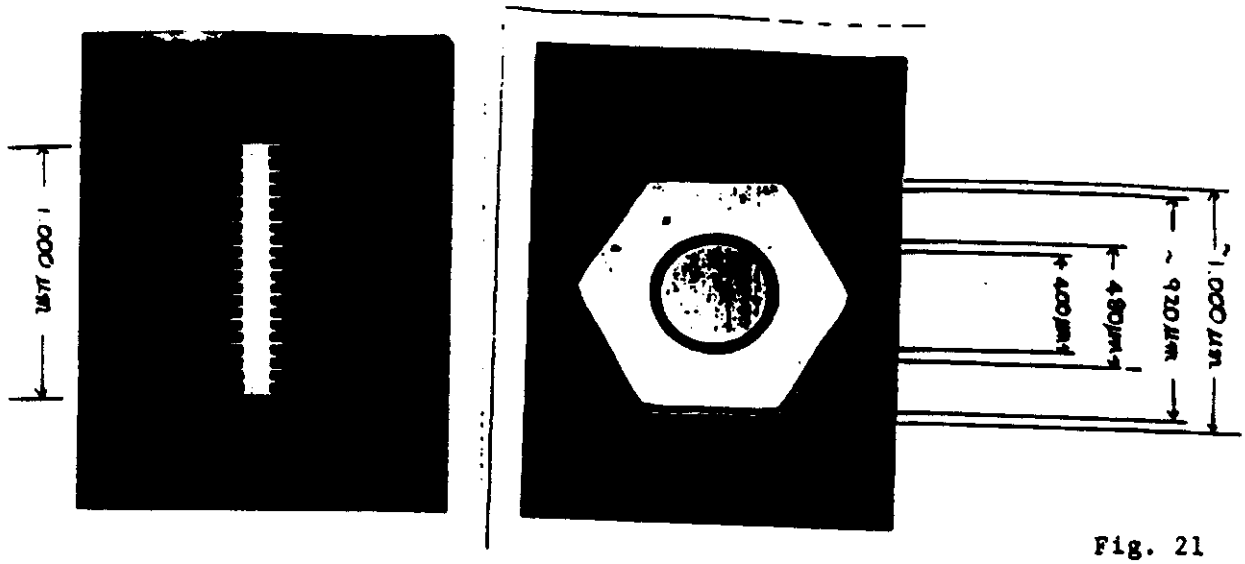

Fig. 21

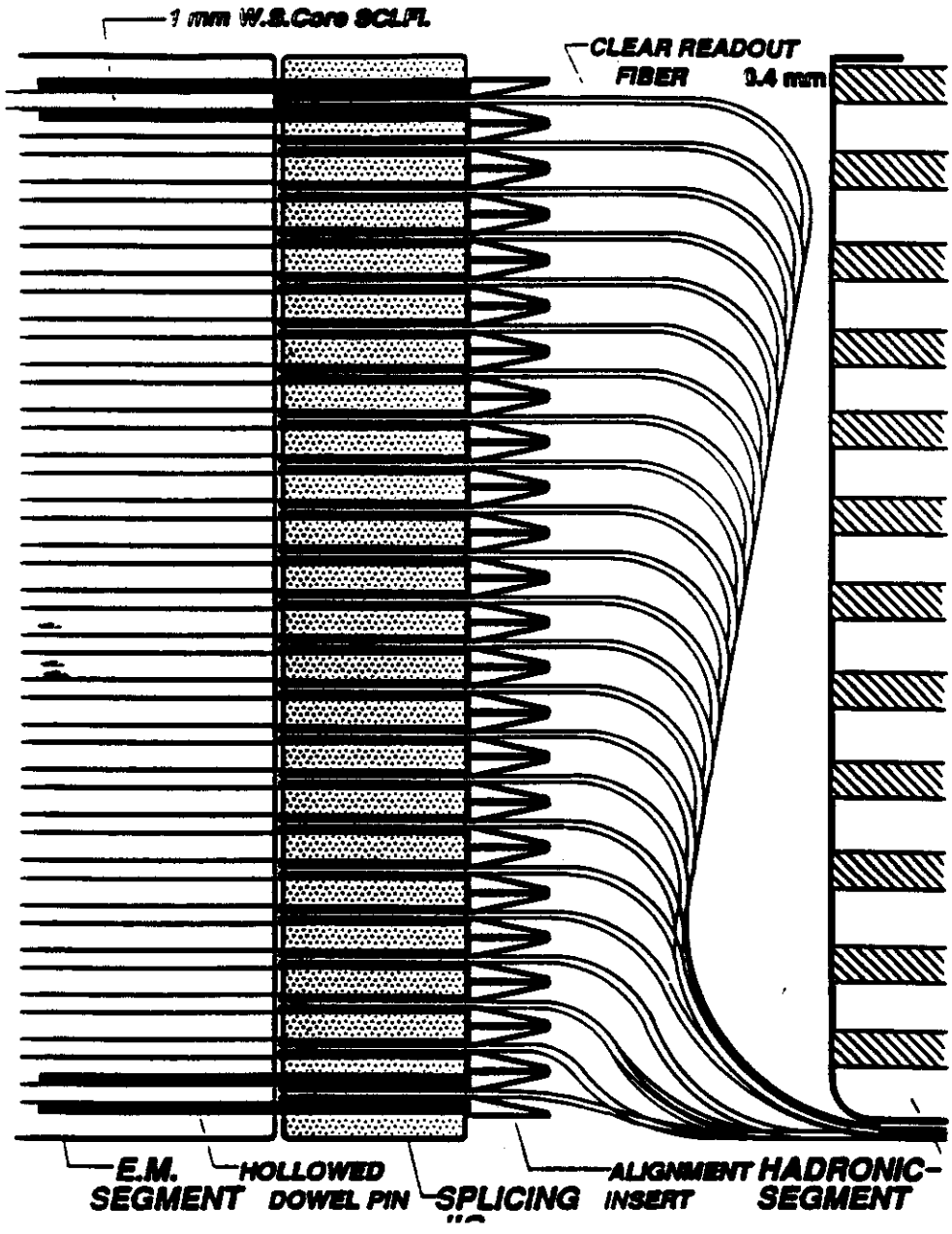
1 mm W.S.Core SCLFI.
CLEAR READOUT FIBER
9.4 mm
E.M. SEGMENT
HOLLOWED DOWEL PIN
SPLICING
ALIGNMENT INSERT
HADRONIC-SEGMENT

Fig. 22

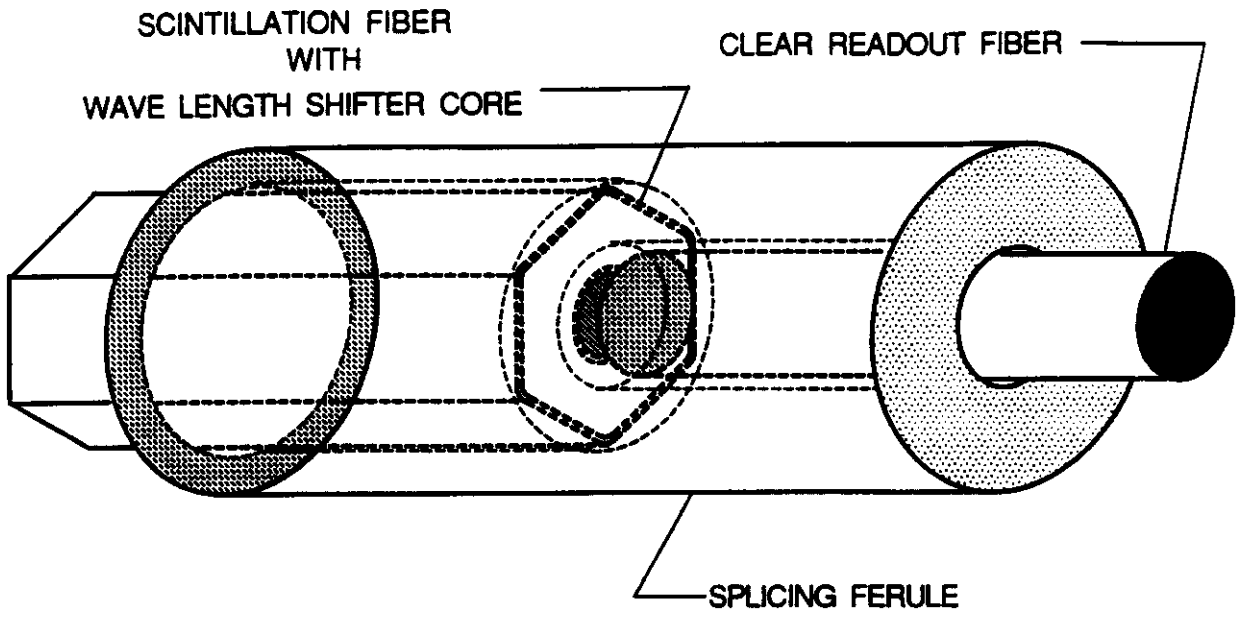

FIBER BY FIBER SPLICING

Fig. 23

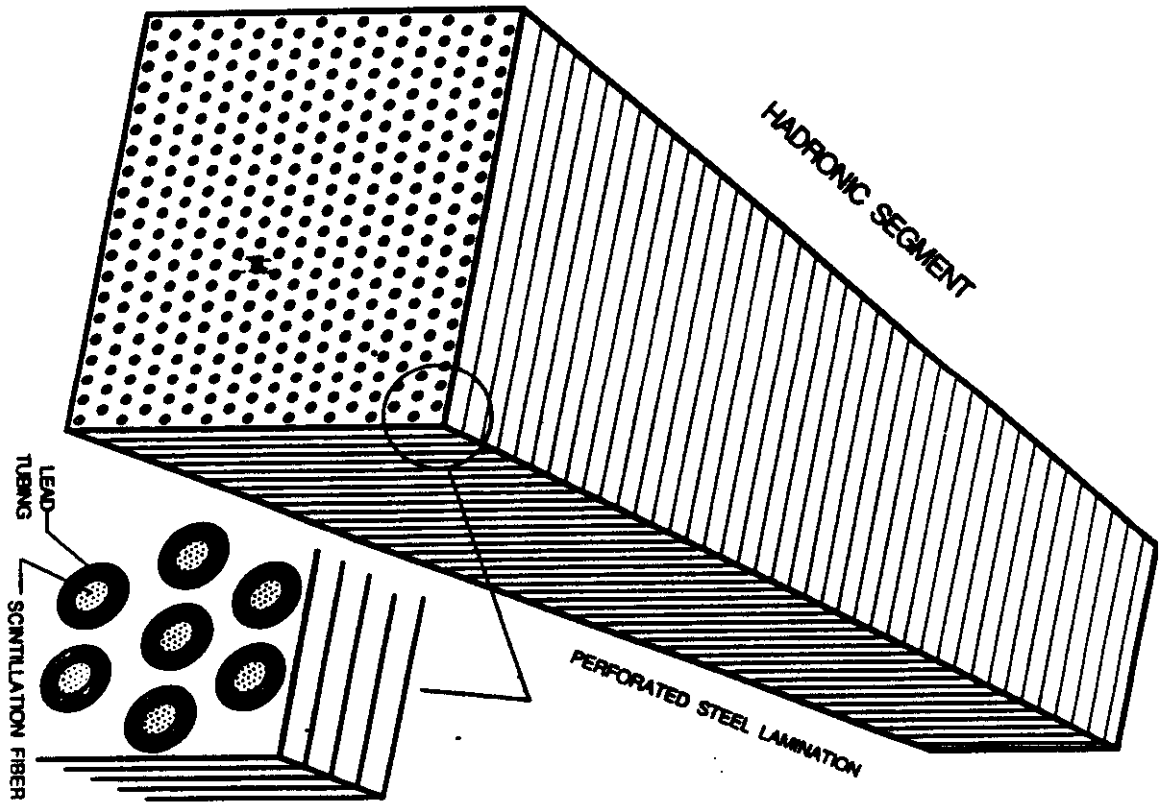

Fig. 24

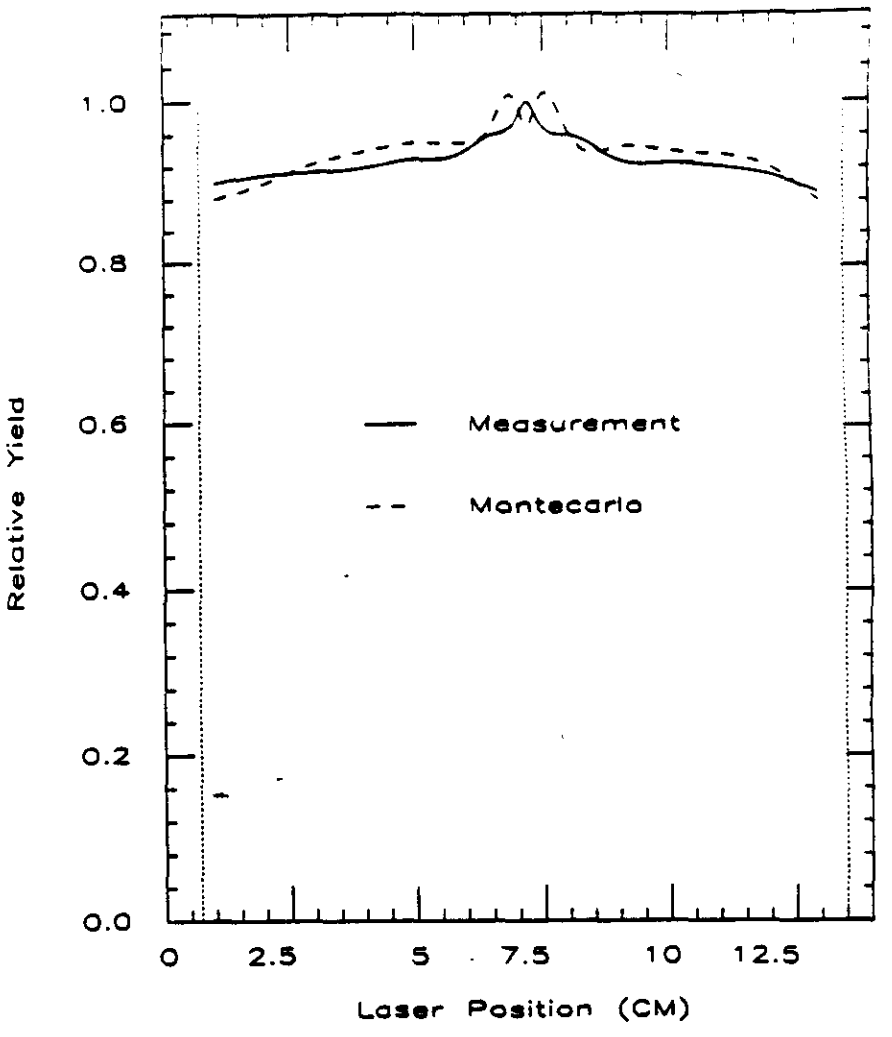
1.0
0.8
0.6
0.4
0.2
0.0
Relative Yield
Measurement
Montecarlo
0
2.5
5
7.5
10
12.5
Laser Position (CM)

Fig. 25

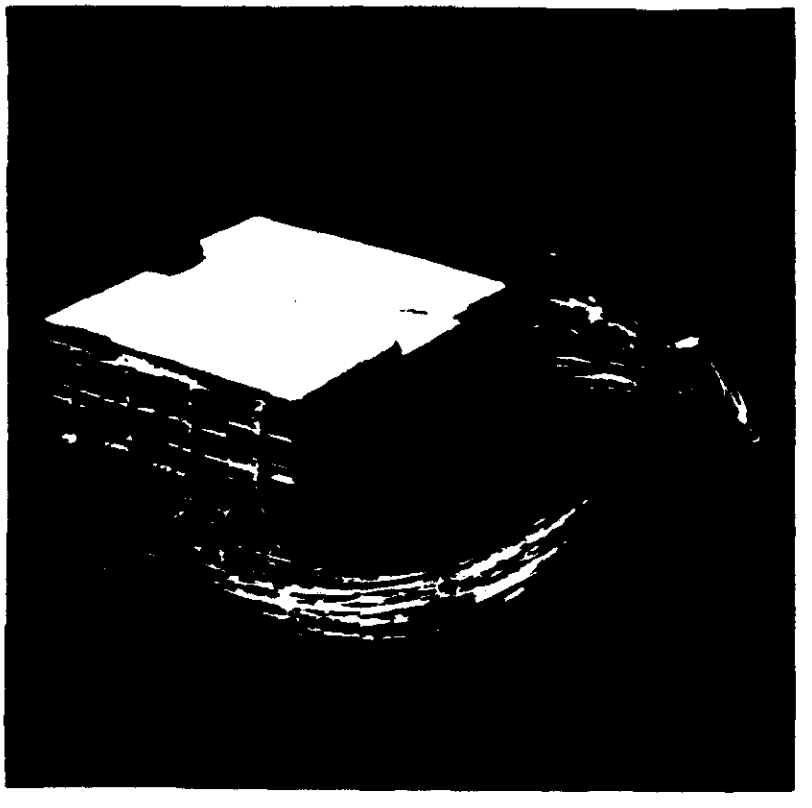

Fig. 26

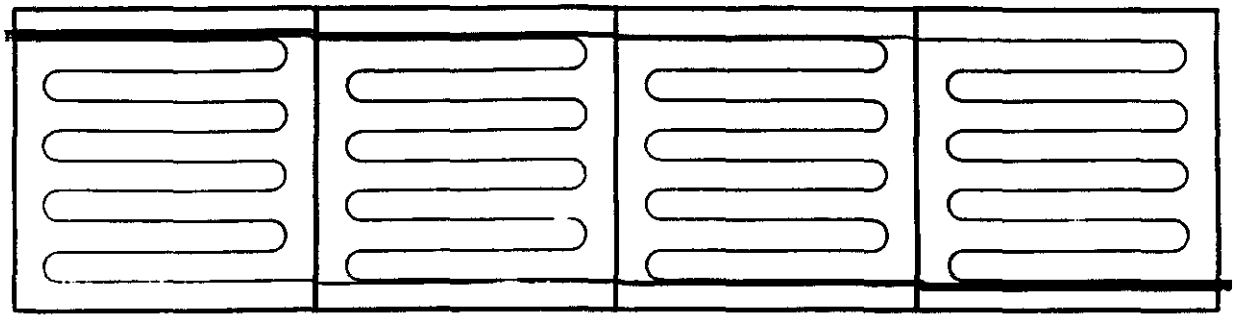

Fig. 27

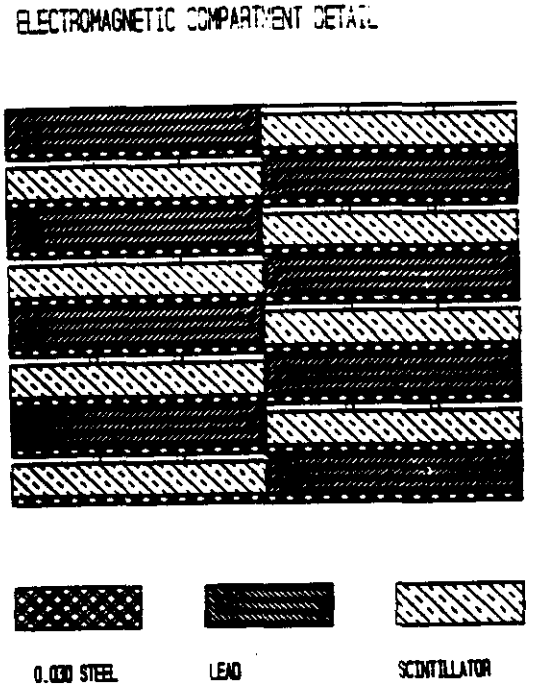

Fig. 28

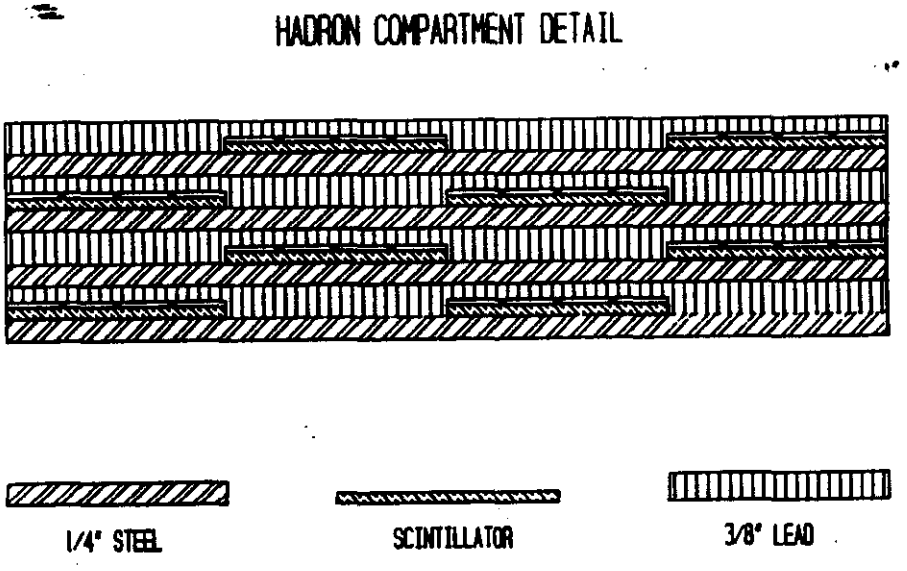

Fig. 29

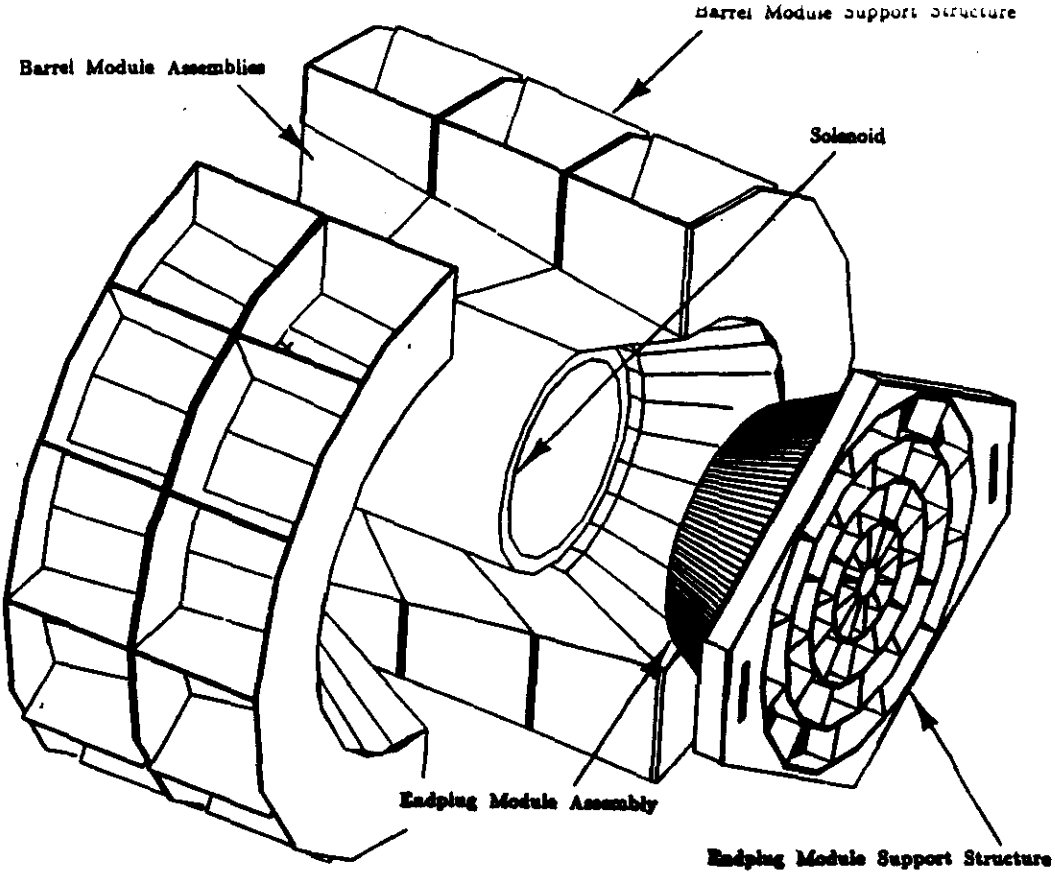

Model of Detector

Fig. 30

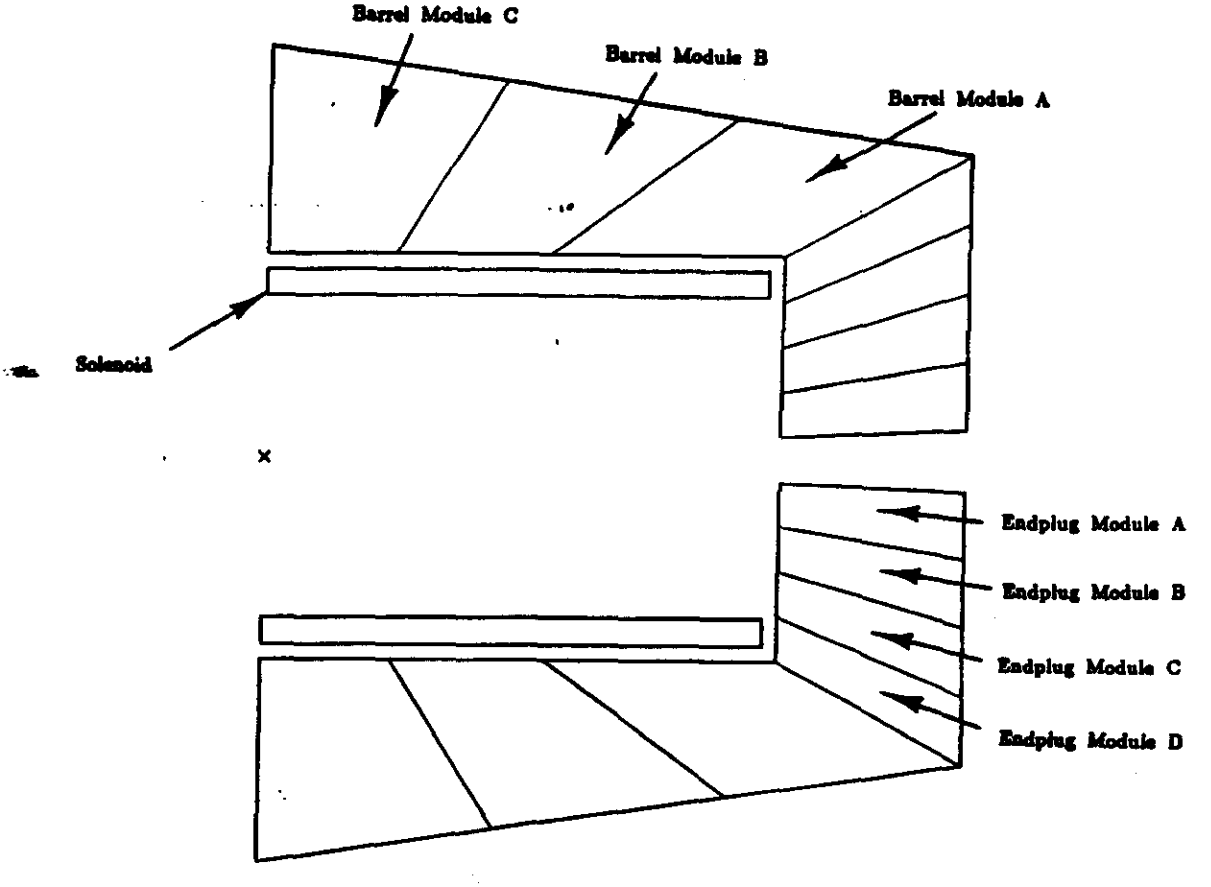

Detector Cross Section

Fig. 31

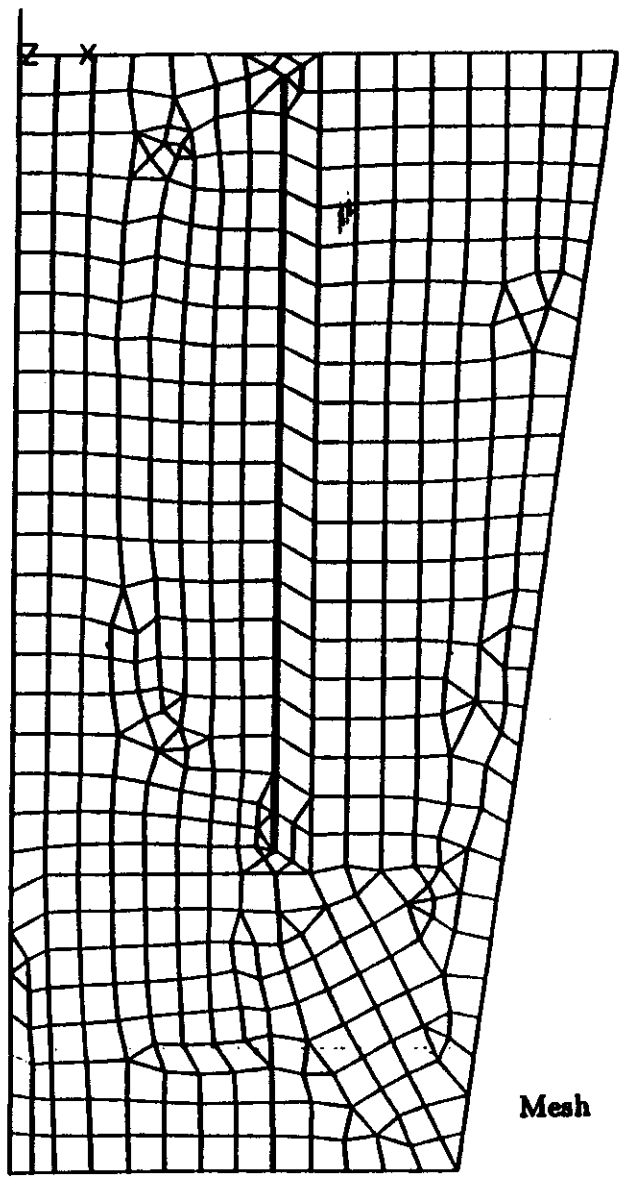

Mesh

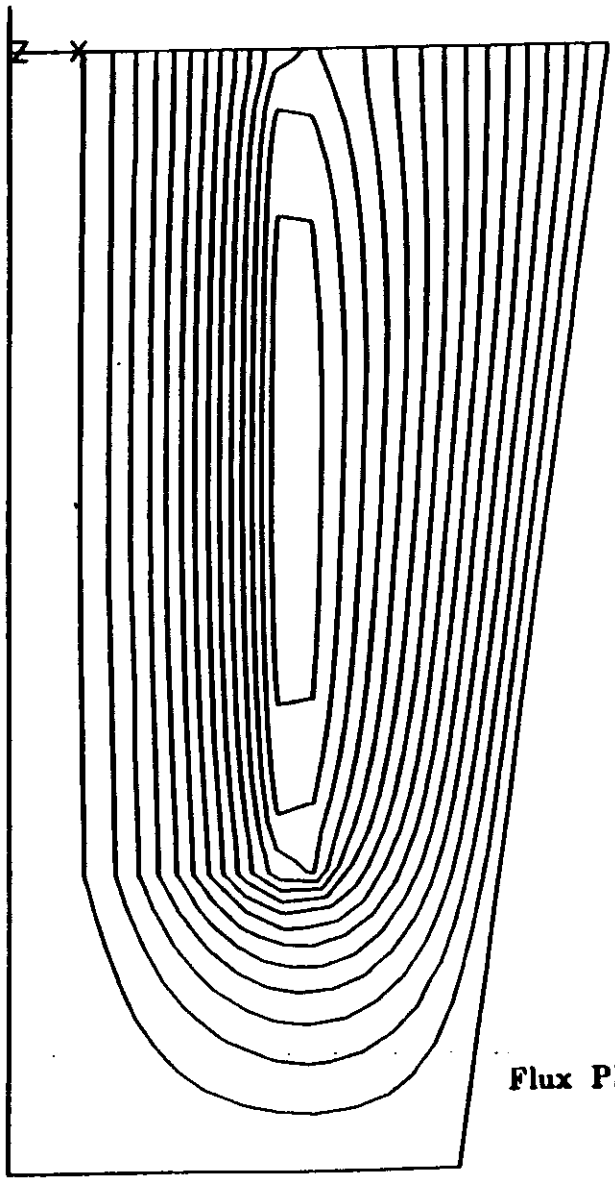

Flux Plot

Fig. 32

Finite Element Magnetic Model

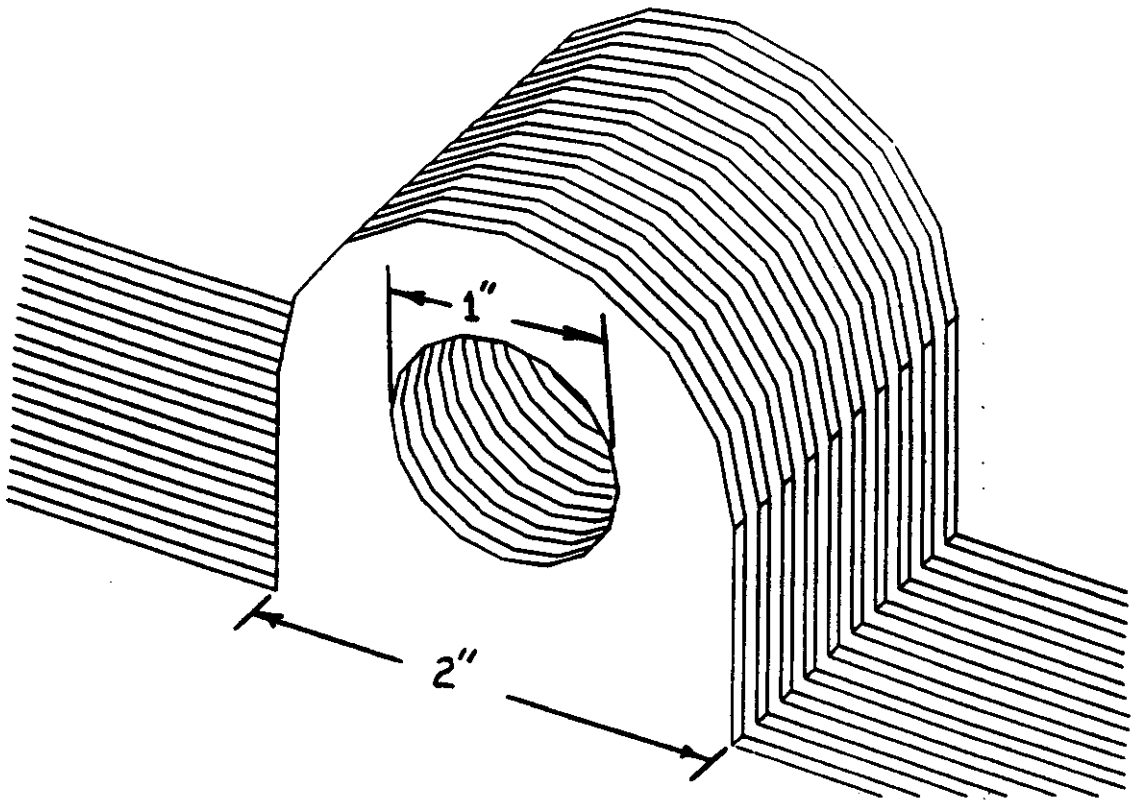

Support Ear Geometry

Fig. 33

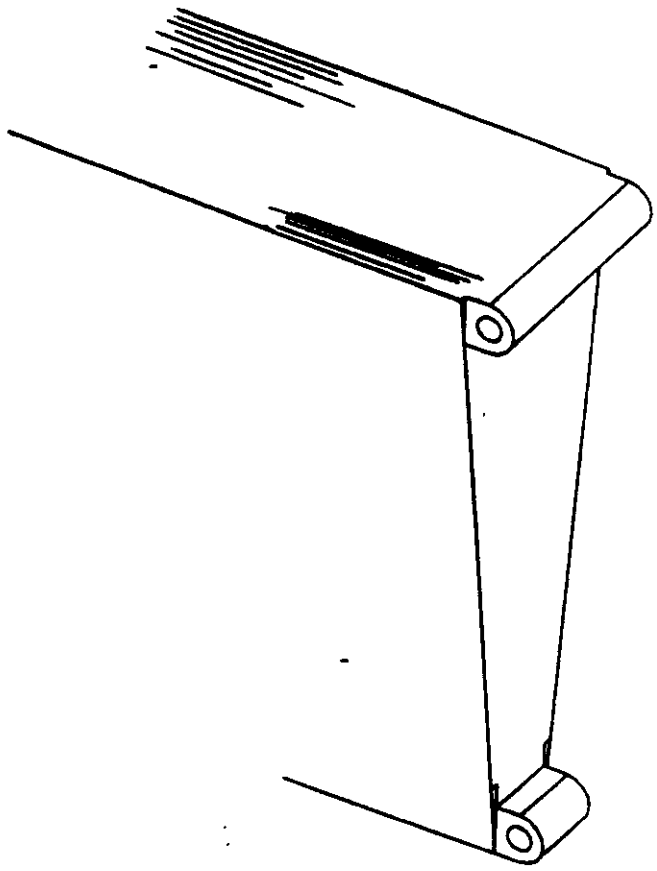

Endplug Module Support Ears

Fig. 34

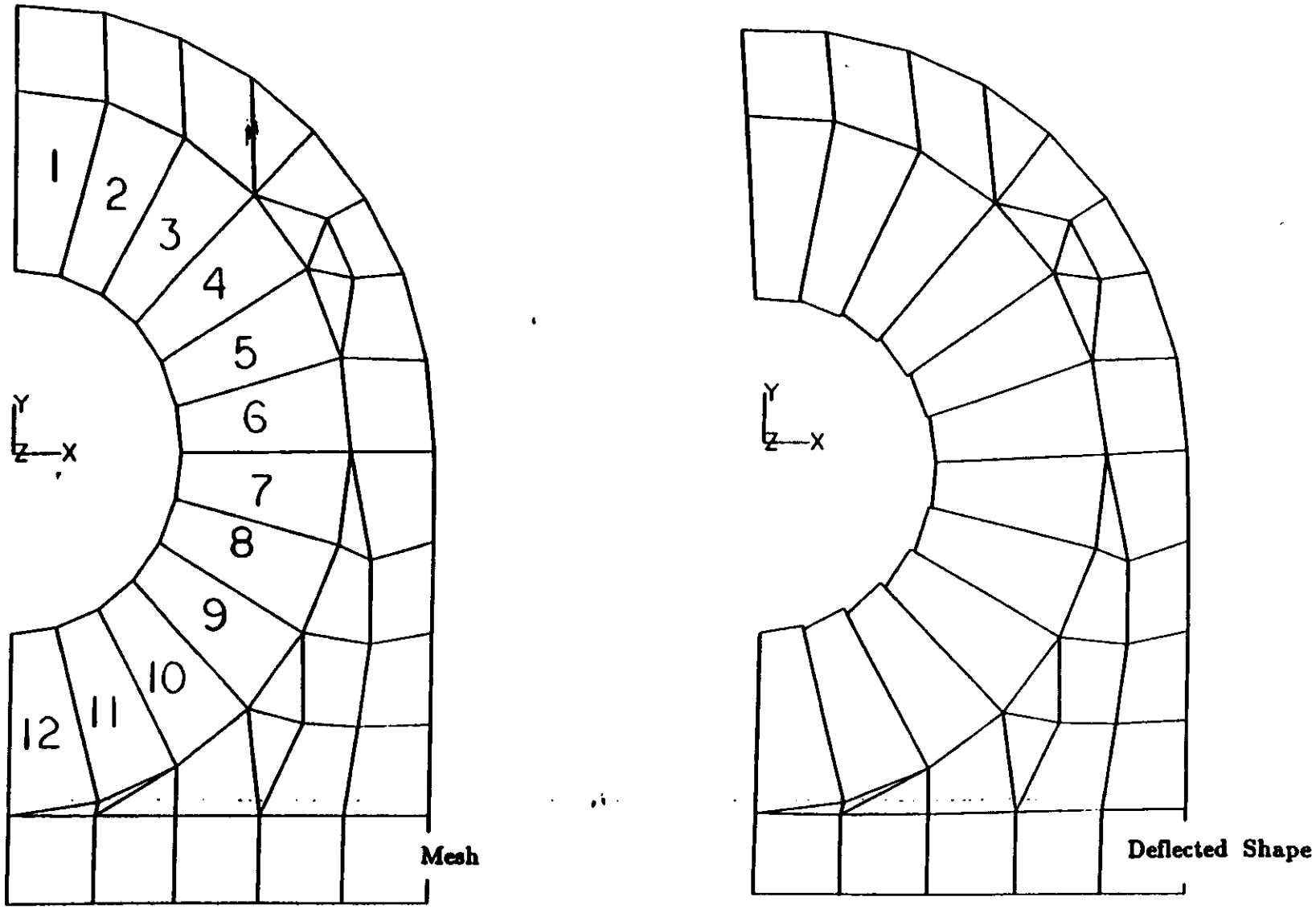

Fig. 35

Finite Element Model of Barrel Assembly

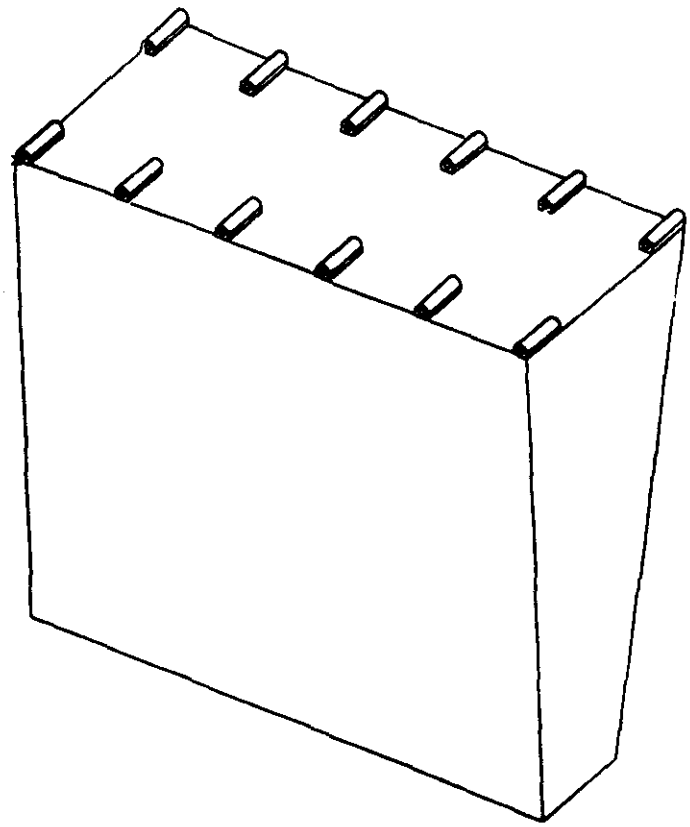

Barrel Module Support Ears Fig. 36

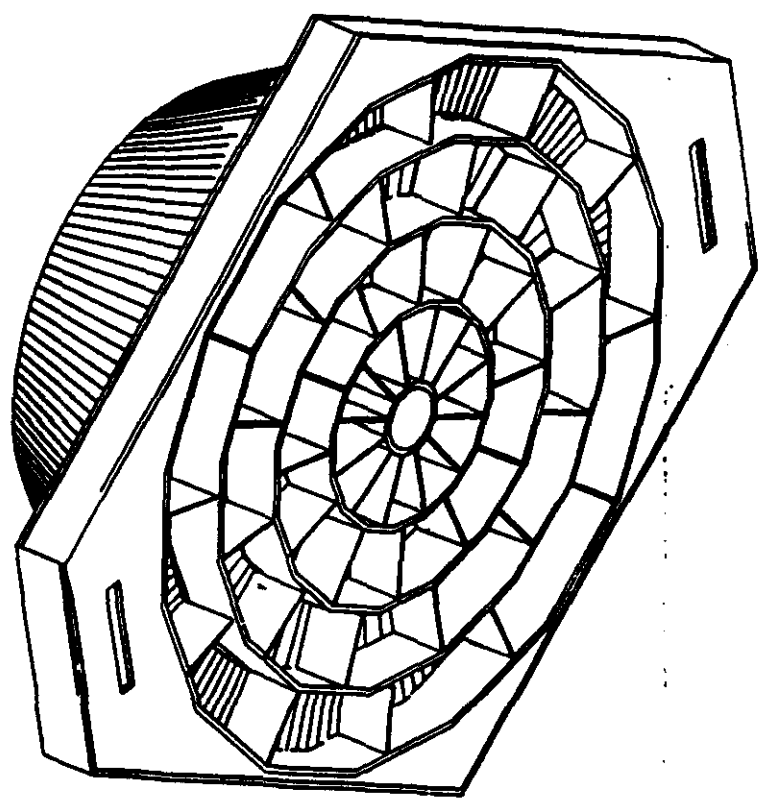

Endplug Module Support Fig. 37

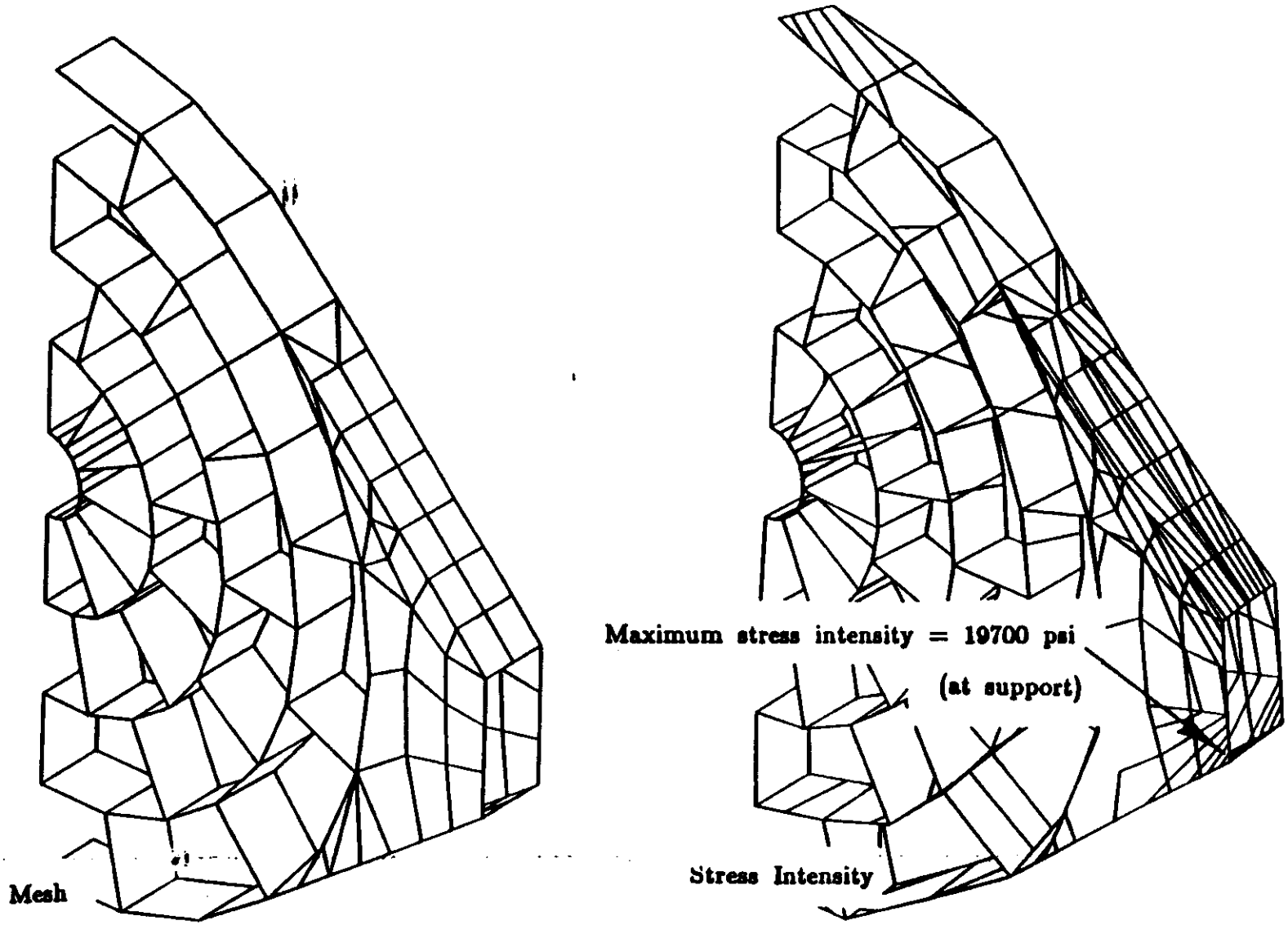

Fig. 38

Finite Element Model of Endplug Support Structure

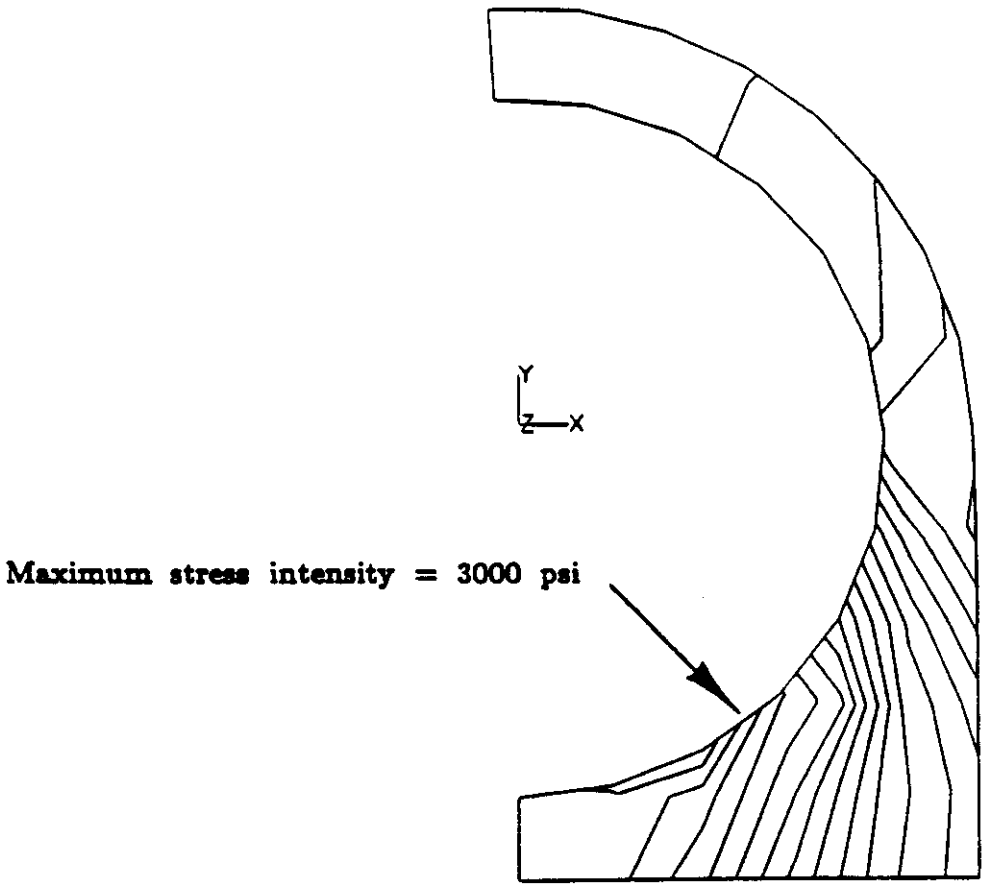

Stress Intensity in Barrel Assembly Support Structure

Fig. 39

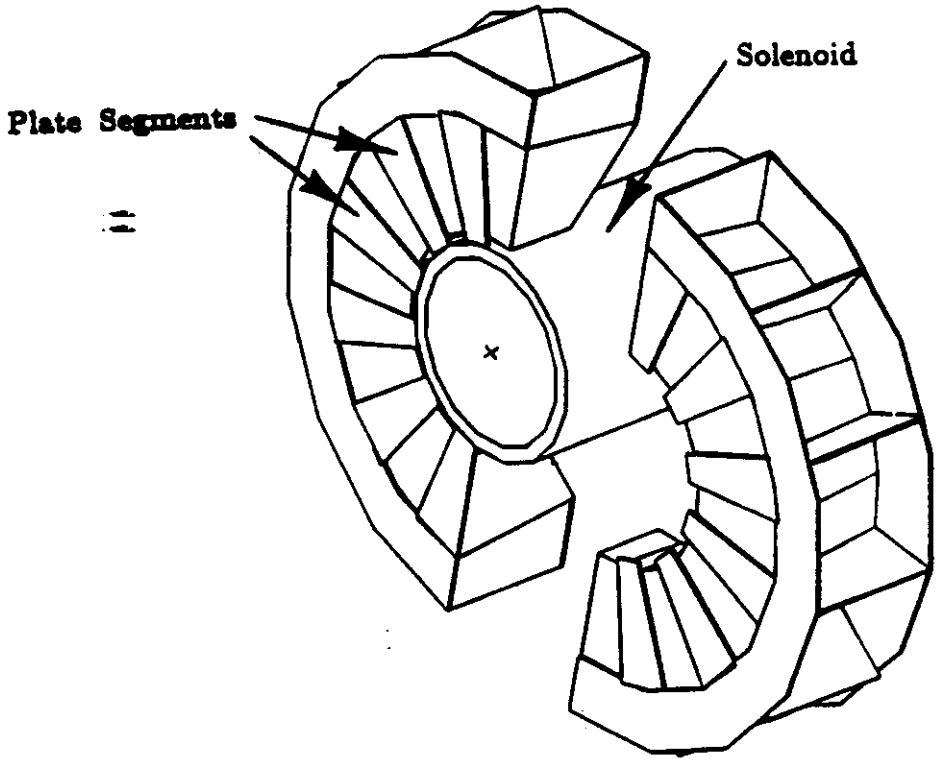

Fig. 40

Solenoid Support at Detector Midplane

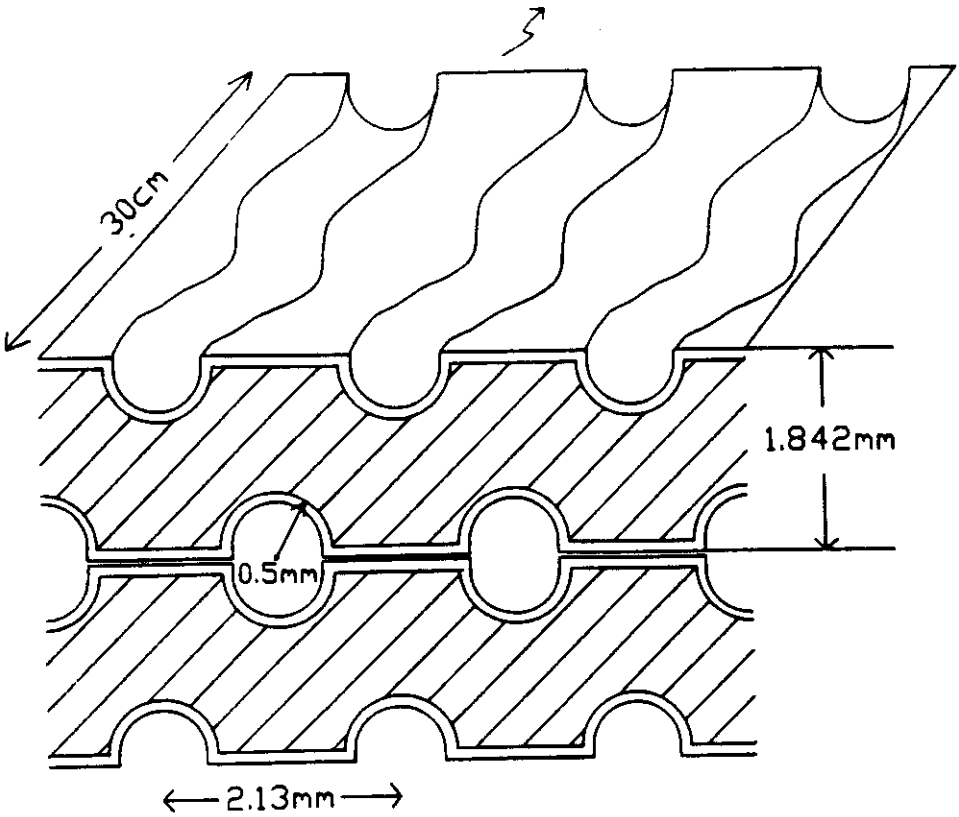
30cm
1.842mm
0.5mm
2.13mm

Fig. 41

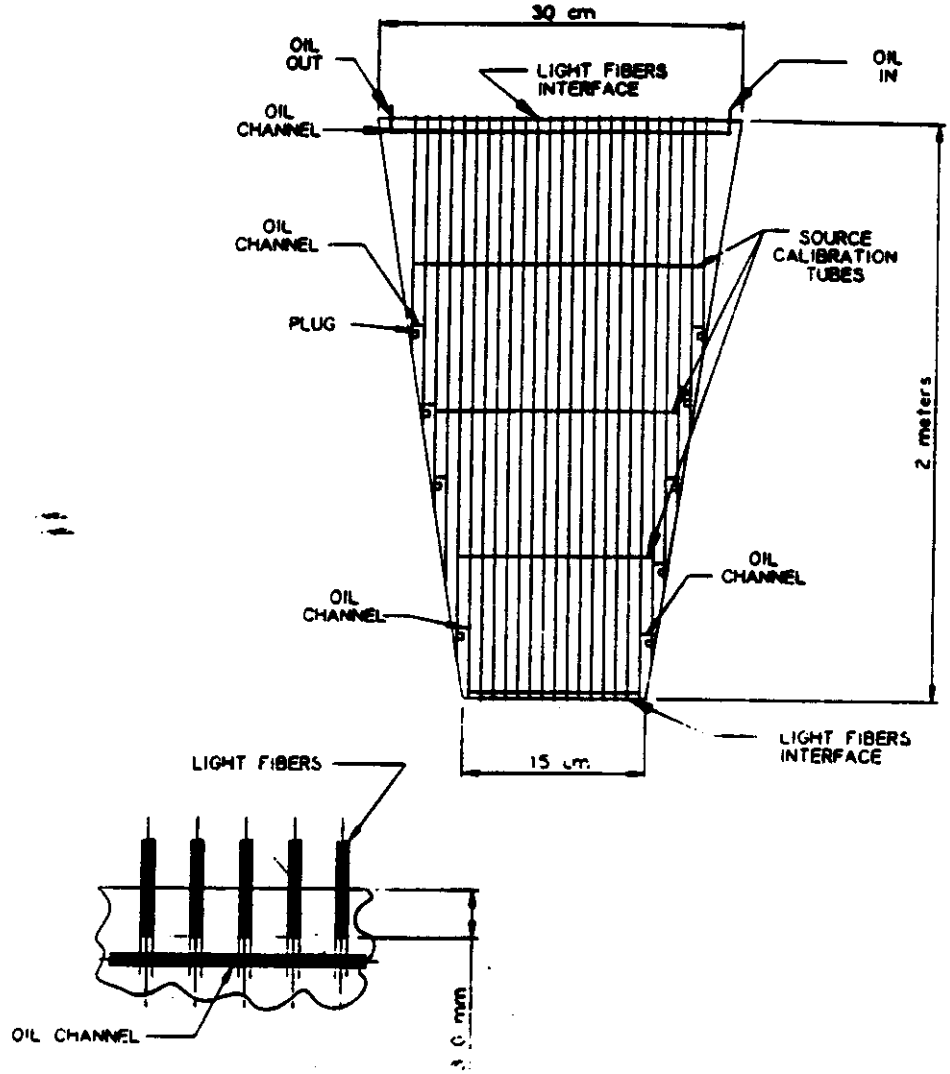
30 cm
OIL OUT
LIGHT FIBERS INTERFACE
OIL IN
OIL CHANNEL
OIL CHANNEL
SOURCE CALIBRATION TUBES
PLUG
2 meters
OIL CHANNEL
OIL CHANNEL
LIGHT FIBERS INTERFACE
15 cm.
LIGHT FIBERS
OIL CHANNEL
6 mm

Fig. 42

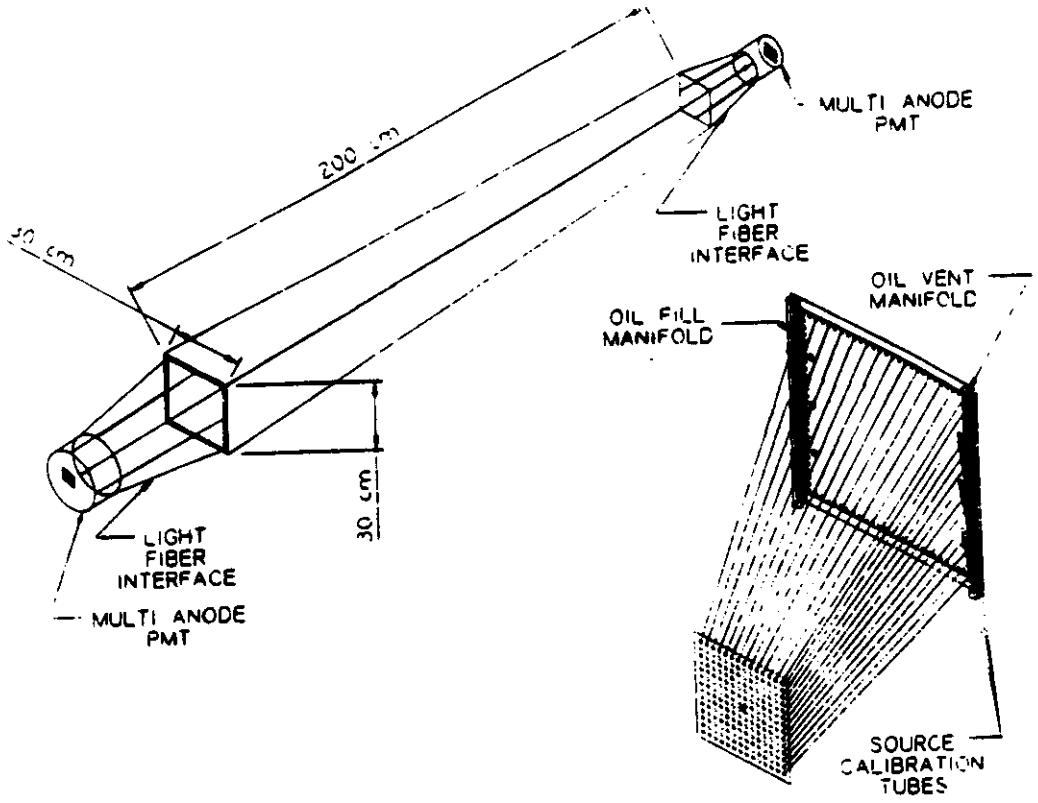
200 cm
30 cm
30 cm
MULTI ANODE PMT
LIGHT FIBER INTERFACE
OIL VENT MANIFOLD
OIL FILL MANIFOLD
LIGHT FIBER INTERFACE
MULTI ANODE PMT
SOURCE CALIBRATION TUBES

Fig. 43

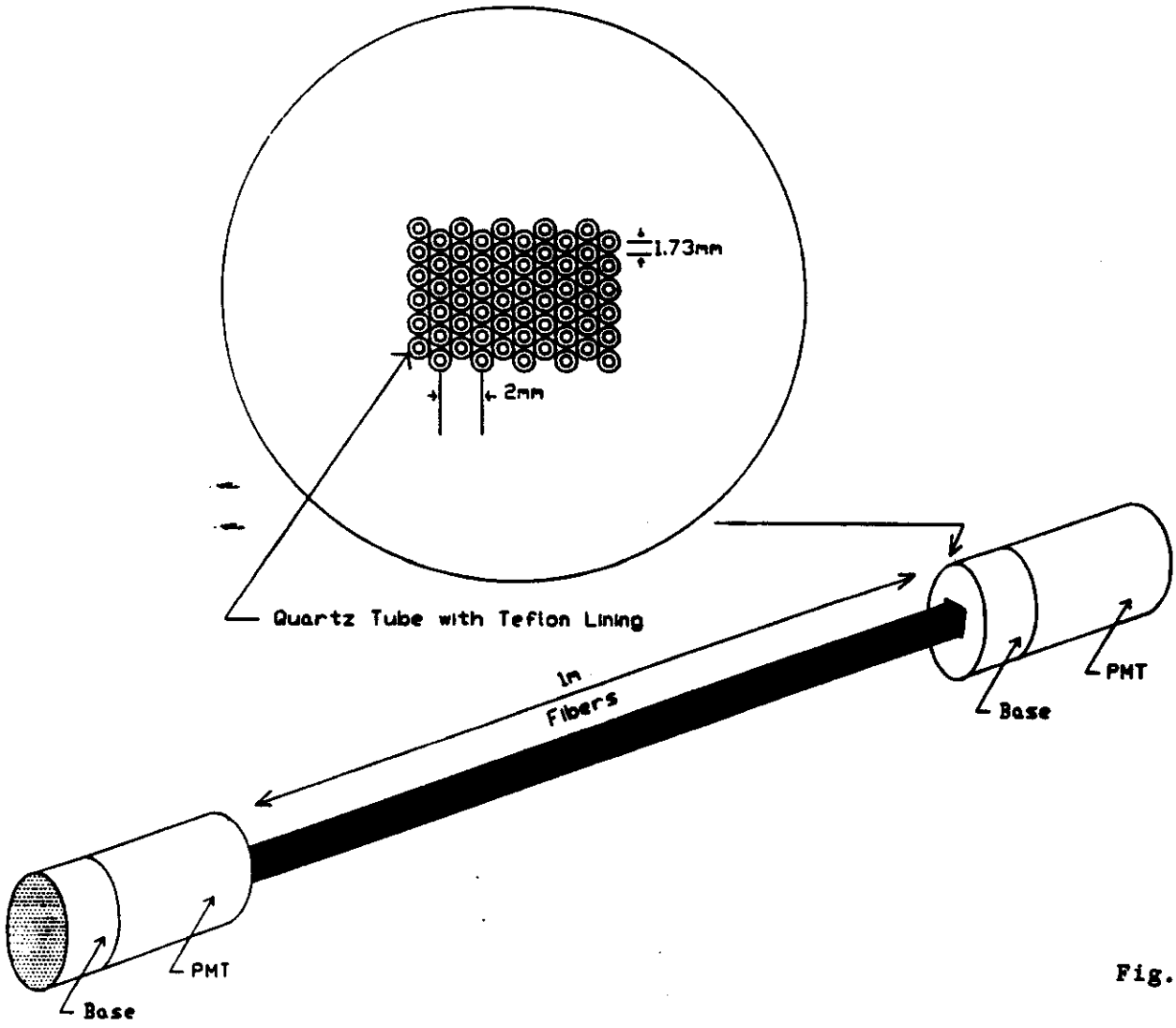
±1.73mm
2mm
Quartz Tube with Teflon Lining
In Fibers
PMT
Base
PMT
Base

Fig. 44

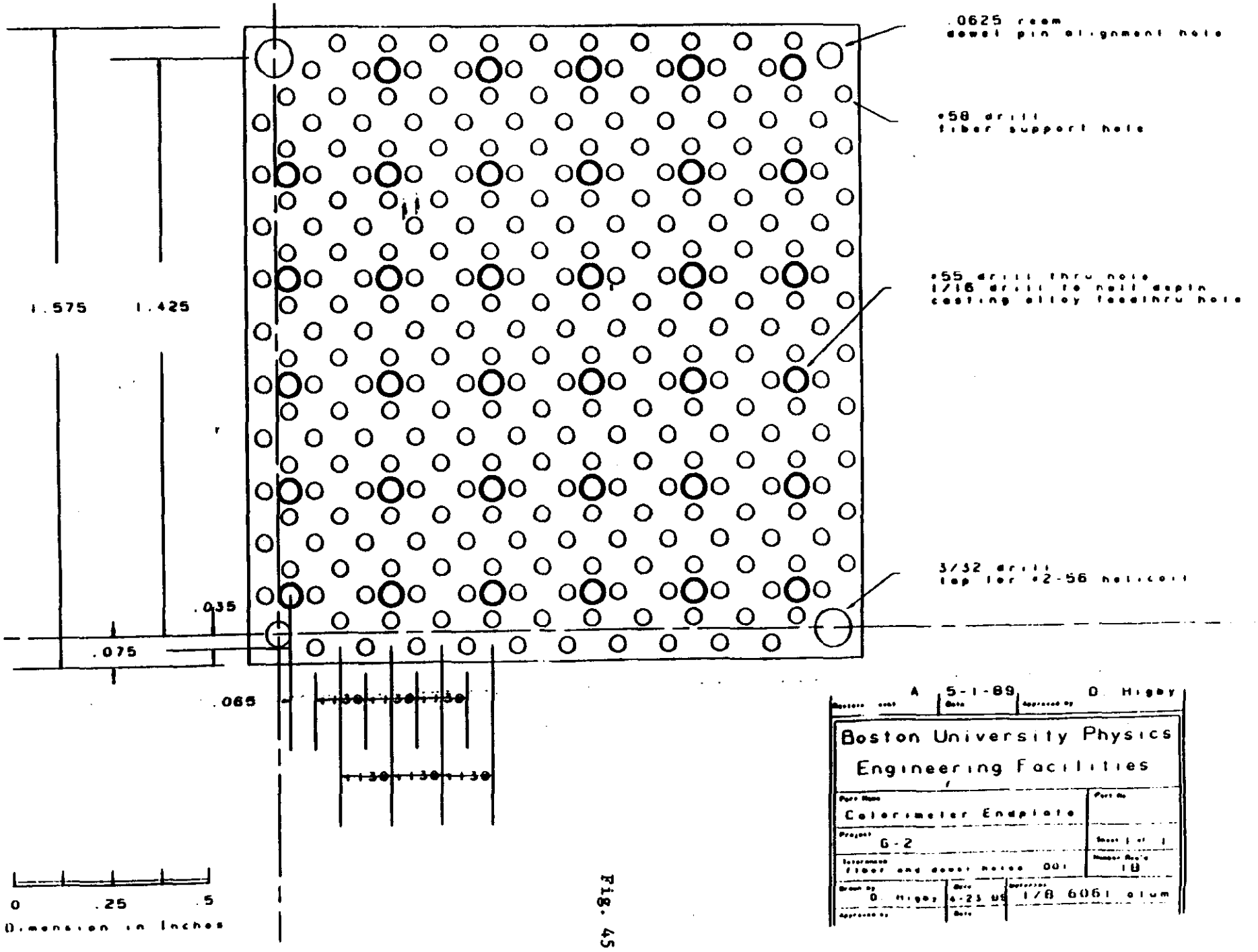

A	5-1-89	D Higey	
Boston University Physics Engineering Facilities			
Part Name: Calorimeter Endplate		Part No.	
Project: G-2		Sheet 1 of 1	
Information: fiber and dowel holes 001		Drawing No.: 18	
Drawn by: D Higey	Date: 4-25-89	Approved: 1/8 6061 alum	
Approved by:	Date:		

Fig. 45

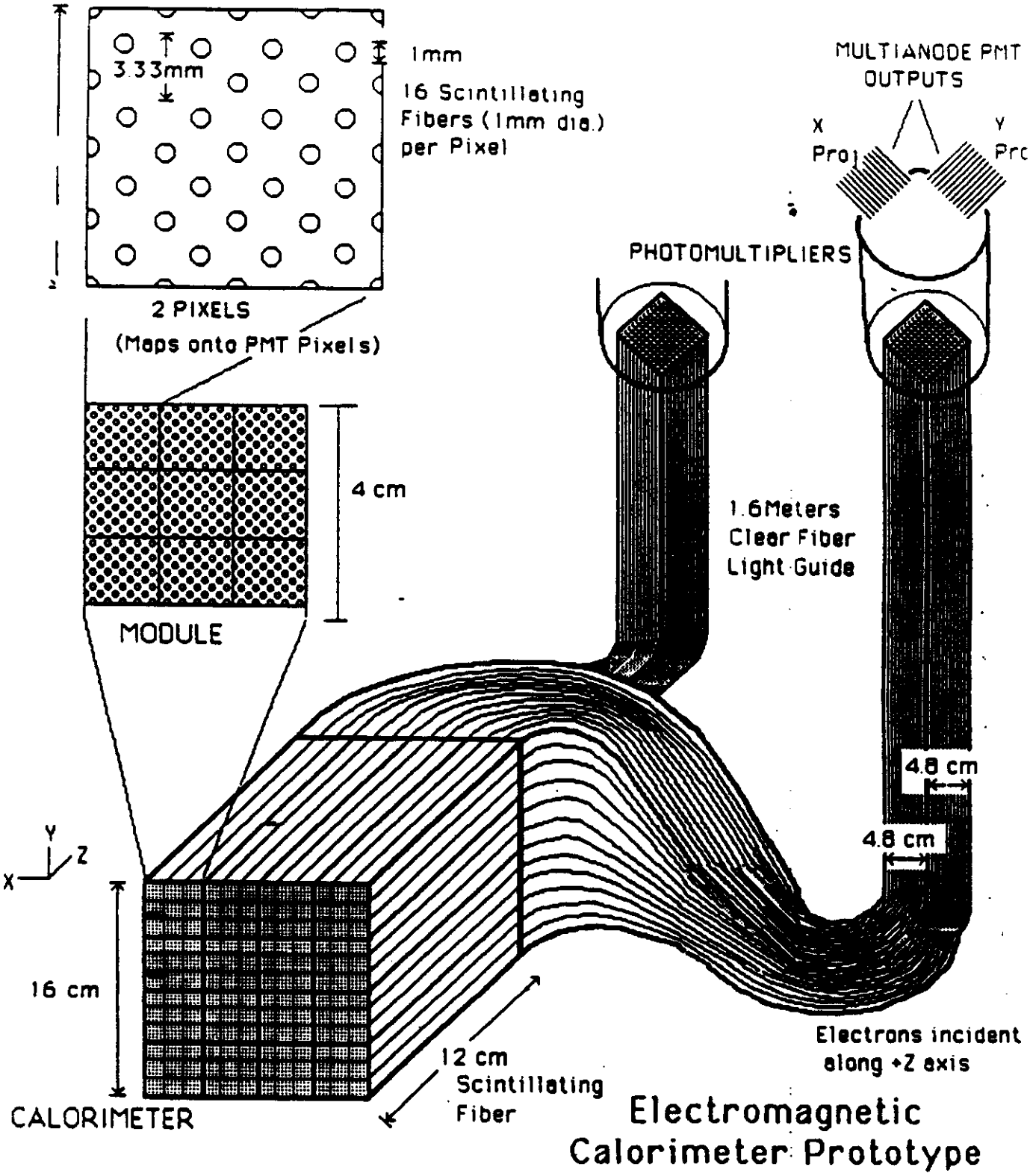

Electromagnetic Calorimeter Prototype

Fig. 46

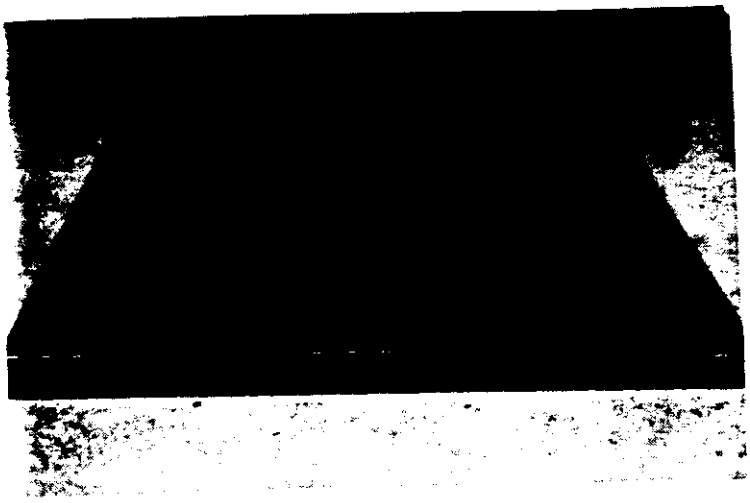

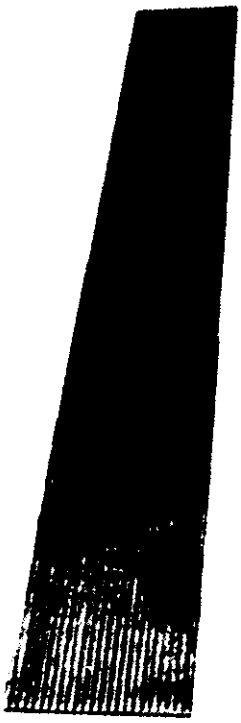

Fig. 47

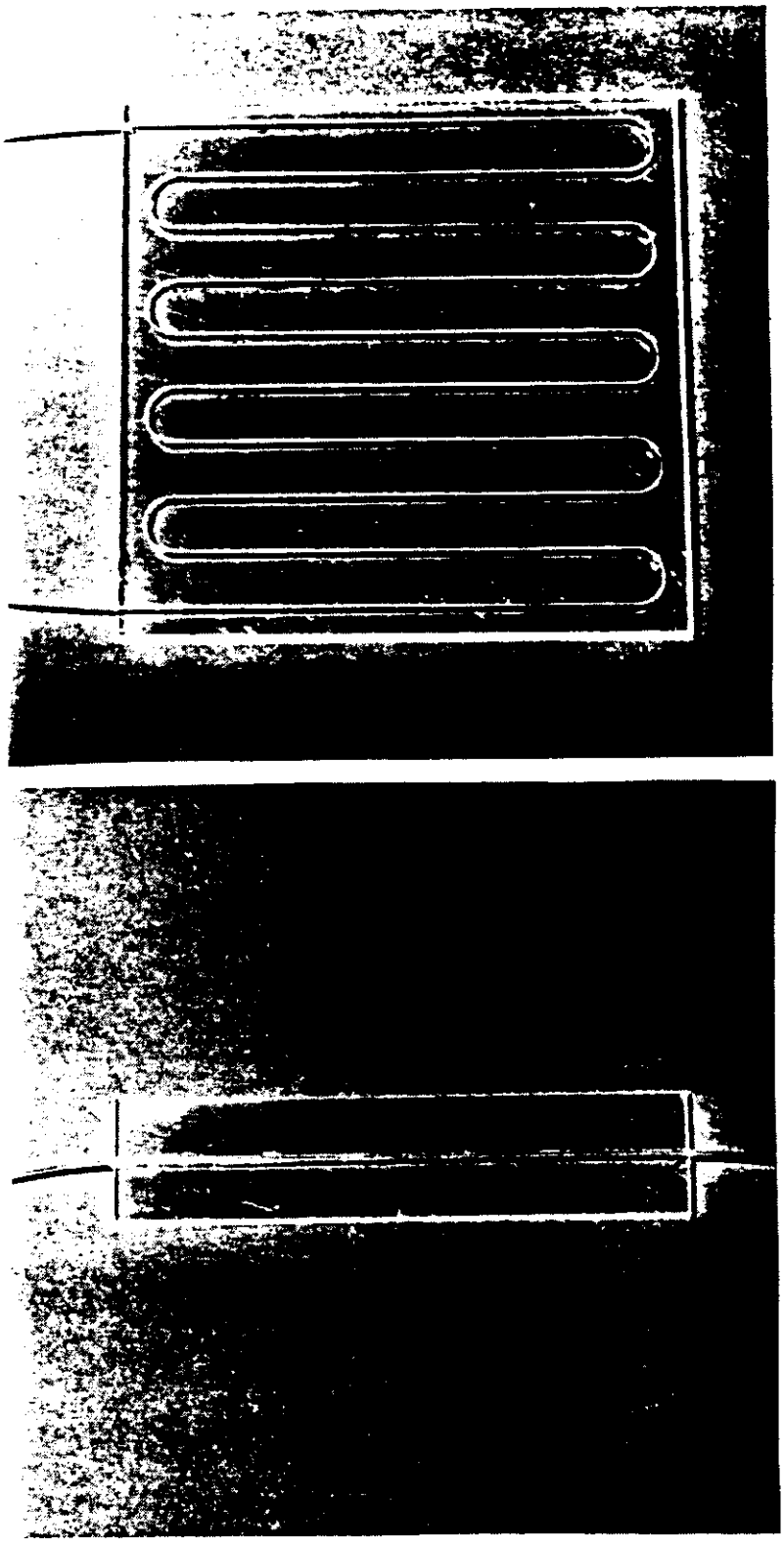

Fig. 48

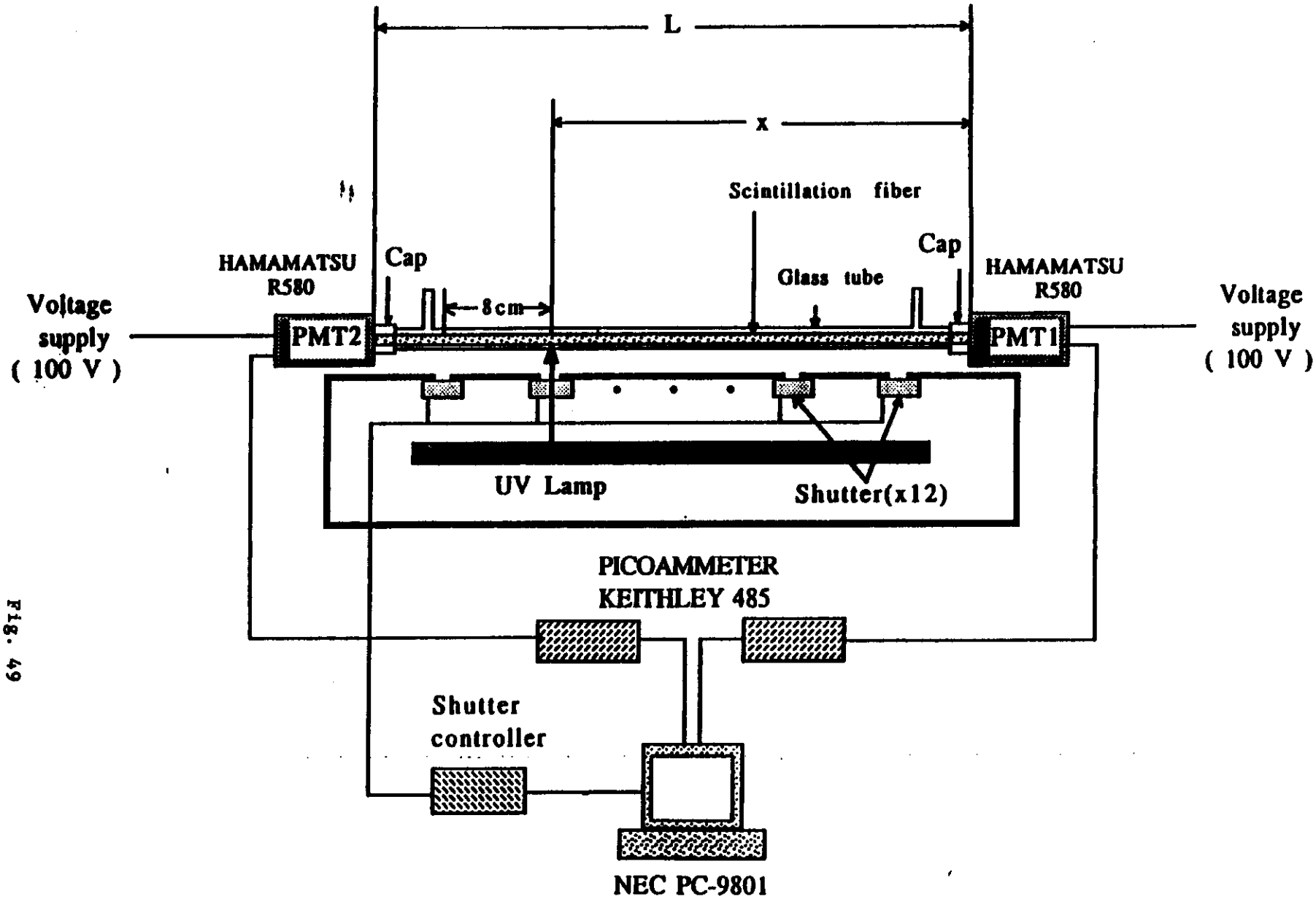
L
x
Scintillation fiber
HAMAMATSU
R580
Cap
8cm
Glass tube
Cap
HAMAMATSU
R580
Voltage
supply
(100 V)
PMT2
PMT1
Voltage
supply
(100 V)
UV Lamp
Shutter(x12)
PICOAMMETER
KEITHLEY 485
Shutter
controller
NEC PC-9801

Fig. 49

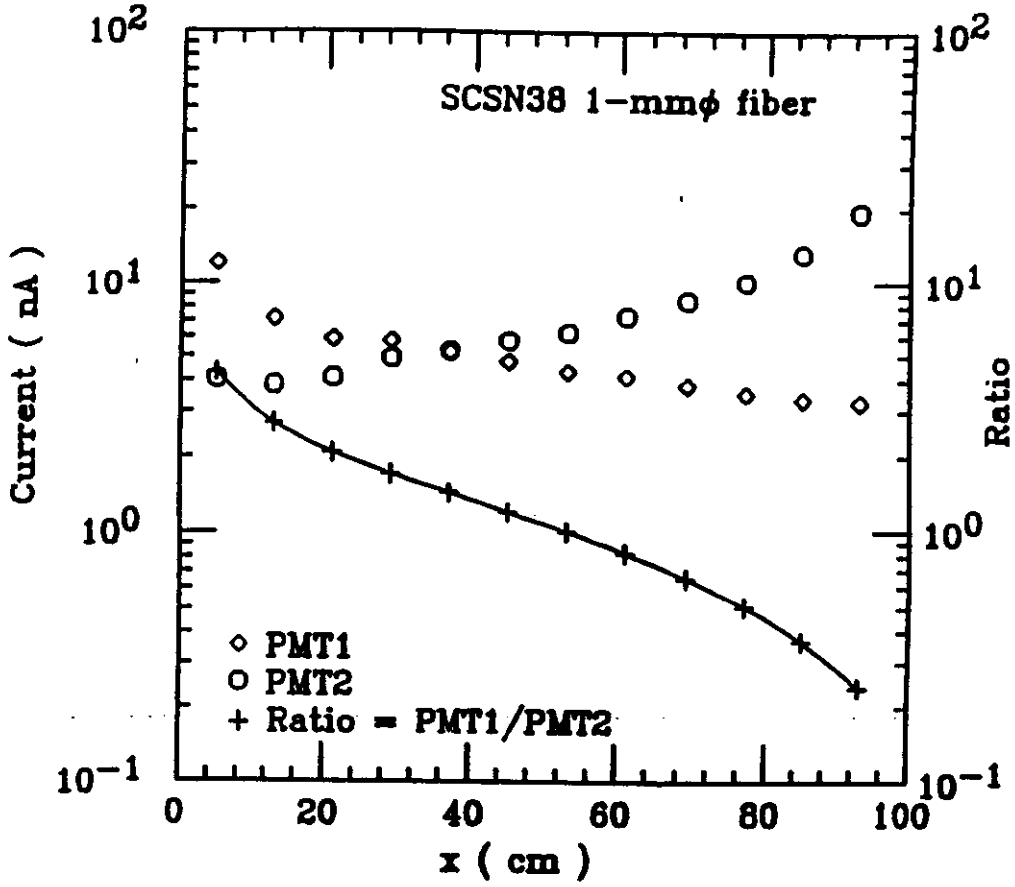
SCSN38 1-mmϕ fiber
Current (nA)
Ratio
x (cm)
PMT1
PMT2
Ratio = PMT1/PMT2

Fig. 50

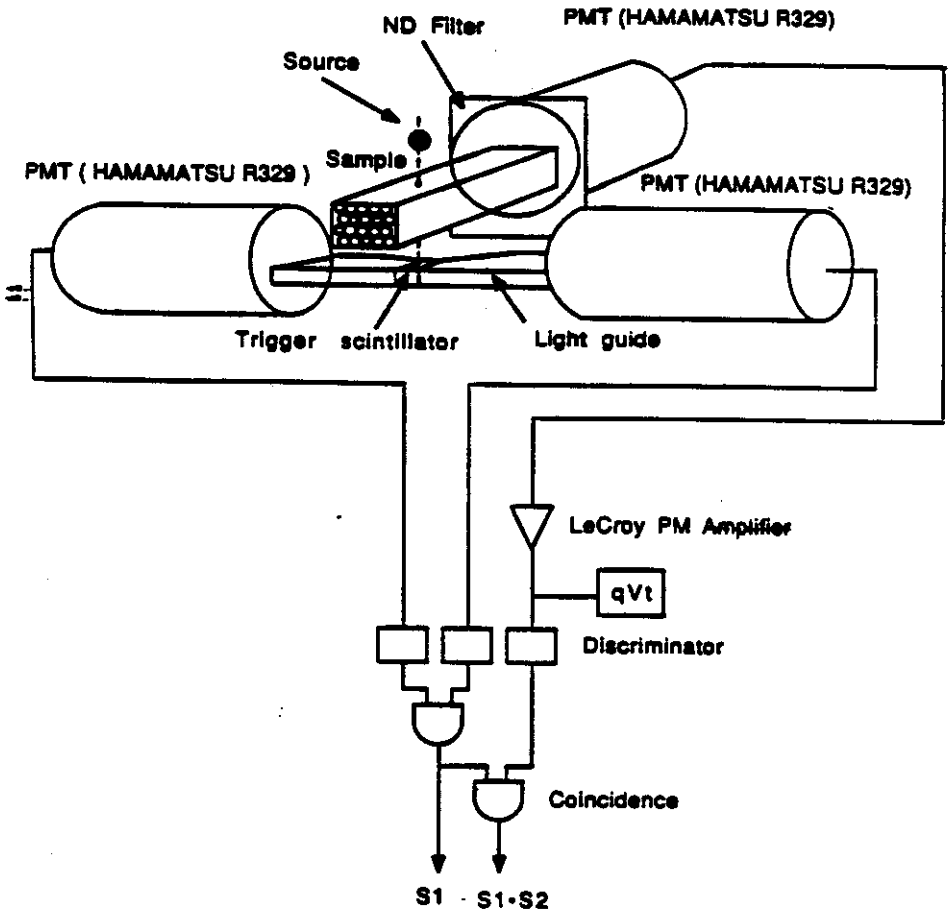
ND Filter
PMT (HAMAMATSU R329)
Source
Sample
PMT (HAMAMATSU R329)
PMT (HAMAMATSU R329)
Trigger scintillator
Light guide
LeCroy PM Amplifier
qVt
Discriminator
Coincidence
S1 · S1·S2

Fig. 51

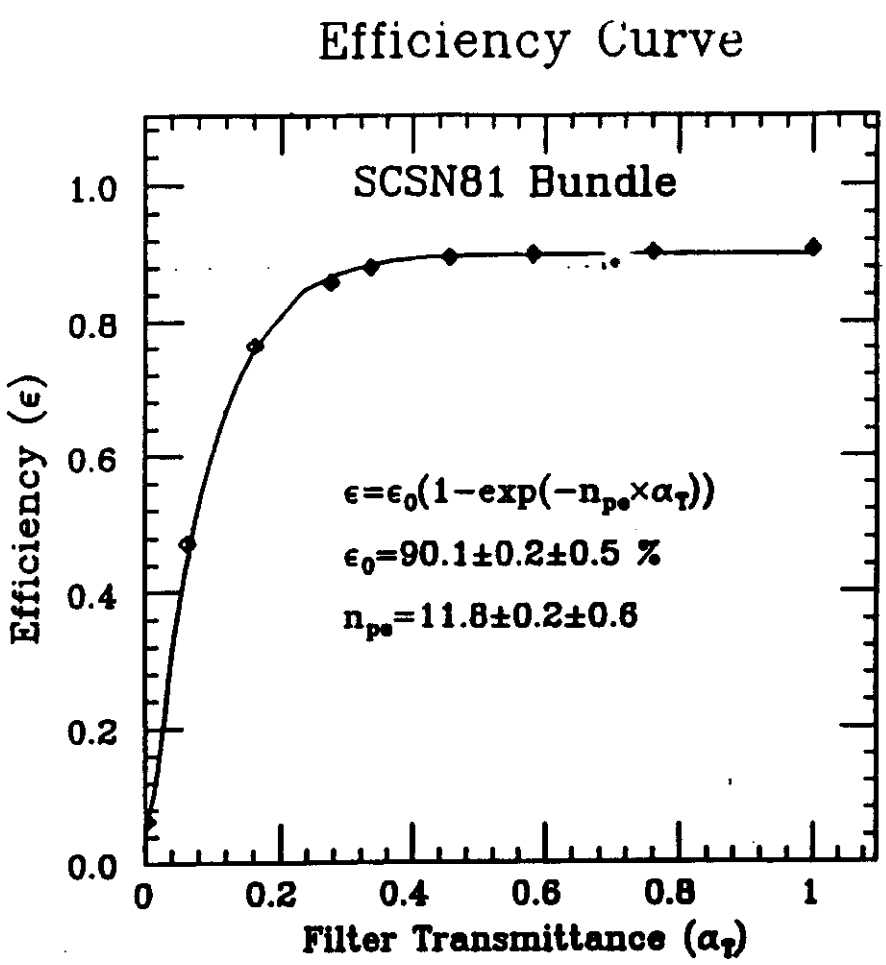
Efficiency Curve
SCSN81 Bundle
$\epsilon=\epsilon_0(1-\exp(-n_{pe}\times\alpha_T))$
ϵ_0=90.1±0.2±0.5 %
n_{pe}=11.8±0.2±0.6
Efficiency (ϵ)
Filter Transmittance (α_T)
0.0
0.2
0.4
0.6
0.8
1.0
0
0.2
0.4
0.6
0.8
1

Fig. 52

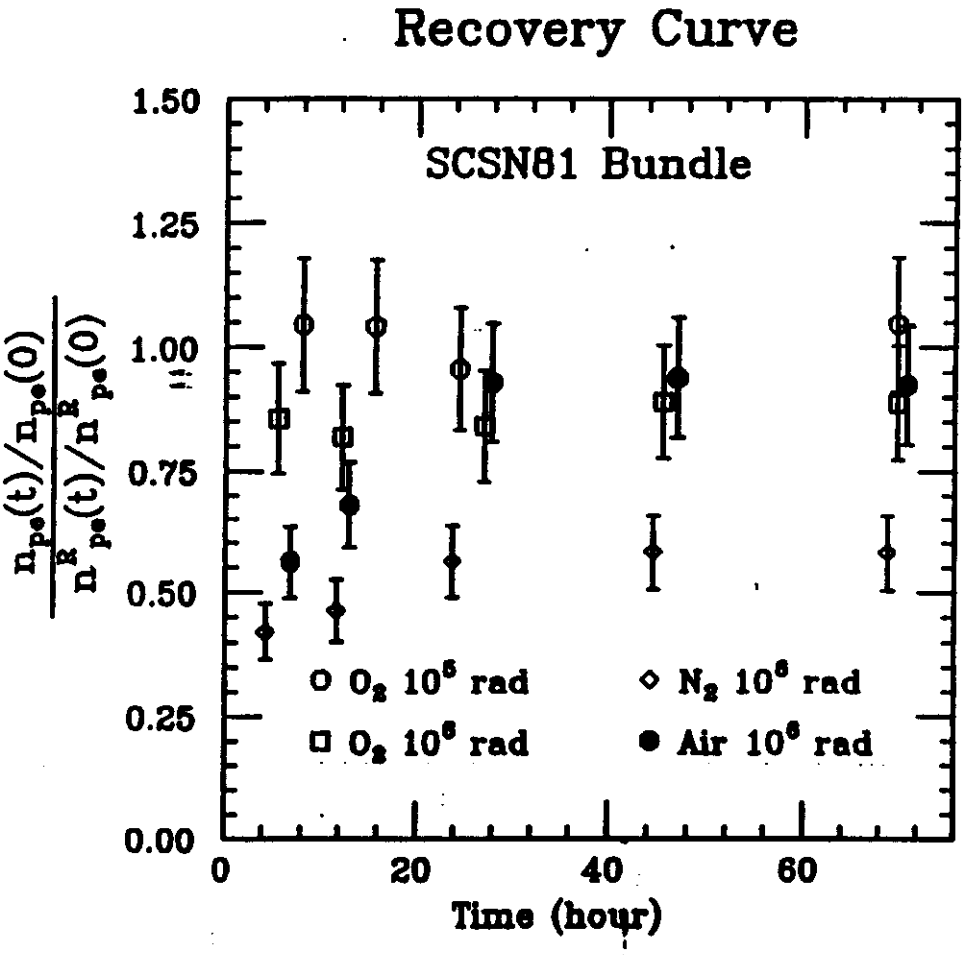
Recovery Curve
SCSN81 Bundle
$\frac{n_{pe}(t)/n_{pe}(0)}{n^R_{pe}(t)/n^R_{pe}(0)}$
O_2 10^5 rad
O_2 10^6 rad
N_2 10^6 rad
Air 10^6 rad
Time (hour)
0.00
0.25
0.50
0.75
1.00
1.25
1.50
0
20
40
60

Fig. 53

The Rockefeller/Yale part of the collaboration has, for the past two years, been working on the design and construction of an imaging pre-radiator. This pre-radiator will be tested in a test-beam at FNAL this coming winter. When various calorimeter modules currently being built by other groups are tested, our pre-radiator will be placed in front of them and read out at the same time.

The group, as part of this project, has developed useful tools for building imaging pre-radiators. These include a winding device to accurately make fiber ribbons, a fast-bus readout for image-intensifiers, GEANT3.13 software to simulate showers and a facility for fiber testing.

Separate work by the SPACAL collaboration include a test beam measurement of the effects of a pre-radiator in conjunction with a spaghetti calorimeter module. These tests were made with a piece of plastic scintillator directly in front of the module preceded by 2.6 RL of lead. These tests have indicated that a factor of five improvement can be obtained beyond that obtained with shower spreading cuts. A further test will be made in the near future using silicon pads as a pre-radiator.

Proposed R&D

The selection of an optimum pre-radiator for the design is an important aspect of the group's R&D program. In order to be able to complete the full engineering design by November 1990 we propose to work on the following items.

i) Optimization of the Rockefeller/Yale imaging pre-radiator for use in a 2 Tesla, 2 meter solenoid with the final calorimeter chosen by this subsystem group. This will include changing the number of fiber layers and the lead thicknesses in the prototype.

ii) The vacuum testing of an existing pixel detector, followed by potting one by Hamamatsu. This image tube will be tested for reading out fibers in a magnetic field.

iii) The initiation of a program of physics simulation in conjunction with the other members of the collaboration with an emphasis on the type of pre-radiator that is required for a general SSC detector.

Milestones and Schedule

1990

i) Vacuum tests of a pixel detector with a source.

ii) Potting of a pixel device inside an image-tube. We will use the most advanced prototype available.

iii) Evaluation of the pre-radiator parameters based on the requirements of the physics and the overall needs of the detector.

1991

i) Development of a specialized pixel detector suitable for use inside an image-tube.

ii) Test Beam studies the image-tube and pre-radiator with the calorimeter selected by this sub-group.

iii) Full engineering design of the pre-radiator for inclusion within a detector proposal.

Milestones and Schedule

1990

i) Vacuum tests of a pixel detector with a source.

ii) Potting of a pixel device inside an image-tube. We will use the most advanced prototype available.

iii) Evaluation of the pre-radiator parameters based on the requirements of the physics and the overall needs of the detector.

1991

i) Development of a specialized pixel detector suitable for use inside an image-tube.

ii) Test Beam studies the image-tube and pre-radiator with the calorimeter selected by this sub-group.

iii) Full engineering design of the pre-radiator for inclusion within a detector proposal.

E. PROTOTYPE STUDIES AND TEST BEAM RESULTS

E.1. BOSTON UNIVERSITY

Our Boston University collaborators have constructed and tested 9 scintillating fiber electron calorimeter modules in the context of experiment AGS 821, a new measurement of the muon g-2. A photograph of these calorimeter modules, with their associated fiber light guide and multi-anode PMT for readout, is shown here as Fig. 45 Each module is 4cm × 4cm × 12cm, with a radiation length of 0.8cm for the lead alloy/plastic fiber composite. Each module contains 288 1mm diameter round scintillating fibers, arranged in a lattice as shown in Fig. 46 At each end of each calorimeter module, fibers pass through a thin aluminum plate which is machined to a smooth surface after casting. This plate is then a 288-fiber "connector plate", with alignment pins and small screws permitting connection (and disconnection) to 288 1mm diameter clear plastic fibers making up a light guide. This light guide is then coupled to a multi-anode photomultiplier for readout of the energy and spatial pattern of individual electron showers. The goal of the g-2 calorimeter was to measure electron energies with good resolution while discriminating against pile-up from simultaneous electrons incident upon the calorimeter at different positions.

A complete electron calorimeter consists of 16 modules, each 4cm × 4cm × 12cm. This modularity is preserved in ordered plastic fiber light guide bundles, which attach separately to calorimeter modules and to the photomultiplier input fixture. This allows for the separate construction and installation of each module, and for the replacement or repositioning of individual modules. The readout of each module is further divided into 3 × 3 'pixels' matching the pixels of a single 12 × 12 multi-anode photomultiplier which can then read out an entire calorimeter. This pixel size matches the typical cross-sectional profile of an electron shower in the calorimeter. Only clear fibers extend beyond the boundaries of the cast block containing scintillating fibers, eliminating background from ambient low-energy charged particles.

Electromagnetic showers are generated in a eutectic alloy of lead/bismuth/tin/cadmium, with scintillating fibers running along the length of the calorimeter. The melting-point of the eutectic metal is 70 degrees C (158 degrees F) and its density is 9.5 g/cm^3. Blocks were cast of this material with embedded scintillating fiber, with no degradation of the scintillation and transmission properties of the fiber. Each module contains 288 fibers (1mm diameter), arranged in 24 "ribbons" of 12 fibers each. The packing density of fibers within the calorimeter is the result of a tradeoff between increased light collection and energy resolution (more fibers) vs. minimizing required photocathode readout area and hence cost. EGS simulations indicated that a packing fraction of 15% (288 fibers/16cm^2) would provide an energy resolution of better than $\frac{18\%}{\sqrt{E}}$. There is, however, no step in our assembly process which precludes a much higher fiber packing fraction.

The metal alloy can be machined to a smooth surface on its four long sides (for stacking), with a thin metal plate on each end. These metal plates can be drilled with countersunk holes for mechanically inserting and fixing the fibers

prior to casting. A 5 micron precision in locating holes for each fiber (with numerically controlled machines at the Boston University Scientific Instrument Facility) can maintain fiber alignment with a similar metal plate on the end of a fiber light guide bundle to within 5% of an individual fiber diameter of 1mm. A calibration fixture may be attached to the upstream end face of each calorimeter in a similar manner.

For each 12cm long module, 288 holes were machined into each of two thin aluminium "spacer plates" which maintained fiber positioning along the length of each module. Slightly larger "flow-through holes" were drilled into each spacer plate, to increase the mechanical rigidity of the cast module. The fibers for each module were fed by ribbons into a "sandwich" of two end plates and two spacer plates, after which the plates were pulled over the fibers to a separation of 12cm. Deburring of the plates and lubrication during the pulling were necessary to avoid damaging the fiber cladding during this procedure, particularly since the Optectron scintillating fibers used exhibited a 5 - 10% variation in fiber diameter. Once the plates were properly positioned, the fiber ends were epoxied into position on the endplates, so that fibers were rigidly held for machining after casting. Vibration of the fiber assembly during casting was sufficient to remove the few small air bubbles which formed, and our final product was very uniform in internal composition.

The 1.6 meter light guide which connects each calorimeter module to a photomultiplier is made of clear acrylic fibers, of a type specially chosen for long (>20 meter) attenuation length at the frequencies emitted by the scintillating fibers. Readout of an entire calorimeter (16cm × 16cm × 12cm deep) is performed with a single Hamamatsu 3" multi-anode photomultiplier. Each photomultiplier contains 144 4mm × 4mm pixels, arranged into 12 'X' rows and 12 'Y' rows for readout as 24 signals. In this way one can read out 24 projections of electron showers within each calorimeter, identifying double-showers separated in either X or in Y.

This device was tested with 1 - 3 GeV electrons in the A2 test beam at Brookhaven National Laboratory. The measured light yield was 500 photoelectrons per GeV of incident electron energy, which could be increased by silvering one end of each scintillating fiber. The measured energy resolution was better than $\frac{20\%}{\sqrt{E}}$, consistent with shower leakage through the sides of a single module and with contamination from pions in the mixed test beam. We measured the efficiency of the optical coupling (two connector plates joined with either optical grease or optical epoxy) as greater than 90%. The light collected after a 1.6m light guide was 80% of that collected by a PMT mounted directly on the calorimeter end plate. Pulse shape was dominated by the PMT rise time of roughly 4ns 10% to 90%, with a FWHM of 6ns for 100mV (1 GeV) pulses.

E.2. FNAL COLLABORATION

We have been very active in prototyping efforts and measurements with the goal of viable scintillator calorimetry for the SSC. A secondary goal involved the use of scintillator calorimetry in an upgrade of the CDF endplug.

Fiber Technology

We have studied many construction schemes for scintillator/fiber calorimetry. We have evaluated and discarded as unfeasible ideas like: Depth segmentation in fiber calorimeters using wavelength shifting fiber ribbons to couple to the fibers (not enough light); FITCAL, i.e. threading wavelength shifting fibers longitudinally through thin scintillator plastic tiles (not enough light, lack of uniformity).

We have developed a new type of fiber: Wavelength Shifting Core fiber in 2 variants, solid and hollow versions, where the clad WLS core is either drawn with the surrounding scintillator in one pass, or is inserted into a hollow-drawn scintillating fiber. This may have application in fiber calorimeters with depth segmentation, where very fine readout fibers from a front compartment can pass directly through the back compartment.

We have prototyped lead manufacture. The Purdue University group has successfully rolled a sufficient number of grooved lead plates to produce a set of electromagnetic prototypes (10x10x30 cm). Figure 47 shows a grooved lead plate rolled by the Purdue members of our collaboration. We are working with industry (Vulcan Lead Co., Able Metal) to devise mass production techniques to roll grooves in lead plates and to machine grooved lead plates. We are exploring casting technologies. Lead casting was used to build a small EM prototype.

We have performed extensive monte carlo studies using GEANT and EGS4 to understand the physics of the fiber calorimeter.

We have started ANSYS structural studies of fiber calorimeters, including the magnetic forces on a solenoid.

Tile Technology

Our experience with tile is more limited, nevertheless this technology, where the tile is read out by a fine waveshifting fiber embedded in the tile surface (or perhaps glued along one or more edges of the tile), seems to be highly promising, both in light yield and in uniformity of response.

We have built tiles and measured light yield and uniformity using cosmic rays and UV lasers. Fig 48 shows a photograph of two geometries of tile studied. These measurements confirmed previous measurements of other groups.

We have developed optics monte carlo programs to aid us in understanding and predicting measurements (both of tiles and of the waveshifter-cored scintillating fibers), and to aid in optimizing light yield and uniformity of response of the final design.

We are investigating techniques of tile manufacture: Laser-cutting, NC milling, and casting. Working with a laser machining company (LMI), we have been able to combine the tile cutting and the groove milling steps into a single process.

We have started ANSYS studies of calorimeter designs.

E.3. University of Illinois PB/SCIFI Group

In the past year, the Illinois component of our collaboration has built many prototypes of Pb/SCIFI detectors and has built nearly 200 final modules in a fully tapered, projective geometry. This task has been related to an effort to complete the forward electromagnetic calorimeter for the JETSET experiment at CERN's low-energy antiproton ring. These detectors have been tested using incident electrons from 35 to 5000 MeV. The detectors exhibit a characteristic resolution described by Sigma/E = $\frac{6.1\%}{\sqrt{E}}$. Our latest tests using an array of the final detectors, light guides, and photomultiplier tubes, confirms this result.

We attribute this excellent performance to several factors. First, a rigorous, and reproducible assembly procedure is used:

This procedure is based on "weaving" fibers on top of precisely grooved lead foils. A machine has been developed which is capable of fabricating large quantities of foils at a very modest cost ($0.70 each, parts and labor). The foils are subsequently cleaned in an ultrasonic bath before inclusion in the detectors. The assembly of a "raw" detector proceeds by

1) placing a plate on a special table with a precise vertical travel,
2) applying a thin but even layer of epoxy, and
3) guiding a properly spaced set of up to 72 fibers across the foil. The procedure is repeated until the detector reaches the desired height. A"weaving" machine has been built at our laboratory and is operated by our group's technician. At the present time, four 8x8x20 cm3 detectors are constructed (simultaneously) in about 10 hours. (We actually make 1 82 cm module and divide it later into smaller segments.) This time can be reduced as discussed below with modest upgrades to the weaving apparatus. Our technique guarantees that the fibers are distributed evenly throughout the volume of the detector with close-packed spacing. This insures the highest resolution given the chosen lead-to-fiber ratio since, in this configuration, sampling fluctuations are minimized. To date, nearly 200 detectors have been built using this apparatus and the detector to detector quality control is well in hand. A straightforward modification of our weaving apparatus would allow us to make 2-meter modules, with different fiber spacing as required for the final calorimeter which is proposed above. We plan to marry our efforts and experience with the plans from the FNAL component of our collaboration in order to produce the next appropriate machine for weaving detectors. This machine will most likely reside at FNAL.

Secondly, high-quality scintillating fibers are used:

These fibers are notably more robust in terms of physical characteristics as compared to those which were employed in earlier similar detectors. Presently, Optectron S101 S fibers form the basic component of the detectors. They have a polystyrene core (n=1.59) and a cladding of fluorinated acrylic (n=1.39). The cladding is approximately 15 microns thick and is capable of withstanding temperatures up to 90 C. This is important to the construction since an optical epoxy (Bicron BC-600) is used to keep the fibers in place. Recently, there has been an explosion of interest in clad scintillating fibers and companies such as Bicron and Kyowa Gas (Japan) have entered the market with a variety of new

products. We have tested several fibers from these companies, including fibers doped with fluors which are particularly radiation resistant such as 3HF. A modified assembly procedure, based on the above description, is used to build "test" calorimeter detectors which are made out of various fibers. A very recent test of radiation damage using Kyowa 3HF fibers and a silicon - based bonding agent was very successful. We plan to explore the performance of other types of fibers and glues in an effort to guide the final selection of ingredients for our main full-sized hadronic modules.

Finally, great care is used in the machining and polishing of the finished detectors.

"Raw" Pb/SCIFI blocks are accurately cut into the required tapered trapezoidal shapes using computer-controlled milling machines . Several polishing steps on the flat face (seen by the photomultiplier tube) are made in order to assure a good transmission of the light from the detector. The detectors are kept clean at all times and are not exposed for long periods of time to UV light which might bleach parts of the fibers. The assembly room itself is outfitted with "UV-less" lighting so that the many spools of fibers which are needed do not deteriorate.

The FSU / UF component of our collaboration has tested a number of scintillating fibers, scintillating plastics, and a variety of epoxies for radiation damage resistance. We are collaborating with several fiber-producing companies in order to develop scintillating fibers which have both long attenuation lengths and which are radiation hard. We have tested numerous glues as well and have found, for example, that the mentioned BC-600 glue (described above) cannot withstand the anticipated radiation dosage in the SSC environment. It turns black at an exposure of less than 1 MR. Instead, a silicon-based glue was used on the calorimeter module built with the 3HF fibers. This glue does not discolor at exposures exceeding 10 MR but it is considerably more difficult to work with. An interesting question we hope to soon answer, is "to what extent does it matter if the glue discolors? " since the glue does not form the optical interface for the fibers. We will continue to explore these tests as a part of this proposal.

E.4. University of Tsukuba

University of Tsukuba is conducting thorough studies of radiation damage to scintillating fibers, in close contact with Kyowa Gas Co. We have tested 1mm diameter fibers made of scintillator SCSN38 and SCSN81 with 20 microns acrylic cladding. Two type of samples were tested: 1 m long for measuring the attenuation length, and bundles of twenty 5 cm long fibers for measuring light yield.

Attenuation Length Measurement

The attenuation length is measured by exciting a 1 m long fiber with UV light, as shown in Fig. 49 . The fiber, in a glass tube, is exposed to UV light (1 cm spot size) via 12 remotely controlled shutters (COPAL-EMS). The fiber is viewed by two Hamamatsu R580 photomultipliers, PMT1 and PMT2, The photomultipliers are operated as a photocell with no dynode amplification by applying 100 V between the photocathode and the first dynode. The currents are

read out by two pico-ampermeters (Keithley 485) and recorded using NEC PC-9801 computer. Fig. 50 shows an example of the resulting current measurement. The ratio of PMT1 and PMT2 currents is fitted with a function

$$\frac{PMT1}{PMT2} = G\frac{\exp(-X/\lambda_L) + C_1\exp(-X/\lambda_S)}{\exp(-(L-X)/\lambda_L) + C_2\exp(-(L-X)/\lambda_S)}$$

to determine short (λ_S) and long (λ_L) components of the attenuation length. Reproducibility of the measurement is monitored by re-measuring periodically a set of reference fibers.

Light Yield Measurement

The relative light yield is determined in terms of the average number of photoelectrons in a photomultiplier, which is determined by measuring the counting efficiency for a ^{106}Ru source. The experimental setup is shown in Fig. 51 . The bundle of scintillating fibers is viewed via ND filters by a Hamamatsu R329 photomultiplier operated at -2.1 kV. The radioactive source ^{106}Ru was used as a source of electrons. Assuming a Poisson distribution of photoelectrons emitted from the photocathode, with the dynode amplification contributing negligible fluctuations, and that the threshold voltage of the discriminator is low enough for a single photoelectron to be detectable, the counting efficiency is given by the equation

$$\varepsilon = \varepsilon_0(1 - \exp(-\bar{n}\,\alpha_T)),$$

where $\bar{n}$ is the average number of photoelectrons when the filters are not inserted and serves as a measure of the light yield of scintillating fibers, α_T is a transmittance of the ND filter, and ε_0 is a constant less than 1. The deviation of ε_0 from unity is mainly due to gamma rays from the ^{106}Ru source, and multiple scattering of electrons. An example of the experimental results for a reference sample of fibers is shown in Fig. 52 .

Study of Radiation Effects

After the measurement of the attenuation length and the light yield fibers are placed in a 2 mm thick aluminium tube with a well defined environment (air, oxygen nitrogen, argon, vacuum). After a six hour period of outgassing fibers are exposed to gamma rays from ^{60}Co source. Dose rates of 2, 100 and 400 krad/hour are used to achieve a total dose of 10^5, 10^6 and 10^7 rads. After irradiation samples are kept in the same environment, and the light yield and attenuation length are measured periodically. Preliminary results, shown in Fig. 53 indicate the beneficial effects of an oxygen atmosphere.

F. DETAILED BUDGET

F.1. EQUIPMENT BUDGET

LAMINATED HADRON CALORIMETER PROTOTYPE ($K)			
COMPONENT	UNIT COST	QUANTITY	TOTAL COST
Scintillating Fiber (Bicron Quote)	$0.5/m	200km	100.
Rolled Lead	$1.45/lb.	3200 lb.	4.6
Manufacturing Machines			25.
Fiber Loading	20.	1	
Rollers	5.	1	
Iron and Bonding			7.
Light Guides			30.
Machining	$30/hr.	1000 hrs.	30.
Assembly, Labor	$10/hr.	2500 hrs.	25.
Electronics			20.
Photomultipliers			20.
TOTAL LAMINATED PROTOTYPE			262.

TILE CALORIMETER PROTOTYPE ($K)			
COMPONENT	UNIT COST	QUANTITY	TOTAL COST
Wavelength Shifting Fiber (Bicron Quote)	$0.5/m	4 km	2.
Scintillator Plate			4.
Machining	$20/hr.	400 hrs.	8.
Assembly, Labor	$10/hr.	400 hrs.	4.
Plastic Casting			10.
Light guides/Optics			12.
Laser-Cutting			8.
N/C Milling			5.
Cosmic-Ray Test Stand			15.
TOTAL TILE PROTOTYPE			68.

2-STAGE/ELECTROMAGNETIC CALORIMETER PROTOTYPES ($K)			
COMPONENT	UNIT COST	QUANTITY	TOTAL COST
Scintillating Fiber (Bicron Quote)	$0.5/m	30 km	15.
Clear Fiber	$0.25/m	32 km	8.
Diffusers/Optics			7.
Casting			12.
Machining	$20/hr.	200 hrs.	4.
Assembly, Labor	$10/hr.	300 hrs.	3.
TOTAL 2-STAGE ELECTROMAGNETIC PROTOTYPE			49.

SPECIALIZED TOOLING ($K)			
COMPONENT	UNIT COST	QUANTITY	TOTAL COST
FIBER CUTTING TOOL			
Flycutting Spindle			7.5
Work Spindle – Drive			6.
Saw Spindle – Drive			2.5
Base			1.0
Machined Parts			10.
Controller			2.
Engineering/Drafting			10.
SUBTOTAL			39.
COMPUTER CONTROLLED PRODUCTION MAPPING FIXTURE			
Cartesian Robot			20.
Sources, Fiber			5.
and Readout			5.
SUBTOTAL			30.
CNC CARBON DIOXIDE LASER PLASTICS CUTTING MACHINE			49.
TOTAL SPECIALIZED TOOLING			118.

ENGINEERING DESIGN ($K)			
TASK	UNIT COST	QUANTITY	TOTAL COST
Manufacturing Engineering	$35./FTE	2.0 FTE	70.
Structural Engineering	$40./FTE	1.5 FTE	60.
Drafting	$30./FTE	0.67 FTE	20.
TOTAL SUBSYSTEM ENGINEERING			150.

FIBER/PM TEST EQUIPMENT ($K)			
COMPONENT	UNIT COST	QUANTITY	TOTAL COST
Fiber Test Station			20.
PMT Test Station			20.
TOTAL FIBER/PM TEST			40.

CALIBRATION ($K)			
COMPONENT	UNIT COST	QUANTITY	TOTAL COST
Laser light injection system			17.
Point sources	0.3	30	9.
Line sources	1.7	3	5.
Remote source drivers			16
PMT current readout and DAQ electronics			10
TOTAL CALIBRATION SYSTEM			57.

BEAM TESTS ($K)			
COMPONENT	UNIT COST	QUANTITY	TOTAL COST
Logistic support			10.
Support frames			10.
Data Acquisition			10.
TOTAL BEAM TESTS			30.

TRIGGER/FRONT END AND DAQ ELECTRONICS ($K)			
COMPONENT	UNIT COST	QUANTITY	TOTAL COST
PM Tube Assemblies	2.	5	10.
FADC/logarithmic	20.	1	20.
Packaging Engineering	20.	1	20.
Electronic Components	10.	1	10.
Trigger gate array	20.	1	20.
Prototype circuit boards	20.	1	20.
TOTAL TRIGGER/DAQ ELECTRONICS			100.

RADIATION DAMAGE ($K)			
COMPONENT	UNIT COST	QUANTITY	TOTAL COST
2 Weeks beam time Illinois Microtron			30.
Beam line equipment - vacuum gauge, table			5.
Fibers, lead, glue for EM prototypes			12.
Multialkali PMTs, bases, HV, counters			8.
Fast Digital Oscilloscope (pulse shape)			5.
Assembly, machining, production			15.
TOTAL RADIATION DAMAGE			75.

PRERADIATOR ($K)			
COMPONENT	UNIT COST	QUANTITY	TOTAL COST
Image tube			30.
Data link TCP/IP			10.
TOTAL PRERADIATOR			40.

F.2. OPERATING BUDGET

BOSTON BUDGET	
COMPONENT	FUNDING ($K)
SALARIES	
Salaries for 1.5 FTE postdoctoral fellow	48.0
Support for 3 FTE graduate students	40.5
TOTAL	88.5
BENEFITS (24.4% for postdocs)	11.7
TOTAL SALARIES AND BENEFITS	100.2
TRAVEL	
Travel = 20.0 Design/Construction work FNAL, 5.0 Test Beam, 5.0 Collaboration Meetings	30.0
TOTAL DIRECT COSTS	130.2
INDIRECT COST (65% off-campus @ 47% + 35% on-campus at 73%, minus underrecovery.)	58.6
TOTAL BOSTON OPERATIONS	188.8
TOTAL BOSTON EQUIPMENT	199.0

BOSTON PERSONNEL		
	% this task	Other tasks
Faculty		
S.T. Dye	25	IMB
J.P. Miller	15	G-2, CP LEAR
B.L. Roberts	15	G-2, CP LEAR
J. Stone	10	MACRO
L. Sulak (P.I.)	40	IMB, G-2
W. Worstell (P.I.)	50	G-2, MACRO
Post-doctoral Research Associates		
S. Klein	10	MACRO
To be named	50	Department HEP
Engineers		
E. Hazen	25	Electronics
D. Higby	75	CAD/CAM
T. Coan	50	Structural
Draftsmen		
S. Glass	25	
R. Bruni	25	
Graduate Assistants		
To be named	3 @ 100	

Responsibility: Engineering Design, EM Calorimeter, Electronics

FAIRFIELD BUDGET	
COMPONENT	FUNDING ($K)
SALARIES	
Two summer student	5.0
One month summer salary	6.0
TRAVEL AND OPERATIONS	
For meetings, collaboration, phone, xerox	5.0
TOTAL DIRECT COSTS	16.0
INDIRECT COSTS @47%	8.0
TOTAL FAIRFIELD OPERATIONS	24.0
TOTAL FAIRFIELD EQUIPMENT	17.0

FAIRFIELD PERSONNEL		
	% this task	Other tasks
Faculty		
D.R. Winn	50	G-2
Summer Student		
To be named	50	Department HEP

Responsibility: Optical calibration, liquid scintillator calorimeter.

FNAL BUDGET	
PROJECT	FUNDING ($K)
SALARIES	
Salaries for 1.5 FTE postdoctoral fellow	42.0
Salaries for 3.0 Summer students	12.0
BENEFITS (25% for postdocs)	11.0
TOTAL SALARIES AND BENEFITS	65.0
TRAVEL	
For meetings, collaboration	30.0
TOTAL DIRECT COSTS	95.0
TOTAL INDIRECT COSTS @46 %	44.0
TOTAL FNAL OPERATIONS	139.0
TOTAL FNAL EQUIPMENT	563.0

FNAL PERSONNEL		
	% this task	Other tasks
Research Physicists		
M. Atac	15	CDF
M. Binkley	10	CDF
A. Bross	35	D0
G.W. Foster(P.I.)	50	CDF
J. Freeman (P.I.)	50	CDF
S. Hahn	15	CDF
J. Hauser	15	CDF
C. Newman-Holmes	25	CDF
M. Mishina (P.I.)	50	CDF
A. Para (P.I.)	50	CDF
D. Theriot	10	
Post-doctoral Research Associates		
S. Tkaczyk	25	
Engineers		
T. Droege	50	
J. Krebs	30	Cryo
R. Wands	50	

Responsibility: Hadron calorimeter, Test beam, Tile calorimeter, Specialized tooling, Radiation hardness.

UNIVERSITY OF FLORIDA BUDGET	
COMPONENT	FUNDING ($K)
SALARIES One summer student	?
Two months summer salary	?
TRAVEL For meetings, collaboration	?
TOTAL DIRECT COSTS	?
INDIRECT COSTS @47%	?
TOTAL FLORIDA OPERATIONS	20.0

UNIVERSITY OF FLORIDA PERSONNEL		
	% this task	Other tasks
Faculty Majewski (P.I.)	50	?

Responsibility: Radiation hardness

FLORIDA STATE BUDGET	
COMPONENT	FUNDING ($K)
SALARIES	
One summer student	?
Two months summer salary	?
TRAVEL	
For meetings, collaboration	?
TOTAL DIRECT COSTS	?
INDIRECT COSTS @?%	?
TOTAL FLORIDA STATE OPERATIONS	20.0

FLORIDA STATE PERSONNEL		
	% this task	Other tasks
Faculty		
K. Johnson (P.I.)	50	?

Responsibility: Radiation hardness

ILLINOIS BUDGET	
COMPONENT	FUNDING ($K)
SALARIES	
0.5 FTE Post-doctoral Research Associate	14.0
TOTAL	14.0
BENEFITS (25% for postdocs)	3.5
TOTAL SALARIES AND BENEFITS	17.5
TRAVEL	
For meetings, collaboration	4.0
TOTAL DIRECT COSTS	21.5
INDIRECT COSTS @47%	10.0
TOTAL ILLINOIS OPERATIONS	31.5
TOTAL ILLINOIS EQUIPMENT	75.0

ILLINOIS PERSONNEL		
	% this task	Other tasks
Faculty		
D. Hertzog (P.I.)	50	?

Responsibility: Radiation hardness

MICHIGAN STATE BUDGET	
COMPONENT	FUNDING ($K)
SALARIES	
0.5 FTE Post-doc	14.0
Undergrad salary	3.0
TOTAL	17.0
BENEFITS (25% for postdocs)	3.5
TOTAL SALARIES AND BENEFITS	20.5
TRAVEL	
For meetings, collaboration	7.0
TOTAL DIRECT COSTS	27.5
INDIRECT COSTS @46%	12.5
TOTAL MSU OPERATIONS	40.0

MICHIGAN STATE PERSONNEL		
	% this task	Other tasks
Faculty		
C. Bromberg (P.I.?)	50	?
J. Huston (P.I.?)	50	?
Post-doctoral Research Associates		
To be named	50	Department HEP
Summer Student		
L. Sorrell	50	Department HEP

Responsibility: Hadron calorimeter: Test beam.

PURDUE BUDGET	
COMPONENT	FUNDING ($K)
SALARIES	
0.5 FTE Postdoctoral fellow (IDC=OFF)	14.0
Undergrad salary (IDC=ON)	4.0
TOTAL	18.0
BENEFITS (16.4% for postdocs)	2.3
TOTAL SALARIES AND BENEFITS	20.3
TRAVEL	
For meetings, collaboration	8.5
TOTAL DIRECT COSTS	28.8
INDIRECT COSTS ON=49%; OFF=25%	8.16
TOTAL PURDUE OPERATIONS	37.0
TOTAL PURDUE EQUIPMENT	40.0

PURDUE PERSONNEL		
	% this task	Other tasks
Faculty		
V. Barnes (P.I.)	25	CDF
A. Garfinkel	25	CDF
Post-doctoral Research Associates		
A. Laasanen	25	CDF
To be named	50	Department HEP
Graduate Assistants		
J. Tonnison	10	CDF
Summer Student		
To be named	50	Department HEP

Responsibility: Source calibration, optics montecarlo simulation.

ROCKEFELLER BUDGET	
COMPONENT	FUNDING ($K)
SALARIES	
Salary for 0.5 FTE postdoctoral fellow	14.5
BENEFITS (23% for postdocs)	3.3
TOTAL SALARIES AND BENEFITS	17.8
TRAVEL	
2 trips 2 people to FNAL for 2 weeks test beam	5.0
Travel to group meetings etc.	2.0
TOTAL TRAVEL	7.0
MATERIALS AND SUPPLIES	6.0
TOTAL DIRECT COSTS	30.8
INDIRECT COSTS @68%	20.9
TOTAL ROCKEFELLER OPERATIONS	51.7
TOTAL ROCKEFELLER EQUIPMENT	40.0

ROCKEFELLER PERSONNEL		
	% this task	Other tasks
Faculty		
P. Meles	50	?
R. Rusak (P.I.)	50	?
A. Vacchi	50	?
S. White	50	?
Post-doctoral Research Associates		
To be named	50	Department HEP

Responsibility: Preradiator

ROCHESTER BUDGET	
PROJECT	FUNDING ($K)
SALARIES One 0.5 FTE senior RA	19.7
Two 0.5 FTE grad students	11.0
BENEFITS (24.4%)	4.8
TOTAL SALARIES AND BENEFITS	35.5
TRAVEL including support for two RA's stationed at FNAL	19.9
TOTAL DIRECT COSTS	55.4
INDIRECT COSTS @30% off-campus rate	16.6
TOTAL ROCHESTER OPERATIONS	72.0

ROCHESTER PERSONNEL		
	% this task	Other tasks
Faculty A. Bodek	50	Department HEP
S. Olsen	10	HEP
Post-doctoral Research Associates P. deBarbaro	50	Department HEP
H. Budd	50	HEP
W. Sakumoto	50	HEP
Graduate Assistants M. Swain	50	HEP
M. Dixon	50	Department HEP

Responsibility: Hadron Calorimeter; Testbeam

TEXAS A & M BUDGET	
PROJECT	FUNDING ($K)
SALARIES	
Salaries for 0.5 FTE postdoc	15.0
Salaries for 0.5 FTE staff scientist/designer	17.9
Support for 0.5 FTE graduate student	12.0
TOTAL	44.9
BENEFITS	10.4
TOTAL SALARIES AND BENEFITS	55.3
TRAVEL	
US trips: meetings/collaborations, 10	5.0
TOTAL DIRECT COSTS	60.3
TOTAL INDIRECT COSTS @31.5 %	19.0
TOTAL TAMU OPERATIONS	79.3
TOTAL TAMU EQUIPMENT	60.0

TEXAS A & M PERSONNEL		
	% this task	Other tasks
Faculty		
T. Bowcock	20	CDF
F. R. Huson	20	E690
P. McIntyre	20	CDF
R. Webb(P.I.)	40	CDF, MACRO
J. White	50	E690
Post-doctoral Research Associates		
To be named	50	Department HEP
Research Staff		
P. Datte	50	TAC
A. David	25	Electronics
N. Diaczenko	25	Mechanics
Graduate Assistants		
S. Zaman	50	Department HEP

Responsibility: Liquid scintillator calorimeter, Test Beam

UCSD BUDGET	
	FUNDING ($K)
SALARIES	
Salaries for 0.5 FTE postdoctoral fellow	14.0
Summer salaries faculty (2 months total)	12.0
Support for one FTE graduate student	11.0
TOTAL	37.0
BENEFITS	4.0
TOTAL SALARIES AND BENEFITS	41.0
TRAVEL	
For meetings, collaboration	12.0
TOTAL DIRECT COSTS	53.0
TOTAL INDIRECT COSTS @ 50%	36.0
TOTAL UCSD OPERATIONS	79.0
TOTAL UCSD EQUIPMENT	40.0

UCSD PERSONNEL		
	% this task	Other tasks
Faculty		
H. Paar (P.I.)	50	TPC/Two Gamma
M. Sivertz	50	TPC/Two Gamma
Post-doctoral Research Associates		
To be named	50	Department HEP
Graduate Assistants		
B. Ong	50	TPC
D. Acosta	50	TPC

Responsibility: PM/Fiber testing; Full scale prototype; EM prototype.

YALE BUDGET	
COMPONENT	FUNDING ($K)
SALARIES	
0.5 FTE Post-doctoral Research Assistant	14.4
TOTAL	14.4
BENEFITS	
NON-TIAA - $7,000 at 28% (JAN-JUN)	2.0
$7.420 at 29% (JUL-DEC)	2.1
TOTAL SALARIES AND BENEFITS	18.5
TRAVEL	
FNAL (2 trips: 3 people for 14 days)	7.0
Meetings, Conferences, Vendor Visits	2.0
TOTAL TRAVEL	9.0
SUPPLIES AND SERVICES	
Telephone, Postage, Copying, Fax	0.5
Stockroom Purchases and Labor	1.0
Computing	.3
Expendable Purchases	1.0
TOTAL SUPPLIES AND SERVICES	2.8
TOTAL DIRECT COSTS	30.3
INDIRECT COSTS	
$30.3K of Total Direct Costs @68%	20.6
TOTAL YALE OPERATIONS	50.9
TOTAL YALE EQUIPMENT	10.0

YALE PERSONNEL		
	% this task	Other tasks
Faculty		
P. Cushman (P.I.)	50	G-2
Post-doctoral Research Associate		
To be named	50	Department HEP

Responsibility: Preradiator

WASHINGTON BUDGET	
COMPONENT	FUNDING ($K)
SALARIES	
0.5 FTE Post-doctoral Research Assistant	14.0
1.0 Graduate Assistant	12.0
TOTAL	26.0
BENEFITS	3.0
TOTAL SALARIES AND BENEFITS	29.0
TRAVEL	14.0
TOTAL DIRECT COSTS	43.0
INDIRECT COSTS	
$43.0K of Total Direct Costs @51%	21.9
TOTAL WASHINGTON OPERATIONS	64.9
TOTAL WASHINGTON EQUIPMENT	10.0

WASHINGTON PERSONNEL		
	% this task	Other tasks
Faculty		
T. Burnett	12	SLD. ALEPH in 1989/90
V. Cook	25	SLD, LAR
K. Young (P.I.)	50	SLD
Post-doctoral Research Associate		
To be named	50	Department HEP
Graduate Student		
To be named	100	

Responsibility: Light collection, test beam data acquisition and triggering

REFERENCES

1. Physics of the Superconducting Supercollider, Snowmass 1986,// Experiments,Detectors, and Experimental Areas for the Supercollider, Berkeley 1987
2. J. Freeman. C. Newman-Holmes. Detector Dependent Contributions to Jet Resolution. Proceedings of Berkeley 1987 Workshop, p.673
3. G.W.Foster. Proceedings of the Fermilab in 1990's Workshop, Breckenridge, 1990
4. L. Balka et al., NIM A267 (1988) 272-279;// S. Bertolucci et al., NIM A267 (1988) 301-314;// S. R. Hahn et al., NIM A267 (1988) 351-366.
5. "The Engineering Development of a Scintillating Fiber Calorimeter", G. Bauer, S.T. Dye, S. Klein, J.P. Miller, B.L. Roberts, J. Rohlf, L. Sulak, D. Winn and W. Worstell, Boston University preprint, June 5, 1989.
6. heavy higgs freeman
7. F
8. R. Wigmans, NIM A256, 273 (1988)
9. A Uranium-Scintillator Calorimeter with Plastic Fiber Readout, NIM A256, 23 (1987)
10. Scintillator Readout Systems Studied in the Development of the ICD, M. Marcin, H. Neal, R. Gufstafson, G. Snow, D0 Note 841
11. R. Fast, et al. "Design Report for an Indirectly Cooled 3-m Diameter Superconducting Solenoid for the Fermilab Collider Detector," TM-1135, Fermilab, Batavia, IL (1982)
12. R.H. Wands and H.J. Krebs, "Magnetic Field and Force Calculations for an SSC Detector Using a Commercial Finite Element Code," Advances in Cryo. Engr. 35: (to be published)
13. S. Dawson *et alSingle Leptons from Heavy Quark Production* Proceedings of the Workshop on Experiments, Detectors and Experimental Areas for the Supercollider, July 7-17, 1987, Berkeley CA.
14. R. Barnett *et alTechniques for finding Supersymmetry at the SSC* ibid.
15. J.S. Whitaker *et al, Physics Parameters for New W's and Z's* and N.G. Deshpande *et alDetection of a new Z' in the Z' to W^-w^- Mode at the SSC* ibid.
16. J.L Rosner and L. Stodolsky , *Direct-Photon Searches as Tests for Unconventional High-Energy Electroweak Interactions* Phys. Rev. D, Brief Reports, 40 (1989) 1676.
17. R Ansorge *et alPerformance of a Scintillating Fiber Detector in th UA2 Upgrade* NIM A265 (1988) 33.
18. C. Back *et al*(The AMY Proposal) TRISTAN-EXP-003 KEK (1984).
19. J. Kirkby *et al, Report of the Compact Detector Subgroup*, in Proceedings of the Workshop on Experiments, Detectors and Experimental Areas for the Supercollider, July 7-17, 1987, Berkeley CA.
20. K. Kuroda , *A New Trend in Photomultiplier Techniques in Future Collider Experiments* NIM A277 (1989) 242.
21. M. Petroff and M. Atac, IEEE Trans. Nucl. Sci. **36**, (1989) 163.

FIGURE CAPTIONS

1) Invariant mass of dijet system form the decay of high P_t W boson
2) Time structure of the signal from SCSN-38 scintillating plastic fibers excited at various points. Fiber has mirror on one end, other end is read out with a photodiode
3) Schematic of an SSC detector chosen as example
4) A composite of the finite element analysis of a lead/fiber barrel calorimeter. An aluminium pipe on the inside and open bridge work on the outside provide support.
5) The deflection (left) and stress (right) for a vertical supertower.
6) Support structure for a barrel and endcap calorimeters, and for superconducting solenoids.
7) Pulse height spectra of 100 MeV (two upper figures) and 88 MeV electron beam recorded in an electromagnetic calorimeter before, immediately after and three weeks after irradiation. The absolute scale of the last measurement is not necessarily the same as for the first two measurements
8) Absorption and emission spectra of dyes in the multistep scintillator developed by Kyowa Gas Co.
9) Emision spectrum of new scintillator developed at Fermilab
10) Structure of the laminated fiber calorimeter
11) Fiber arrangement in a calorimeter
12) Projective tower build of parallel plates
13) Monte Carlo simulation of 100 GeV electromagnetic and hadron showers. Top figure shows the number of towers with energy deposition exceeding 0.5 GeV. Bottom figure shows the distribution of the fraction of total energy deposited in towers with minimal energy deposition in 'side' fibers. Towers were 5 x 5 cm at the front face, 10 x 10 cm at the back
14) Pulse height spectra of 40 GeV electron beam as a function of the angle of incidence,[22]
15) Electromagnetic section of the calorimeter: double bend of the plates provides large incidence angle, preserving projective nature of the tower
16) Change in the e/π due to different light attenuation as a function of the attenuation length
17) Contribution to the energy resolution for hadronic showers due to light attenuation as a function of the attenuation length
18) Structure of the segmented fiber calorimeter
19) Wavelength shifter core fiber design
20) Examples of ray tracing through the composite fiber
21) Photograph of the wavelength shifter fiber developed by Kyowa Gas Co.
22) Splice of the scintillating fibers and clear read-out fibers
23) Fiber by fiber splicing
24) Hadron segment design
25) UV laser scan of a prototype tile
26) Photograph of a tile stack for cosmic ray studies
27) Structure of tile plates.
28) EM calorimeter structure using tiles

29) Hadron calorimeter structure using tiles
30) A model of a detector
31) Detector cross section
32) Finite element magnetic model
33) Support ear geometry
34) Endplug module support ears
35) Finite element model of barrel assembly
36) Barrel module support ears
37) Endplug module support
38) Finite element model of endplug support structure
39) Stress intensity in barrel assembly support structure
40) Solenoid support at detector midplane
41) Example of scheme to construct TIR channels
42) Wedge design showing filling,venting and calibration channels
43) Another view of a wedge design
44) One of the test setups for studying TIR channels
45) BU scintillating fiber EM calorimeters
46) BU scintillating fiber lattice endplate
47) A photograph of a lead plate rolled by Purdue University.
48) A photograph of a tile prototype
49) Setup for measurements of attenuation length
50) Currents in PMT1, PMT2 and their ratio, as a function of position
51) Test stand for measurement of relative light yield
52) Efficiency of the SCSN81 reference bundle as a function of the transmittance of ND filters
53) Recovery of the attenuation length of a function of time, for different environments